



Circulation in the Strait of Juan de Fuca

Some Recent Oceanographic Observations

G. A. Cannon, Editor

J. R. Holbrook and R. A. Feely, editorial assistants

Contributing Authors

Coastal Physics, PMEL

G. A. Cannon, R. L. Charnell, N. P. Laird, H. O. Mofjeld, D. J. Pashinski, J. D. Schumacher

Chemistry and Biology, PMEL

E. T. Baker, D. M. Damkaer, R. A. Feely, J. D. Larrance

Deep Sea Physics, PMEL

D. Halpern, J. R. Holbrook

Numerical Studies, PMEL

J. A. Galt, J. Karpen, J. E. Overland, C. H. Pease, R. W. Stewart

Oceanographic Division, NOS

B. B. Parker

Remote Sensing Studies, PMEL

C. B. Sawyer

**Pacific Marine Environmental Laboratory
Seattle, Washington**

June 1978

U.S. DEPARTMENT OF COMMERCE

Juanita M. Kreps, Secretary

National Oceanic and Atmospheric Administration
Richard A. Frank, Administrator

Environmental Research Laboratories
Boulder, Colorado
Wilmot Hess, Director

NOTICE

Mention of a commercial company or product does not constitute an endorsement by NOAA Environmental Research Laboratories. Use for publicity or advertising purposes of information from this publication concerning proprietary products or the tests of such products is not authorized.

CONTENTS

| | |
|--|----|
| Executive Summary | v |
| Abstract | 1 |
| 1. Introduction | 1 |
| 2. Physical setting | 3 |
| 2.1 Geography | 3 |
| 2.2 Tides and tidal currents | 4 |
| 2.3 Winds | 6 |
| General description | 6 |
| Recent observations. | 9 |
| Model results. | 12 |
| 3. Oceanography | 16 |
| 3.1 Surface drifter observations. | 16 |
| 3.2 Suspended sediments. | 17 |
| 3.3 Western Strait currents and water properties | 22 |
| Mean flow | 23 |
| Variations | 25 |
| Winter wind forcing | 25 |
| 3.4 Eastern strait–San Juan Island currents | 31 |
| 3.5 Plankton observations. | 34 |
| 4. Oil-spill trajectory modeling | 36 |
| 4.1 Model description | 36 |
| 4.2 Sample trajectories | 37 |
| 5. Other studies | 42 |
| 6. Summary and conclusions. | 44 |
| 7. Acknowledgments. | 47 |
| 8. References | 48 |

EXECUTIVE SUMMARY

The Strait of Juan de Fuca is a major shipping route for both the United States and Canada. Tanker traffic is likely to increase in these waters now that the Trans-Alaskan pipeline is complete. Much new work has taken place since the publication of the most recent oceanographic description of this estuary over fifteen years ago. The present report was written at the request of the NOAA Administrator to provide an up-to-date, comprehensive synthesis of results of the most recent studies for use in decisions regarding these waters. The primary emphasis of the NOAA efforts has been on transport mechanisms that might affect the redistribution of spilled oil. Additional field studies east of Port Angeles are continuing through 1978.

These studies have shown that a variety of transport processes exist in the Strait of Juan de Fuca that could result in considerable redistribution of spilled oil, or any other contaminant, throughout the region. Winds appear to be the primary factor causing significant variations in the more normal net flow of surface water out to sea. In addition, winds appear to direct the flow toward the shores of the Strait. Large flow variations occur during every season but summer. The evidence presented, while not yet complete, indicates the strong possibility of significant volumes of a spilled contaminant reaching beaches within the estuary instead of being transported out of the estuary. The probability of such a beaching increases significantly the farther into the estuarine system the potential spill occurs. Likewise, the probability of an accident leading to a spill increases with distance into the system because of narrowing channels near the San Juan Islands and intersecting traffic lanes north of Admiralty Inlet, the entrance to Puget Sound.

Tidal currents are the strongest component of the flow in most of this estuarine system, and because of their large magnitude in the more restricted passages they are navigational hazards. Tidal fronts form north and south of the San Juan Islands in waters that are major traffic lanes, and near-shore eddies and backwaters occur nearly everywhere on the down-current side of headlands. Both of these phenomena tend to concentrate floating or suspended material. However, current-meter and satellite observations of the Fraser River plume indicate that variable wind-

driven currents, rather than tidal currents, dominate the relatively shallow water near Cherry Point, one of the major oil terminals in the region. Drift cards released south of San Juan Island in the middle of the eastern basin of the Strait, an intersection of major traffic lanes, were found on all beaches surrounding the eastern basin. Drift cards that progressed farther seaward tended to ground on Vancouver Island in winter and on the Olympic Peninsula in summer. A computerized oil-spill trajectory model, while still incompletely developed, also indicated several possibilities of flow ending on beaches in the eastern basin. Moored current meter observations in the western basin showed that, during intervals of coastal storms, the surface currents flowed into rather than out of the Strait for a few days. This flow was accompanied by intrusions of coastal ocean water as far as 90 km from the mouth and retention of surface water within the system. The speed and duration of the intrusions implied that ocean water on occasion could possibly reach as far east as Whidbey Island.

There remain a number of unanswered questions. The flow patterns that distributed the drift cards around the eastern basin are unknown. Also, it is not clear whether the intrusions of coastal water enter the eastern basin, or to what extent storm-related conditions drive the circulation there. These questions are being addressed during the present field investigations. Another limitation is that the oil-spill trajectory model has been run only for a typical March and no summer cases have yet been run; additional calculations are being made this year. Also, time has not allowed inclusion of data on the winter current reversals in the model. As yet, little is known about processes occurring in the near-shore zone extending about a mile or so offshore throughout the estuary, in the passages between the San Juan Islands, at the mouth of the Strait, and at the junction with Admiralty Inlet. These areas must await future research.

This report was used for environmental planning even before the final draft was completed. The summary and conclusions were presented as "Comments on vessel traffic management in Puget Sound waters and environmental factors entering therein" at U.S. Coast Guard hearings on April 20-21, 1978, in Seattle.

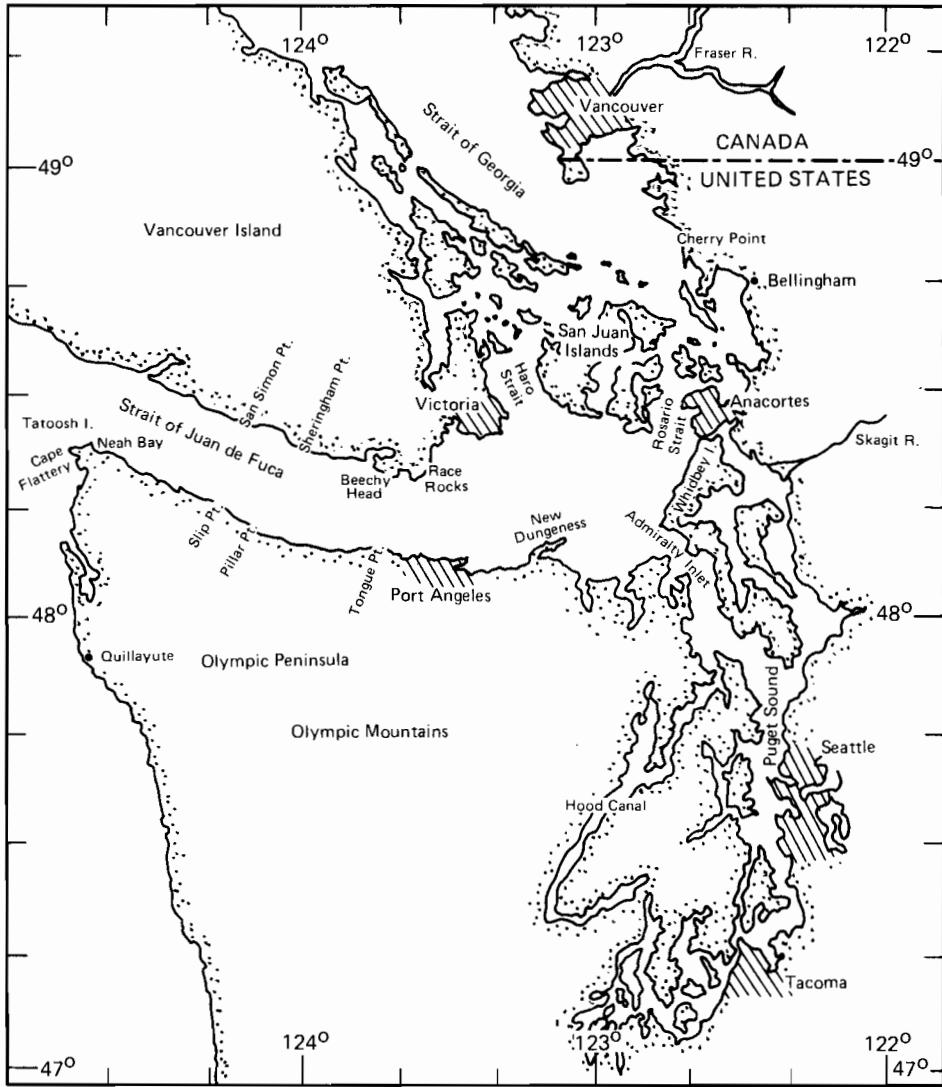


Figure 1. Strait of Juan de Fuca, showing nearby features and connecting waterways. Additional place names in and north of the San Juan Islands are shown in Fig. 39.

CIRCULATION IN THE STRAIT OF JUAN DE FUCA: SOME RECENT OCEANOGRAPHIC OBSERVATIONS

G. A. Cannon, ed.

ABSTRACT. Oceanographic research in the Strait of Juan de Fuca and some of its adjacent waterways, emphasizing transport mechanisms that might affect the redistribution of spilled oil, has focused on near-surface circulation and its driving mechanisms. Moored current meters, surface drift cards, satellite images of suspended sediment, and an oil-spill trajectory model were used. The largest flow variations were found during fall-winter-spring. Drift cards tended to ground on Vancouver Island in winter, on the Olympic Peninsula in summer, and on beaches in the eastern basin of the Strait throughout the year. Trajectory model experiments also showed flow ending on beaches in the eastern basin. Numerous tidal fronts were observed north and south of the San Juan Islands, and near-shore eddies occurred everywhere on the down-current sides of headlands. Both of these phenomena tend to concentrate floating or suspended material. Moored current meters showed winter intrusions of oceanic surface water almost to Port Angeles lasting several days to over a week. Outflow often occurred only in the deeper water, with surface water being retained within the system. Winds appeared to be the major cause of all flow variations. Indications were that significant volumes of any contaminant would probably reach beaches within the estuary.

1. INTRODUCTION

The Strait of Juan de Fuca estuary is the principal approach from the Pacific Ocean to the major Canadian and United States population centers (Vancouver, Seattle, et al.) located on the Strait and on the adjacent waters of the Strait of Georgia and Puget Sound (Fig. 1). The region is a spectacular environment for living and recreation, and its abundant resources provide a substantial base for economic development. Decisions on questions regarding new and alternate uses of these waters require knowledge of various aspects of the marine environment. However, the most recent description of oceanographic features of the Strait of Juan de Fuca is more than fifteen years old (Herlinveaux and Tully, 1961). While several studies have occurred since then, most have been limited to descriptions in isolated reports or have not yet appeared in reports or scientific publications.

In 1975 the Pacific Marine Environmental Laboratory (PMEL) of NOAA initiated investigations into several oceanographic aspects of this system with major emphasis on circulation. Be-

cause of the potential for increased tanker traffic, the primary objective of these investigations was to describe the important transport mechanisms that might affect redistribution of spilled oil. Field studies included primarily physical oceanographic and meteorologic measurements to observe surface circulation and to determine causes for its variations. Because the surface and deeper water constitute a coupled system, some aspects of flow through the total water column also were measured. Additional studies included suspended sediment investigations partly using satellite observations, oil-spill trajectory model developments that included a coupled meteorological model, and biological observations of seasonal plankton distributions. The mooring studies discussed in this report have been west of Port Angeles. Mooring studies east of Port Angeles are taking place during 1978 and cannot as yet be reported.

Since the fall of 1973 the National Ocean Survey (NOS) of NOAA has carried out several detailed circulatory surveys in the Strait of Juan de

Fuca, the Strait of Georgia, and the connecting waterways through the San Juan Islands. The primary objective of their surveys was to obtain information on tides and tidal currents, along with supporting auxiliary data. This information was to provide increased understanding of these water systems needed in general for safer navigation and more specifically for possible increased oil tanker traffic. Some of these surveys have been carried out jointly with PMEL investigators. NOS observations presented in this report have been made primarily east of Port Angeles and in the passages of the San Juan Islands.

The purpose of this report is to summarize and synthesize some of the scientific information of this recent oceanographic research in the Strait of Juan de Fuca so that it is available in one source for environmental planning. Most of the material

presented here has come either from recently published reports or from studies that are in various stages of being published. More details will be found in the referenced reports. This report primarily describes studies conducted by NOAA and, where appropriate, refers to other known work in the area. It emphasizes circulation and water movement because the majority of recent research has been dominated by efforts in these areas. The Other Studies section mentions ongoing work east of Port Angeles. No attempt has been made to relate this work to ecosystems studies, and no implications have been drawn regarding oil transportation or oil-port siting. Other recent works have examined some of these topics (e.g., Little, 1977).

The Summary and Conclusions section is a brief self-contained synopsis of this report.

2. PHYSICAL SETTING

2.1 Geography

The Strait of Juan de Fuca is a submarine valley extending from the Pacific Ocean to the channels of the San Juan Archipelago, Whidbey Island, and Admiralty Inlet. It is bounded on the north by the low Seymour Mountains on Vancouver Island in Canada and on the south by the higher Olympic Mountains in Washington State. The Strait contains two basins with depths exceeding 100 m. These are separated by an effective sill (cross-channel ridge) projecting southward from Victoria at about 60-m depth. Seaward of this sill the outer (or western) basin deepens to more than 200 m at Cape Flattery, and these depths continue seaward along a glacial channel across the entire continental shelf. This western basin is about 20 km wide and 90 km long. Landward of the sill is the deeper inner (or eastern) basin which connects to the Strait of Georgia primarily through Haro Strait with a secondary sill of about 90 m near the north side of the San Juan Islands. Shallower depths connect across the 64-m Admiralty Inlet sill into Puget Sound. Intermediate depths are found in Rosario Strait, which is the third main passage of major shipping importance. This eastern basin topography is more complex with numerous banks and shoals (Fig. 2). More details are given by Parker (1977).

The western Strait of Juan de Fuca may be considered a weakly stratified, partially mixed estuary with a surface-to-bottom salinity difference of 2^{0}_{00} – 3^{0}_{00} (Herlinveaux and Tully, 1961). Although there are important cross-channel variations, the along-channel mean flow is characterized by the classical estuarine circulation with seaward (westward) transport near the surface and landward (eastward) transport near the bottom. This circulation is maintained by river water which enters the system and sets up a longitudinal sea-surface slope directed toward the mouth. The near-surface flow is driven primarily by the longitudinal sea-surface slope (barotropic forcing) while the deeper return flow is driven by

the longitudinal density gradient (baroclinic forcing). These two driving forces are balanced by the internal and bottom frictional forces generated by strong tidal mixing.

Fresh water entering the inland waters is primarily river runoff, with the Fraser River accounting for approximately 80% of the total (Waldichuck, 1957). Precipitation varies considerably (49–250 cm/yr) within the drainage basins. Most of the drainage areas are high mountainous regions, and winter snow storage plays a major role in establishing the runoff (Fig. 3). Precipitation is greatest during winter and at higher elevations, but drainage does not occur until spring warming.

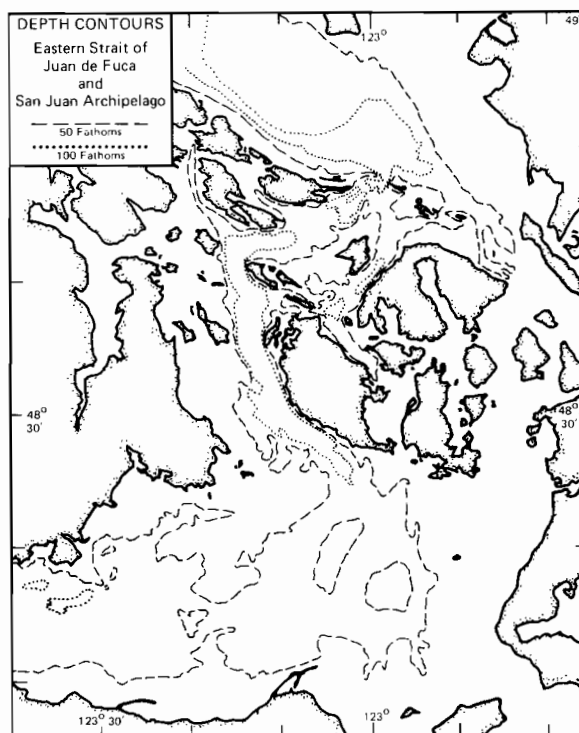


Figure 2. Topography of the eastern basin of the Strait of Juan de Fuca and the San Juan Islands waterways. Based on Parker (1977).

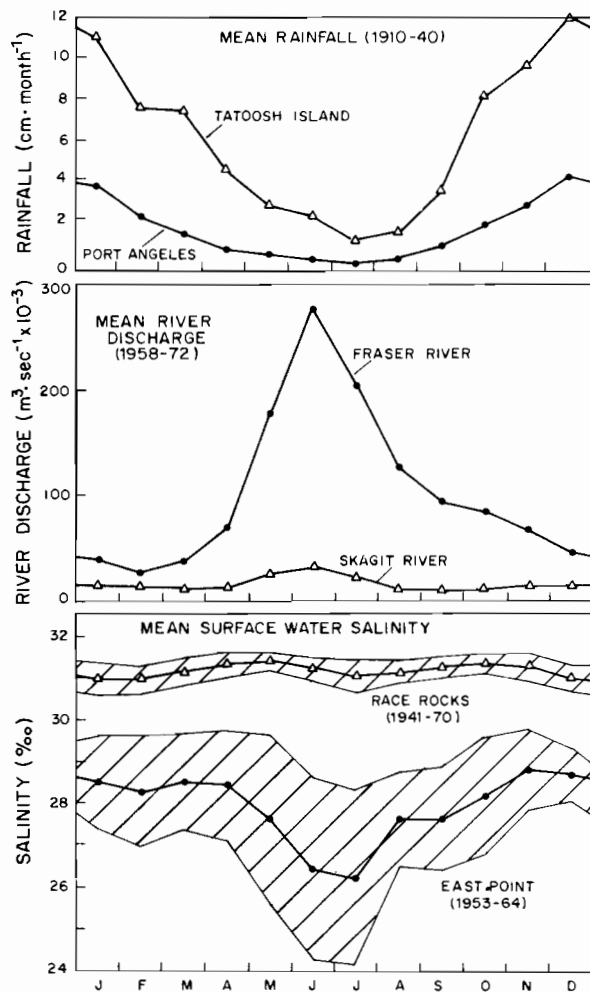


Figure 3. Seasonal variations in monthly rainfall, river discharge, and surface salinity. From Holbrook and Halpern (1978).

Consequently, the Fraser River has maximum discharge in June. Its winter mean discharge represents only approximately 12% of its June peak. The Skagit River (the largest river emptying into Puget Sound proper), however, has maximum discharges in both summer and winter. The volume of the maximum Fraser discharge in June over one semidiurnal tidal period is less than 1% of the tidal prism (volume of water between high and low tide levels). The spring freshet lowers the surface salinity north of the San Juan Islands at East Point (east end of Saturna Island, shown in Fig. 39) by several parts per thousand, while south of the San Juan Islands at Race Rocks, the surface salinity remains higher and undergoes smaller seasonal and monthly variations. One important aspect of tidal mixing in the passages of the San Juan Islands is the moderating effect on seasonal freshwater fluctuations in the Strait of Juan de Fuca. Tidal mixing in Admiralty Inlet similarly moderates runoff entering from Puget Sound.

2.2 Tides and Tidal Currents

Observations from various sources indicate that tidal currents dominate the flow regime in these waters. Superimposed on the tidal motions are the estuarine and wind-driven currents that transport floating and suspended material through the system. The tidal currents represent navigational hazards. In addition, they tend to disperse floating and dissolved constituents away from shorelines and to concentrate those constituents in near-shore eddies and at tidal fronts.

Both the diurnal and semidiurnal tides enter the system from the Pacific Ocean as progressive, long waves. (Figs. 4 and 5 show the M_2 semidiurnal tide; the diurnal is in Parker, 1977.) Each wave propagates through the topographically complicated San Juan Archipelago, producing a complex current pattern in this region with strong currents in Haro and Rosario Straits (Fig. 6). Strong currents also occur in Admiralty Inlet as the tides propagate into Puget Sound (Fig. 7). The tidal current regime south of the San Juan Archipelago (eastern basin of the Strait of Juan de Fuca) appears to be extremely complex. The volume transported through a cross-section near Neah Bay during a flood tide is approximately 20 km^3 and 25 km^3 for the M_2 and K_1 components, respectively, and the resulting tidal prism during spring tides is nearly 2% of the volume of the system (P. B. Crean, Environment Canada, personal communication).

Further analysis of the tide and tidal current regimes in the Strait of Juan de Fuca, Strait of Georgia, and Puget Sound systems is underway at the National Ocean Survey using a semi-analytical model, and at Environment Canada using a numerical model. It is well established by the early work of Redfield (1950), as well as by more recent work, that reflection of the tides in the Strait of Georgia produces standing tides in that region. Around the San Juan and Channel Islands (Canadian), the tidal currents in any given channel are often controlled by the differing water level at the two ends of the channel. Because of their shorter wavelength, the semidiurnal tides such as M_2 have minimums in their range near Victoria (Fig. 5) while diurnal tides such as K_1 (not shown) have progressively increasing ranges moving landward from the Pacific Ocean.

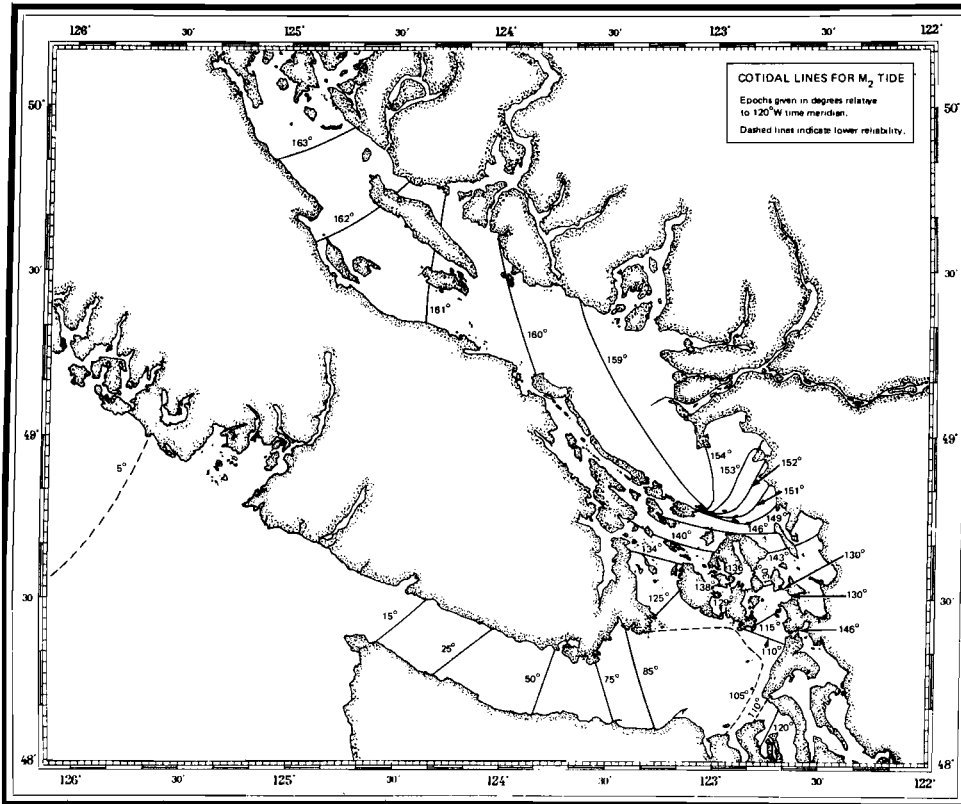


Figure 4. Cotidal line chart for the M_2 tide in the Strait of Juan de Fuca-Strait of Georgia system. From Parker (1977).

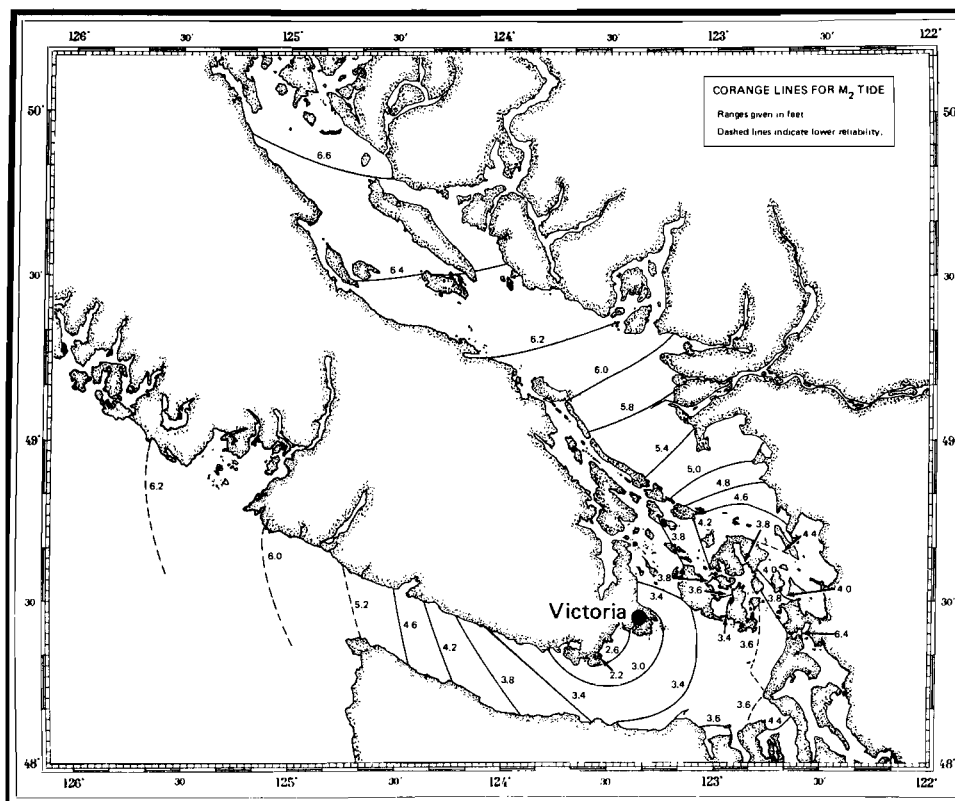


Figure 5. Corange line chart for the M_2 tide. From Parker (1977).

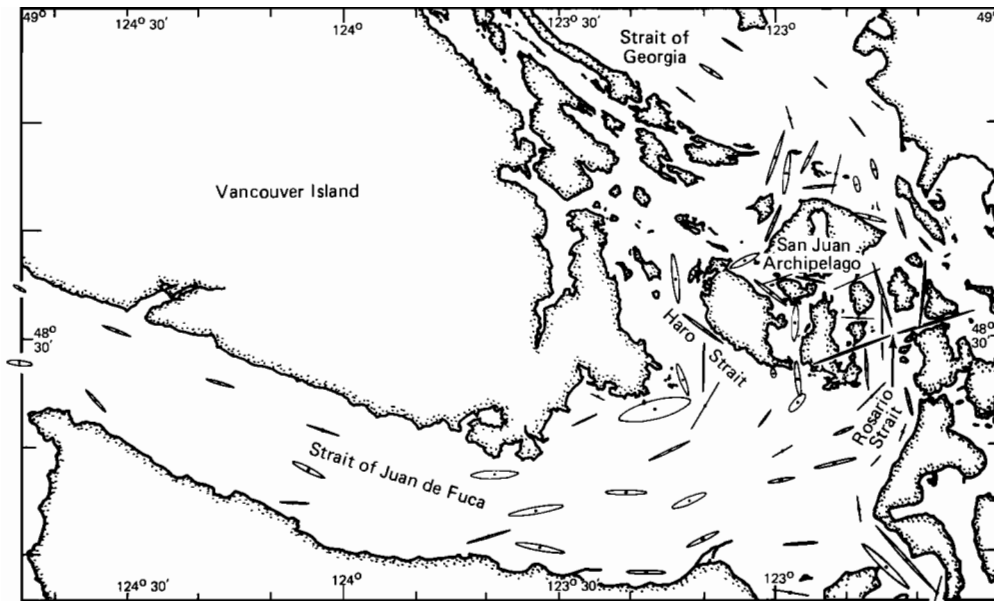


Figure 6. Tidal current ellipse chart for the tide in the Strait of Juan de Fuca–Strait of Georgia system. Direction ellipse points indicates direction of tidal current flow. Size of ellipse indicates intensity of flow. From Parker (1977).

While a regional description of the tidal range appears to be reasonably accurate, the tidal currents appear to be much more sensitive to local variations in water depth and details of the shore line than are the tidal ranges. For example, the tidal currents near Cherry Point are relatively small (Schumacher et al., 1978), while much stronger tidal currents occur offshore from Cherry Point and in the passages leading to the Strait of Juan de Fuca (Fig. 6). On the other hand, the tidal ranges showed much less variation (Fig. 5).

Moored current meter arrays do not allow a detailed analysis of tidal fronts or discontinuities, but these can be observed in aerial and satellite images. Such fronts are common near points of land in the Strait of Juan de Fuca–Puget Sound region (C. A. Barnes, University of Washington, personal communication; see Section 3.2 below). Tidal fronts act as down-welling centers where floating material such as oil could be injected into the deeper layers of the water column. Vertical dispersion also occurs in passages with strong tidal currents, which produce mixing through the generation of turbulence.

The vertical distribution of the tidal currents is relatively simple in the Strait of Juan de Fuca and in the passages through the San Juan Archipelago. In these regions, the tidal currents are relatively independent of depth near the surface, decrease in amplitude below the surface layers, and form a bottom boundary layer with active generation of turbulence during strong current intervals. To the north of the passages in the southern Strait of

Georgia, internal waves are formed during flood tides. The currents associated with these waves change across the shallow pycnocline formed by the Fraser River effluent (Gargett, 1976).

2.3 Winds

General description. Major perturbations to the seaward, near-surface estuarine flow can occur as a result of the near-surface wind field. Wind stress can act directly on the surface, transferring momentum or energy downward by vertical mixing. It also can act indirectly by raising the sea level at the mouth of the estuary (piling up water) and thereby modifying the sea-surface slope within the estuary, which in turn dominates the near-surface circulation. Thus, knowledge of local and adjacent wind fields is essential to any description of near-surface water motion. The conventional directions from which the wind blows are used in the following description.

The predominant winds along the ocean coast are southwesterly (i.e., from the southwest) in winter and northwesterly in summer, paralleling the general coastline, and this pattern is reflected in measurements of typical winter and summer mean wind stress fields off the Washington coast (Nelson, 1977). In the Strait of Juan de Fuca the winds are controlled by orographic factors. In general, seaward or easterly winds dominate in winter while landward or westerly winds occur more frequently in summer (Harris and Rattray,

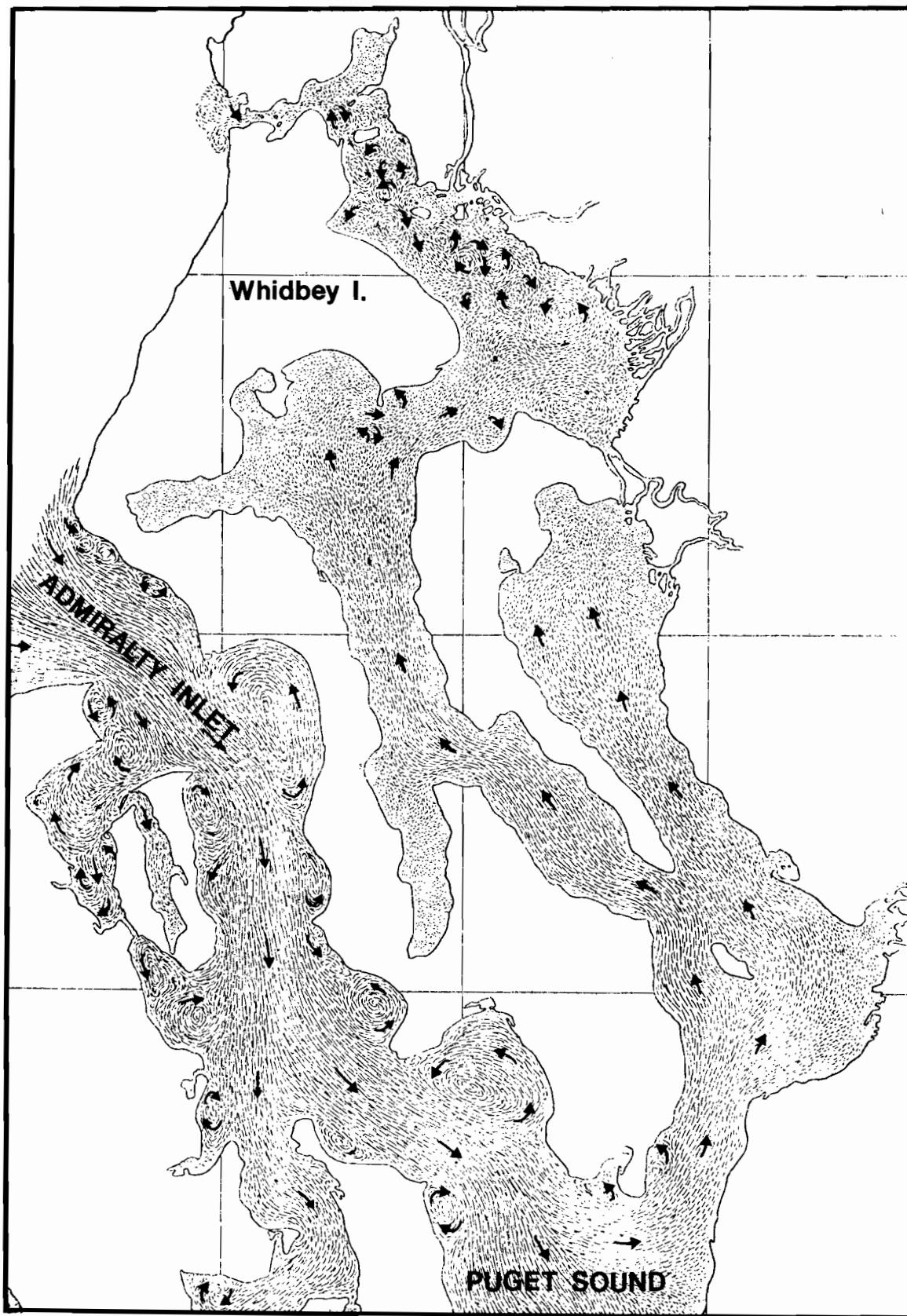


Figure 7. Artist's rendering of surface tidal currents during flood tide in Admiralty Inlet as observed in a hydraulic model of the Puget Sound system. From McGary and Lincoln (1977).

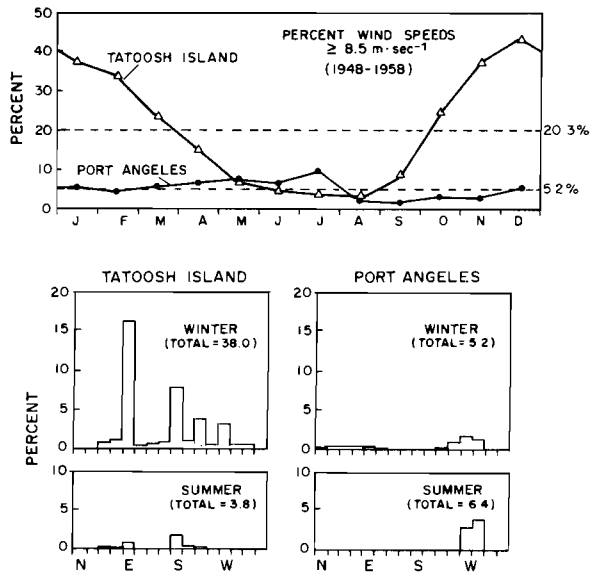


Figure 8. Seasonal distribution of winds greater than 8.5 m/sec at Tatoosh Island and Port Angeles. From Holbrook and Halpern (1978). Winter and summer histograms are for December-February and June-August, respectively.

1954). The seasonal variation of winds at Tatoosh Island off Cape Flattery shows that during winter months 38% of all winds observed have speeds greater than 8.5 m/sec (Fig. 8). The southerly and easterly directions shown in the Tatoosh histogram suggest that winter winds reflect the combined influence of the large-scale wind systems along the coast and the locally steered winds in the Strait. In contrast to Tatoosh, during winter months at Port Angeles only 5% of the wind speeds are greater than 8.5 m/sec. The Port Angeles winds are generally westerly which is consistent with the apparent divergence region west of Port Angeles suggested by Harris and Rattray. However, about 1%-2% of all observations showed strong northeasterly winds.

The winter season (December-February) weather is dominated by cyclonic storms moving over or to the north of the region, interrupted infrequently by periods of high pressure. Gale force (17-24 m/sec) or higher winds occur frequently near Tatoosh Island with southerly gales persisting two or three days accompanied by high sea and swell. While it is difficult to generalize all weather types, there seem to be two typical storm patterns. In the first, pressure patterns are associated with a large low-pressure area in the Gulf of Alaska (Fig. 9-A). The center of the low pressure is usually stationary with the frontal system moving rapidly across the Pacific. Often the cold front will rapidly approach the coast, stall, dissipate offshore, and then move inland, leading to difficulties in providing forecasts. The second type of storm includes disturbances that form in the central Pacific between the Aleutian low and the Central Pacific high and skirt across the Pacific, commonly on an east-northeasterly trajectory, reaching land over Vancouver Island (Fig. 9-B). Such systems are steered by a strong westerly component in the flow at upper levels in the atmosphere. Occasionally the large-scale flow pattern of upper air will shift as it did in winter 1976-77 when the storm track occurred to the south of Oregon. For frontal systems associated with low-pressure centers passing to the north of the Strait of Juan de Fuca, the general pattern of surface winds just offshore is prevailing south to southwesterly flow backing to west-northwest as the cold front passes. At some time during most winters an upper level ridge of high pressure will develop over northwest Canada (Fig. 9-C). This is accompanied by a surface high over Puget Sound basin. The corresponding weather includes clear skies, near-freezing temperatures, and very stable air in the surface layer. Winds in the Strait are from the east, increasing in magnitude from east to west.

Summer is characterized by the offshore build-up of the eastern Pacific high pressure (Fig. 9-D).

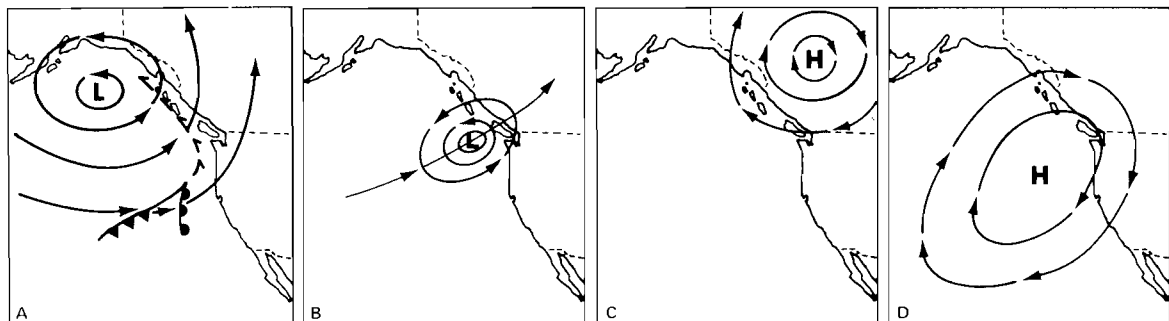


Figure 9. Typical storm patterns affecting the Washington coast. Adapted from Maunder (1968) in Overland and Vimont (1978).

The high pressure leads to a dry season with many clear days and prevailing winds from the west to northwest. Superimposed upon the mean flow is a strong diurnal oscillation associated with the sea breeze. Victoria and Port Angeles show a component of wind continuously from the west with maximum speed occurring at about 1800 local time and near zero speed in the early morning hours. Over 75% of all wind observations during the summer months at Port Angeles are from the western quadrant.

The spring season is not significantly different from winter except that temperatures begin to rise, the frequency of cyclonic disturbances decreases, and their distribution over time is irregular. The autumn season is another transition period. A common characteristic of early fall is an Indian summer, the result of continuing high pressure.

Topography plays the major role in influencing the winds in the Strait of Juan de Fuca. Due to the rotation of the earth, winds tend to blow clockwise around a high and counterclockwise around a low as viewed from space in the northern hemisphere. However, in places where topography prevents the free flow of air, such as the passageways of northwest Washington, winds invariably blow from high to low pressure in a direction dictated by the orientation of the terrain. The Strait of Juan de Fuca is very prone to this type of channeling since the air is often stably stratified, decreasing the possibility of vertical motion of air parcels. For example, when winter high pressure exists in the interior of Washington State, the pressure is higher inland at Bellingham than at Quillayute on the coast (Fig. 10). The airflow accelerates through the Strait with the weak winds at Port Angeles and strong east winds at Tatoosh. These are the so-called gap winds (Reed, 1931). Winds are from the north in the Puget Sound-Seattle area.

The local air flow is complicated further by inertia, the tendency of the air to flow in the same direction. Just before the passage of a storm with coastal winds from the southwest, the flow is channeled through Puget Sound and around the Olympic Mountains (Fig. 11). However, the air flow overshoots in the lee of the mountain forming an area of calm winds in the vicinity of Port Angeles. As the storm moves northeastward the winds in the Strait shift to westerly and the convergence zone formed in the lee of the mountain moves south. This case of westerly winds in the Strait was typical during one of the winter series of recent observations described below and later in Section 3.3. These westerly winds appeared to be a regularly occurring event during winter. Other examples are in Overland and Vimont (1978).

Recent observations. During the late winter of 1976 (February–May), the winter of 1976–1977 (November 1976–February 1977), and the summer of 1977 (June–September), over-the-water and shore-station wind measurements were made in conjunction with current observations in the western basin of the Strait, as described in the Oceanography section. Over-the-water winds were measured from surface buoys located at Sites A, B, and C (Fig. 12) and were recorded by vector-averaging wind recorders. Details of the measurement techniques and preliminary analysis are given in Holbrook and Halpern (1978).

The predominant wind patterns during the three deployments were different (Fig. 13). During the first winter's deployment, coastal winds were southwesterly, while Strait winds were westerly as measured at Race Rocks and Port Angeles. No over-the-water winds were recorded. During the second winter experiment, coastal winds were southeasterly, and Strait winds measured from the surface buoys were predominantly easterly, in contrast with the winds of the first winter. During the summer experiment, Strait winds measured from the surface buoys were westerly with a strong diurnal sea-breeze component. The second winter generally was analogous to that described by Harris and Rattray (1954), while the mean conditions during the first winter were entirely different.

During the first winter experiment, winds were measured at NOS and Environment Canada shore stations (Fig. 14). The two most predominant winter wind patterns occurred on February 15 and March 3, 1976. The first was characterized by southerly winds off the coast (Tatoosh Island) and over the inland waters (Point Wilson at the entrance to Admiralty Inlet and Smith Island) and weak and variable winds over the middle Strait (Port Angeles, Race Rocks, and New Dungeness spit east of Port Angeles). On March 3, winds at all stations were northeasterly and were generally associated with a high pressure system located over the Cascade Range.

Other statistical studies showed that the total wind variance was 81% greater during winter than during summer. The along-channel wind variance accounted for most (76%–84%) of the total variance and was primarily distributed at lower frequencies with 87%–90% below 0.04 cycles per hour (cph). The only significant spectral peaks occurred during summer and were associated with the sea-breeze effect. Of the along-channel variance at frequencies below 0.04 cph, 72%–85% was coherent between Sites A and C, and phase lags in this frequency range were not significantly different from zero. Of the along-channel total wind energy, 56%–74% was linearly

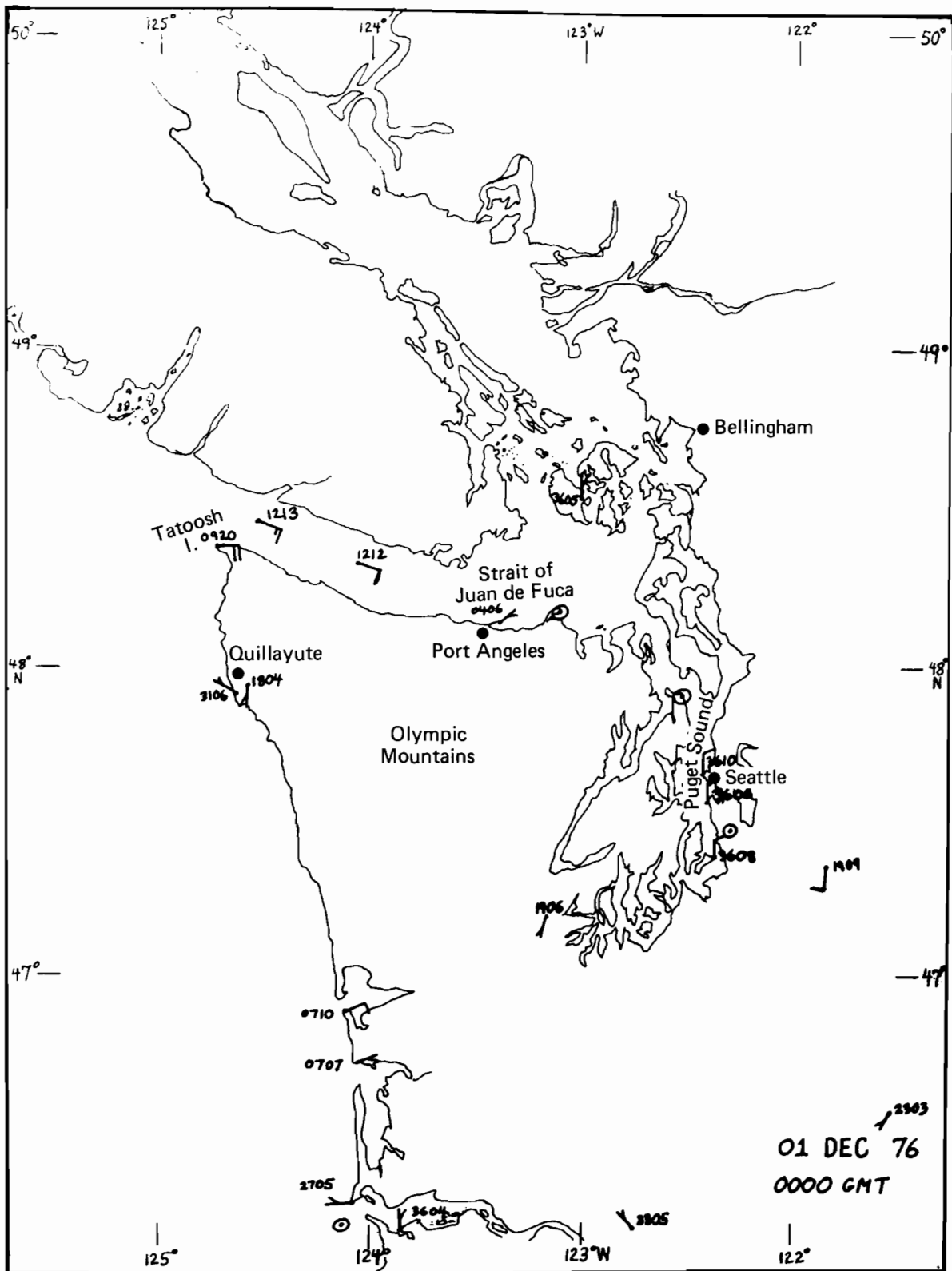


Figure 10. Sample wind patterns with interior high pressure. Barbs on wind arrows each represent 10 knots (5.1 m/sec). From Overland and Vimont (1978).

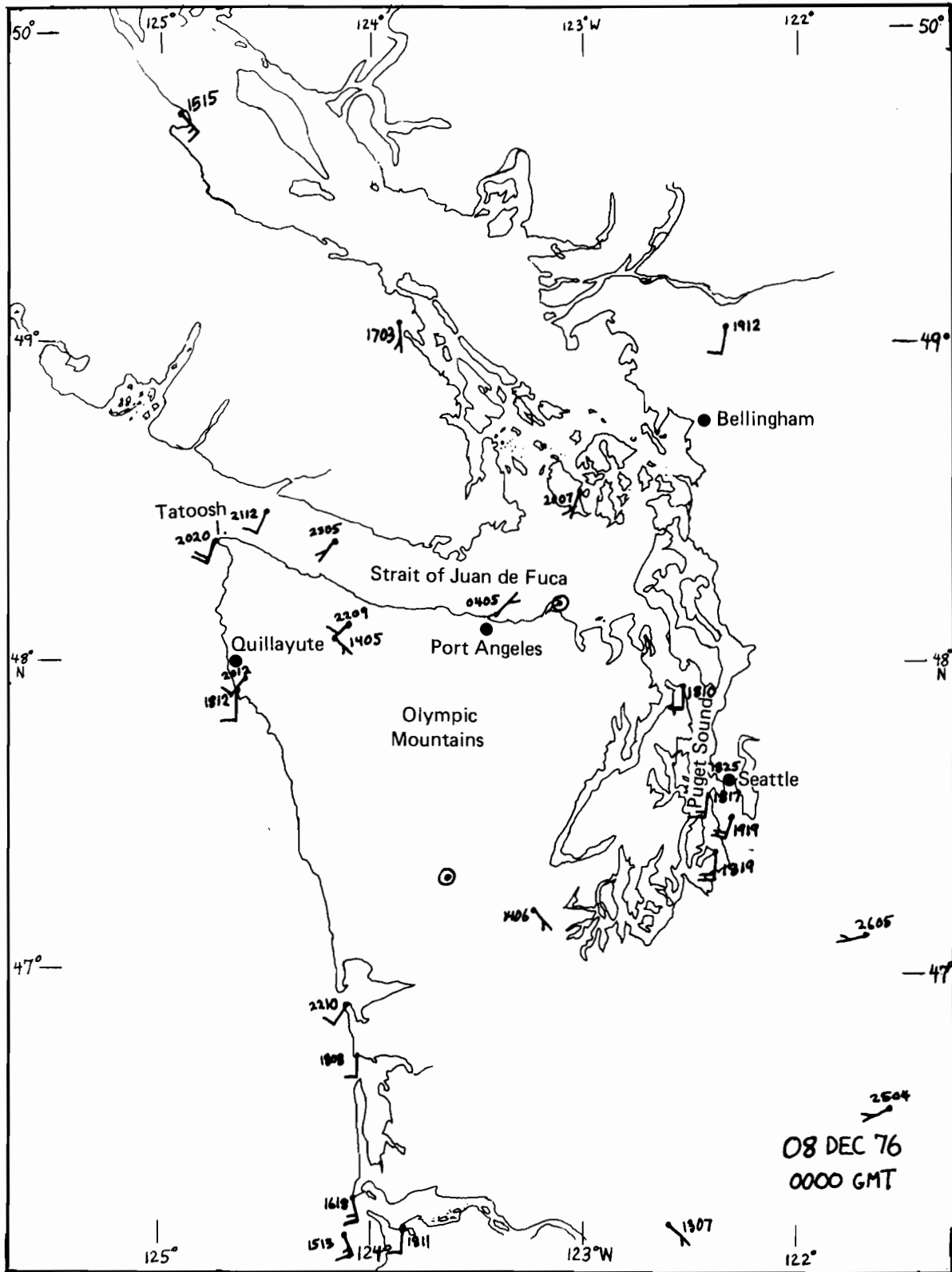


Figure 11. Sample wind patterns during southwest storm winds on the coast. From Overland and Vimont (1978).

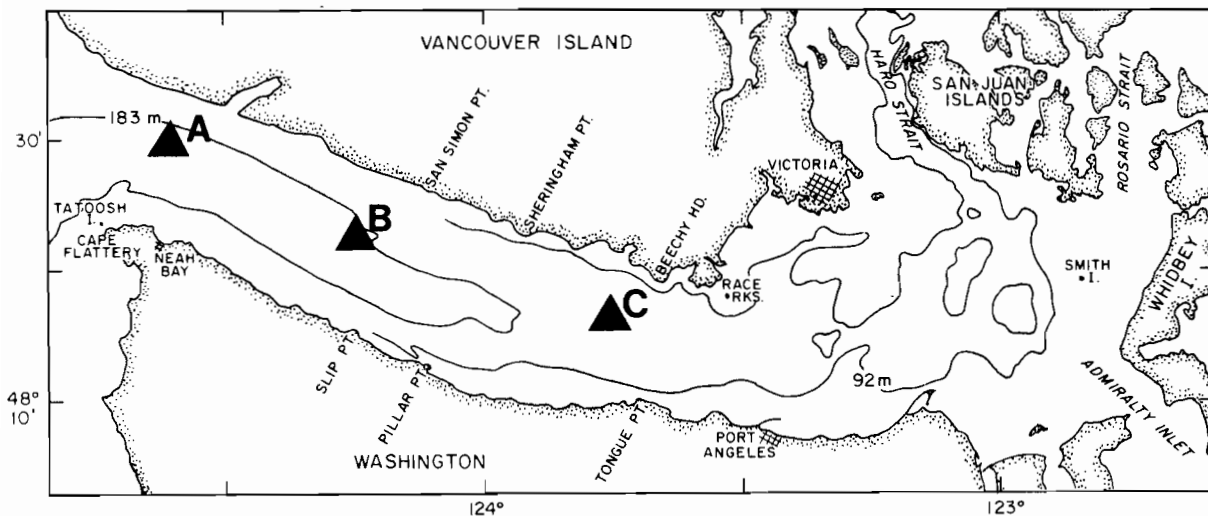


Figure 12. Surface mooring locations A, B, and C. From Holbrook and Halpern (1978).

correlated over the length of the western Strait (70 km). Winter correlation coefficients (0.86–0.90) were higher than summer (0.75–0.84). The across-channel wind components were not significantly correlated between Sites A, B, and C. During summer only, wind speeds increased with up-channel (landward) distance due to orographic funneling (first suggested by Reed, 1931) and possibly with increased strength of the sea breeze.

Correlations between over-the-water winds and shore-station winds showed north-south components were not significantly correlated. The east-west components were in general significantly correlated with those measured at shore stations. During winter, east-west winds at Race Rocks and Tatoosh Island were most representative of western Strait winds over the open water. During summer, comparisons were best with winds at Race Rocks and Sheringham Point. Winds measured on Ediz Hook at Port Angeles during winter were least representative of winds over the water.

The atmospheric pressure difference between Bellingham, located northeast of the San Juan Islands, and Quillayute, located on the Washington coast, was assumed to be representative of the longitudinal atmospheric pressure gradient (Fig. 15). Hourly and low-pass filtered values were strongly correlated with the along-channel component of winds measured at Site B and at Race Rocks. Out-channel winds occurred when atmospheric pressure over inland regions (Bellingham) was greater than over the Pacific coast (Quillayute). Maximum (above 10 m/sec) winds were associated with pressure differences in excess of 4 mb. There was a correspondence between along-channel winds with speeds of 2.5 m/sec and the along-channel atmospheric pressure gradient

of 1 mb/200 km. The best estimators of along-channel winds in the western Strait were found to be the atmospheric pressure difference between Bellingham and Quillayute airports and the regularly measured winds at Race Rocks.

Further discussion of the marine meteorology of western Washington is given in Overland and Vimont (1979), Holbrook and Halpern (1978), Lilly (1978), Maunder (1968), and Phillips (1966). Also, a new technique of airborne wind measurements recently has been developed for application to atmospheric models and/or oil-spill prediction (Oliver and Gower, 1977).

Model results. The winds over western Washington are dominated by the effects of topography. The Strait of Juan de Fuca, being a narrow cut in the coastal mountains between Puget Sound and the ocean, is particularly rich in local features with large changes in wind speed and direction over short distances. The location and shape of these features are continually changing in response to the changing large-scale weather situation. Thus, a major limitation of coastal meteorological forecasting is the inadequate specification of the local wind field at the spatial resolution necessary to resolve wind drift, local waves, and vessel or oil-spill leeway. Typically, this is due to the difficulty of estimating near-shore wind fields directly from large-scale pressure patterns or from widely scattered and often unrepresentative wind measurements. To this end a numerical meteorological model was developed for use in conjunction with the field measurement program to determine regional wind patterns for the oil-spill trajectory model (described below in Section 4) and to explore the physical processes that

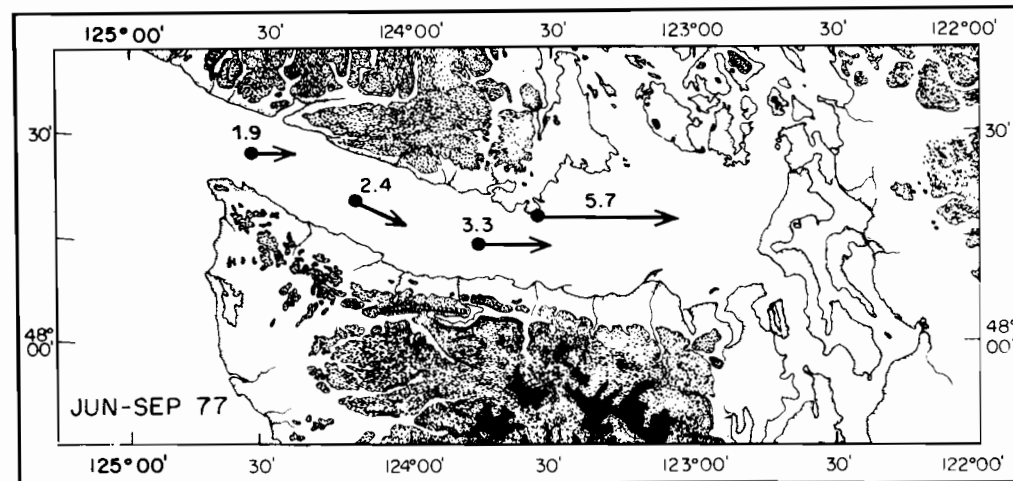
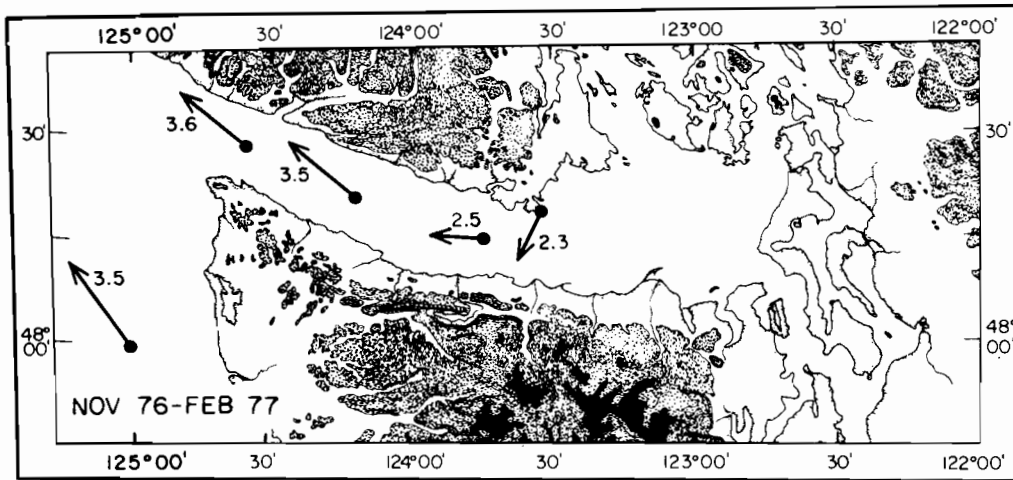
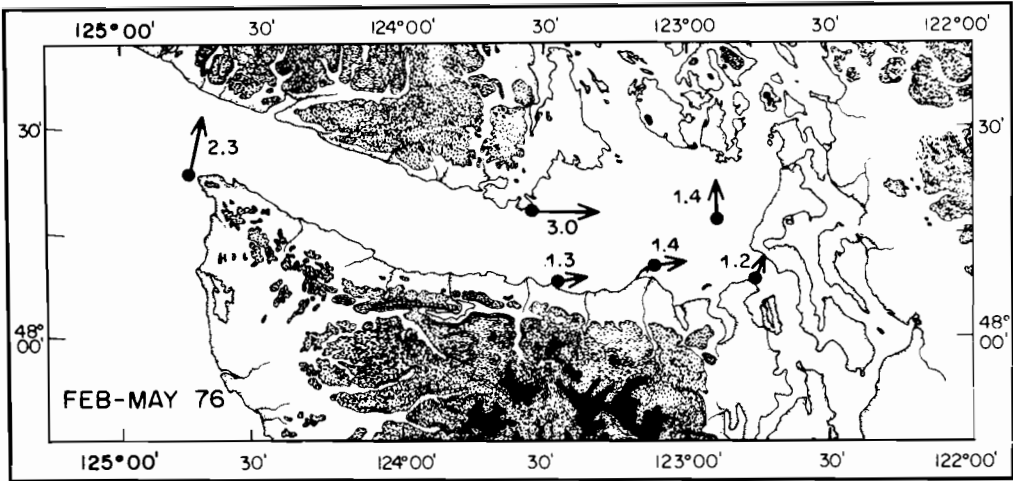


Figure 13. Vector mean winds (m/sec) during each of the three experiments showing direction to which the wind blows. From Holbrook and Halpern (1978).

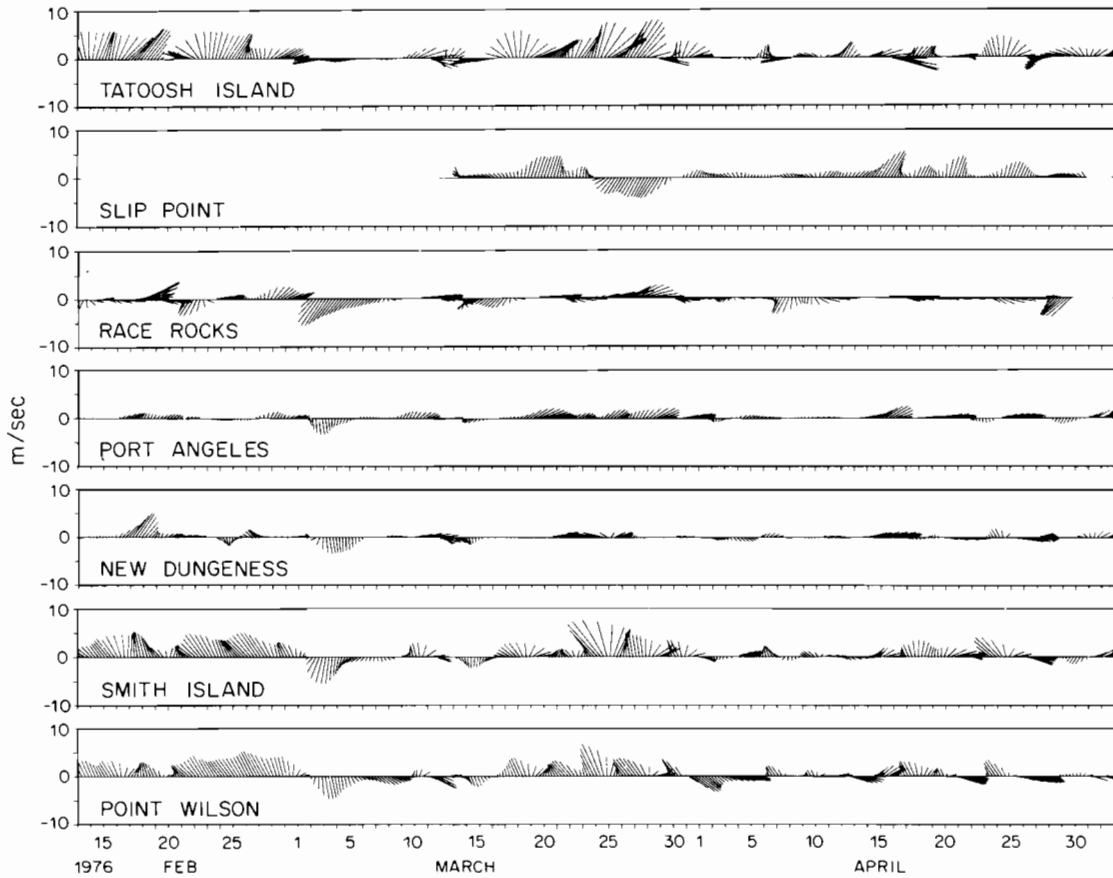


Figure 14. Low-pass filtered wind vectors measured at shore stations during the first winter experiment and plotted at 6-h intervals. From Holbrook and Halpern (1978). The vectors point in the direction toward which the wind blows.

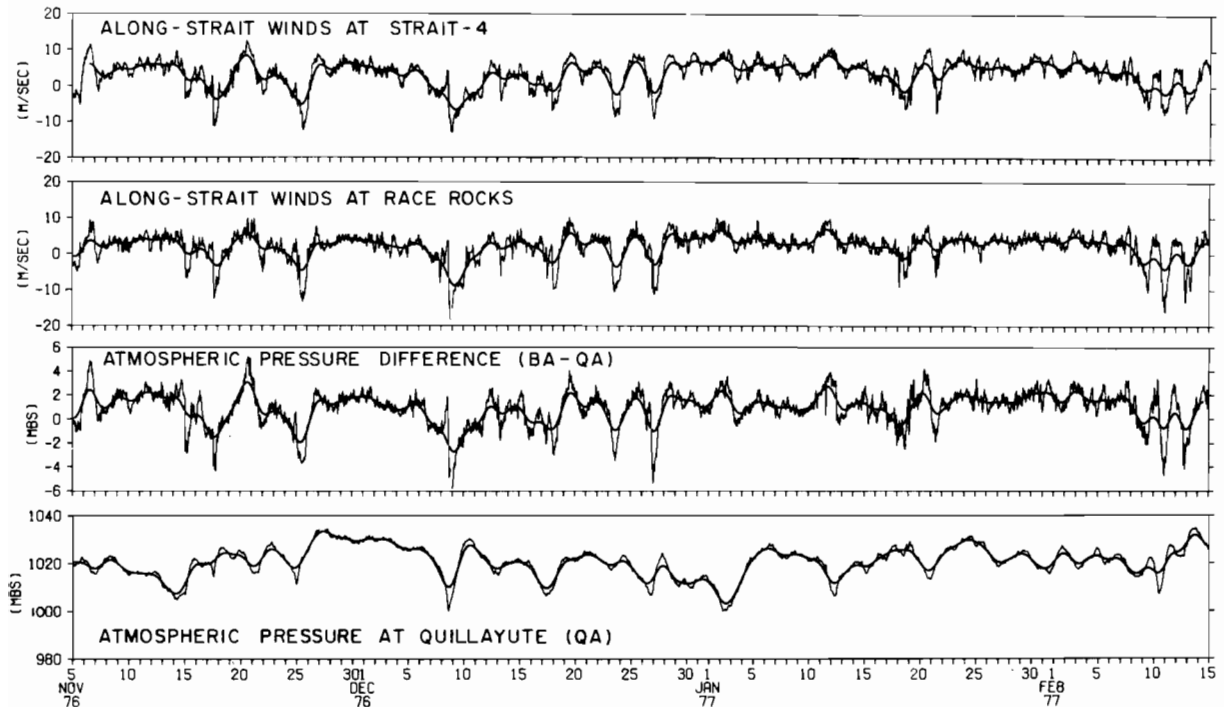


Figure 15. Along-channel winds related to the atmospheric pressure difference between Bellingham (BA) and Quillayute (QA) showing hourly and low-pass filtered values. From Holbrook and Halpern (1978).

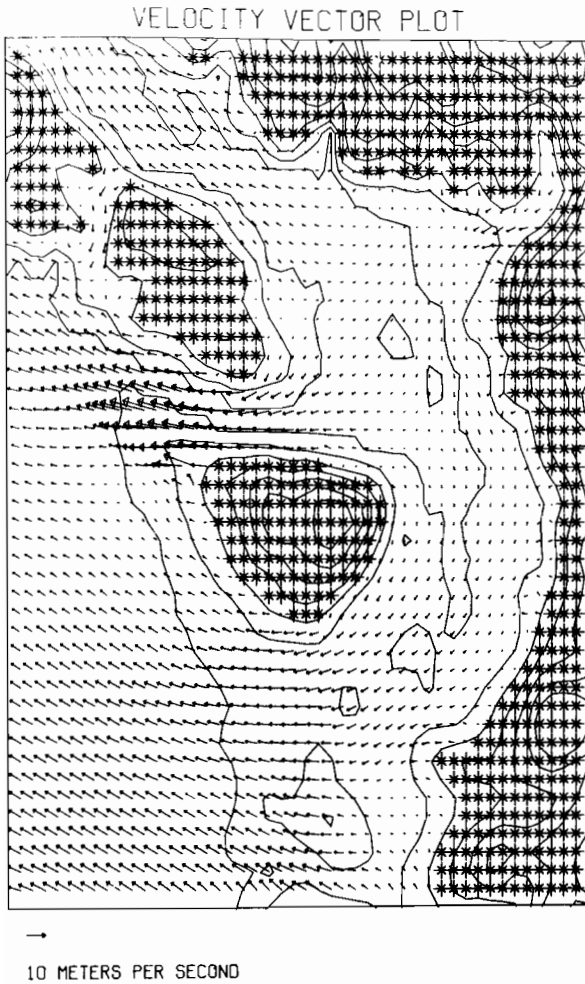


Figure 16. Sample model winds showing easterly winds in the Strait of Juan de Fuca. From Overland et al. (1978).

create the local patterns. The intent of the model was first to specify the large-scale pressure field, stability of the air, local land elevations, and the distribution of land and water, and then to use the equations of momentum to estimate the local wind field. A complete description of the model with initial validation experiments is given in Overland et al. (1978). The model domain extended south to include all of the Olympic Mountains, because it was determined that the winds in the Strait of Juan de Fuca were sensitive to the volume of air channeled through Puget Sound.

Figure 16 shows the result of running the model for the case of east winds in the outer part of the Strait (Fig. 10). High pressure was to the east of the region. Major features were light northerly winds in Puget Sound and the strong winds in the western end of the Strait of Juan de Fuca. Stability restricts the flow to regions below the mountain-tops where the air is accelerated along the east-west pressure gradient out through the Strait of Juan de Fuca. The divergence of the air flow after reaching the ocean created a local low pressure

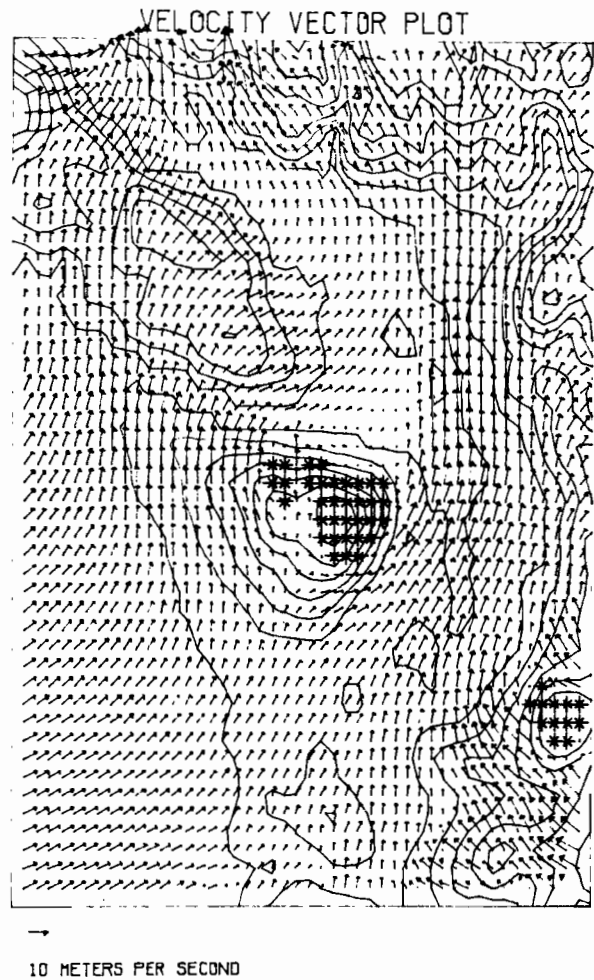


Figure 17. Sample model winds showing southwesterly winds along the coast. From Overland et al. (1978).

offshore which further accelerated the flow in the Strait to speeds much greater than would be estimated for simple geostrophic flow with the same pressure gradient. The model indicated a general flow of air out of the Puget Sound basin at the surface with replacement of the air by subsidence from above.

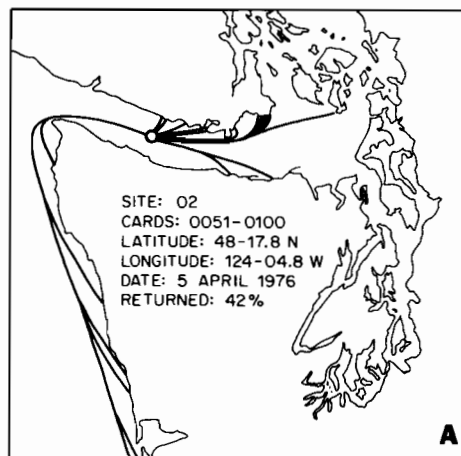
Figure 17 shows a case for southwesterly flow typical of the synoptic situation before the passage of a cold front (Fig. 11). The local wind vectors show the channeling by the Cascade and Olympic Mountains. Winds over Puget Sound were stronger and more southerly than offshore. A region of light winds was evident in the lee of the Olympic Mountains, which the model interpreted as a locally induced low-pressure center. Similar numerical experiments indicated that the position of the eddy and the magnitude of the pressure gradient that developed along the axis of the Strait of Juan de Fuca were very sensitive to the volume of air channeled through Puget Sound, which depended in turn on the orientation of the offshore flow.

3. OCEANOGRAPHY

3.1 Surface Drifter Observations

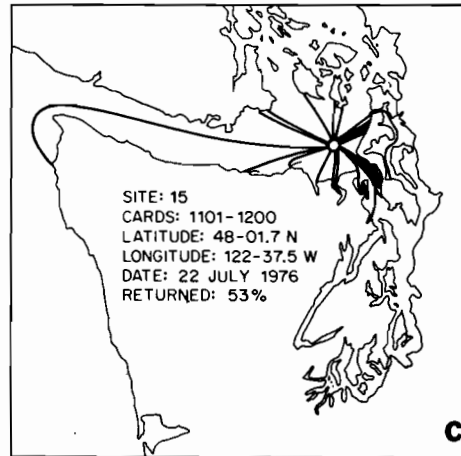
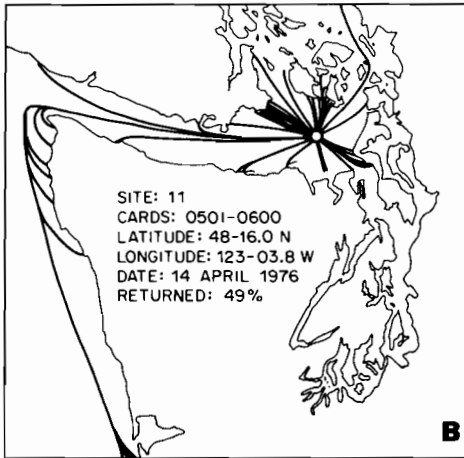
A program of surface drift cards, or drifters, was initiated to determine potential flow trajectories in the Strait of Juan de Fuca and Puget Sound systems. During six cruises in 1976-77, 5000 drift cards (flat plastic cards about 6 by 12 cm) were released throughout the Strait and parts of Puget Sound at 55 sites when conductivity-temperature-depth observations were being made or when current-meter stations were deployed or recovered. All releases were south of the passages between the San Juan Islands. Of the total released 29% had been recovered as of November 1977. Many of the cards were covered with oil and tar at time of recovery. Total recoveries from the Sound and Strait have been 40% and 20%, respectively. Cards released in the Strait had a greater chance of reaching the ocean and hence were lost to the study as indicated by the generally lower percentage recovered. Seasonal dependence for recoveries was less clear. However, recovery distributions appeared consistent with seasonal wind patterns.

There was an overall tendency for cards released in the Puget Sound-Strait of Juan de Fuca system to migrate seaward. This is because near-surface transport resulting from the estuarine circulation within the system generally moves seaward. For all cards released, approximately 24% of the recoveries were from locations seaward of the release site; 7% were from areas landward of the release site; and the balance were from locations in the general vicinity of the release site. A mean seaward drift of 6 km/day was calculated and the cards appeared to be waterborne for days to weeks. The majority of the drifters from the interior of the Puget Sound-Strait of Juan de Fuca system were returned in 2-4 days by people who found them and responded to the message on them, and those drifters exiting the system were returned within 3-4 weeks. More details of the program and computational techniques are described by Pashinski and Charnell (1978).



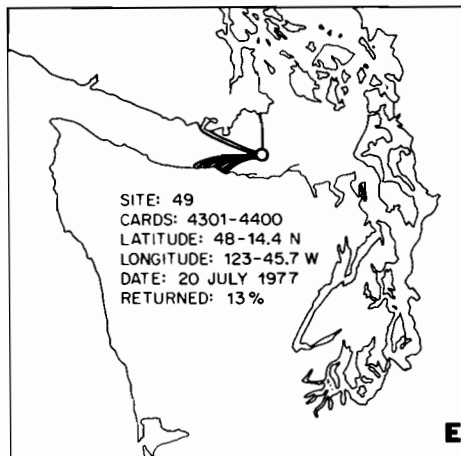
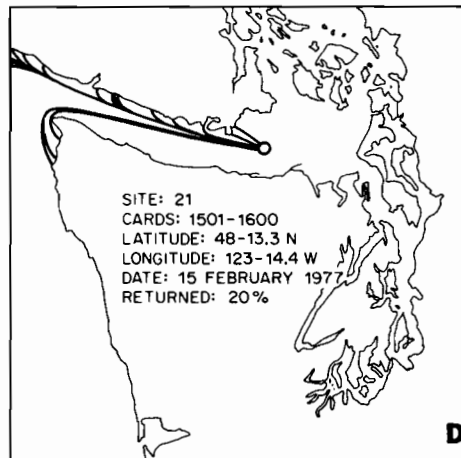
During the summers of 1976 and 1977 releases were distributed along the entire Strait of Juan de Fuca. The general drift was similar in both years. There was a seaward migration of most cards released near the mouth of the Strait into the Pacific. Cards exiting the Strait immediately grounded on the north coast of Washington or were lost to the study. Of those released in the eastern Strait, few apparently reached the ocean. Recovery was high, and most cards were found within a few tens of kilometers of the release point. Cards were found on Whidbey Island, the San Juan Islands, and along the south coast of the Strait (Fig. 18-C). Both summers showed this same pattern. Cards released within Puget Sound flowed out Admiralty Inlet into the eastern Strait and then were dispersed similarly around the eastern Strait basin. Releases closer to the southern shore of the entire Strait moved seaward and tended to ground on the southern shore (Fig. 18-E).

The releases which grounded on the U.S. shore in July 1977 were concurrent with a tracked drifter study in the western Strait (Ebbesmeyer et al., 1977). Their tracked drifters experienced an across-channel flow to the south under the influence of a diurnal fluctuating west wind during each of three days. Releases were made between Slip Point and Pillar Point only on the southern half of the Strait and were tracked only during daylight hours. During ebb flow the tracked drifters moved parallel to the shore, and during flood they moved toward the shore. No sightings or recoveries were reported on or near Canadian shores. There was a dominance of occurrences of beachings in the lee of Slip Point and in the lee of Pillar Point, which indicated that these were possible entrapment areas. Drift card responses described by Pashinski and Charnell from this same period were predominantly under the same wind influence. During winter 1977 cards were released primarily in the western Strait basin. This release



represented the highest number of cards deployed at any time and the lowest return rate (13%). The majority grounded along the west coast of Vancouver Island, but a few moved out of the Strait, then south along the northern Washington coast (Fig. 18-D).

Spring releases were made both years throughout the Strait. There was a high incidence of recovery along the Washington-Oregon coast from both eastern and western Strait releases, but very few cards were recovered along Vancouver Island outside of the Strait (Fig. 18-A). Recoveries for those released in the eastern Strait exhibited a pattern identical to a summer release shown earlier (Figs. 18-C and 18-B), except for the added large incidence of coastal recoveries in spring. Current observations farther west, described in Section 3.3, showed weak currents at this time. Cards released at one eastern station in the Strait were blown due east by high west winds, and 93 of 100 cards were found along a short stretch of beach on Whidbey Island. Cards released in Admiralty Inlet moved out into the eastern Strait and spread out as described above for summer releases. More work is needed to determine the dispersion paths between release and recovery sites within the eastern basin of the Strait (e.g., Fig. 18-B).



3.2 Suspended Sediments

Baker et al. (1978) studied the surface trajectories of sediment plumes originating from the Fraser and Skagit Rivers. These plumes are natural tracers of the flow patterns of the fresher water that is discharged into the Strait of Georgia-Strait of Juan de Fuca system. Where the plumes meet saline water, there is an abrupt change that is marked by a sharp edge between the river water and the darker sea water. The water masses separated by this frontal surface also have

Figure 18. Surface drifter recovery locations for various release sites and times. From Pashinski and Charnell (1978).

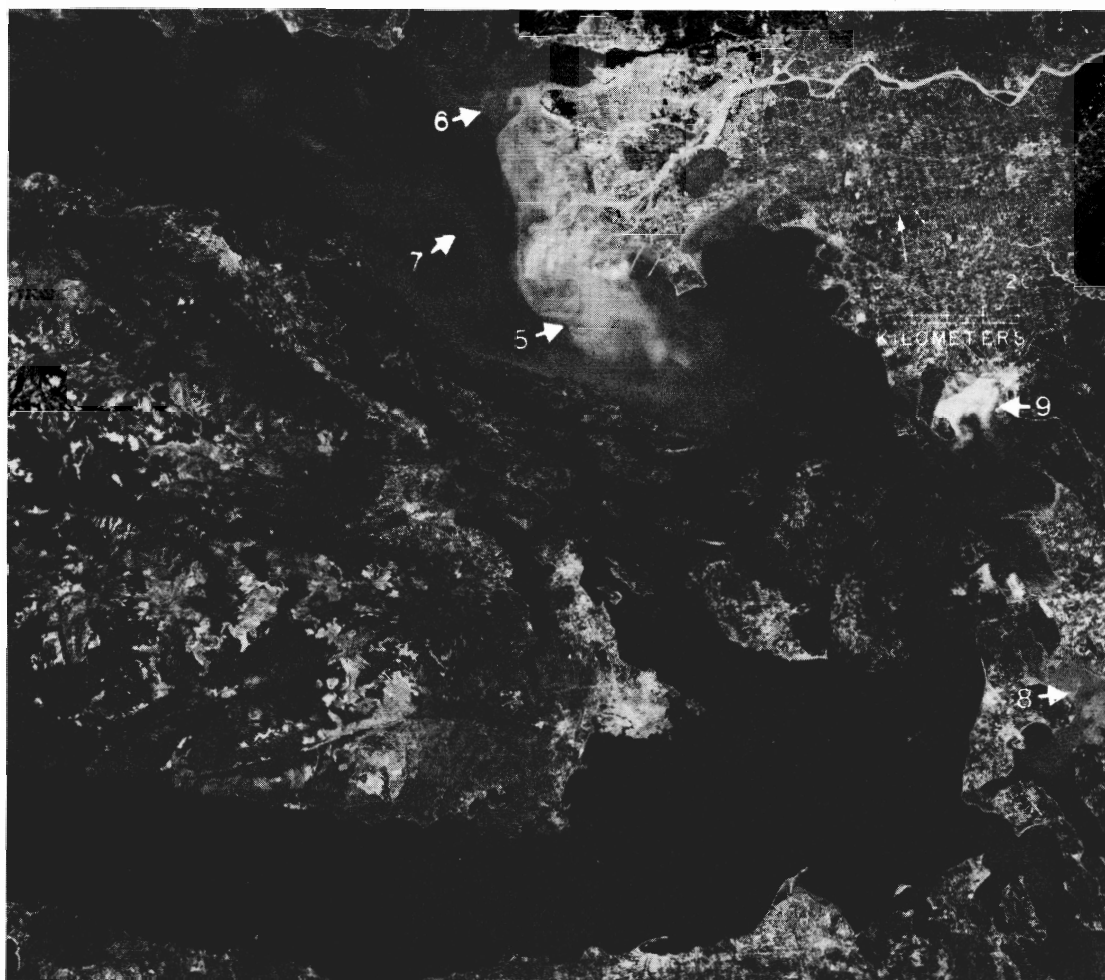


Figure 19. MSS Band 5 of LANDSAT image 1727-18290, showing a southeasterly dispersal (5) of suspended sediments from the Fraser River into the Strait of Georgia on July 20, 1974. Time of image acquisition was 1029 PST, between major ebb current and slack water. The dispersal pattern suggests movement of Fraser River sediments along Saturna, Mayne, and Galiano Islands and into Trincomali Channel from Porlier Pass. Suspended sediments from the North

Arm of the Fraser appear to flow to the northwest and to the northeast into Burrard Inlet (6). A cyclonic eddy (7) can be observed north of Galiano Island. Sediment discharge from the Skagit River into Skagit Bay (8), and from the Nooksack River into Bellingham Bay (9) is clearly visible. Several tidal fronts are also observed in the Strait of Juan de Fuca. From Baker et al. (1978).

differing velocities, and where the surface velocities are convergent, there must be downward movement at the front. For example, oil spilled in Delaware Bay, between Delaware and New Jersey, moved toward fronts and spread out along them (Klemas and Polis, 1976). The combination of downward motion with the presence of suspended particles to which oil might attach suggests that a convergent front is the place where oil would be most likely to sink below the surface, greatly increasing the hazard to marine life.

Suspended matter concentrations and compositions determined by using water samples collected in situ with 10-liter Scott-Richards bottles have been used to describe the seasonal variations of particulate distributions. However, due to the physical limitations of operating from a single

vessel, the data were not entirely synoptic and were integrated over several tidal cycles. In order to obtain synoptic information about plume trajectories, a set of LANDSAT satellite images from 1972-1977 has been examined. The sediment plumes in the LANDSAT images appeared lighter in tone than the less turbid water. However, the LANDSAT imagery only provided information about the upper few meters of the water column. Fortunately, previous studies have shown that the brackish water is generally confined to the upper 5-10 m (Waldichuck, 1957). Therefore, the LANDSAT imagery could be used to study the migration patterns of the brackish water, providing the sediment loadings were sufficiently higher than the surrounding water. The amount of useful information about seasonal variations of sus-

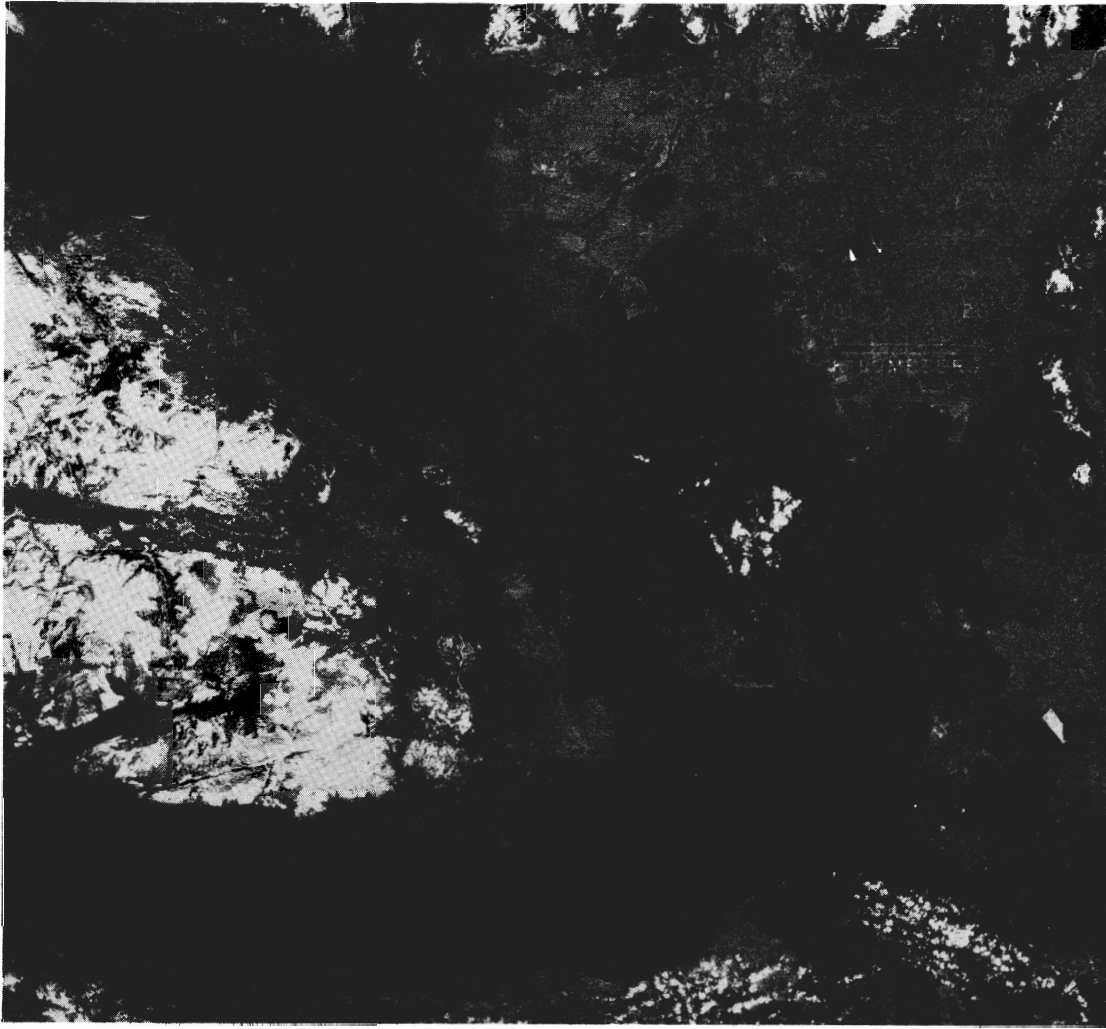


Figure 20. MSS Band 4 of LANDSAT image 2417-18220 on March 14, 1976. Time of image acquisition was 1022 PST, between minor ebb current and slack water. The image shows limited dispersal of suspended sediments into the nearshore waters south and southeast of the mouths of the Main, Middle, and North Arms of the Fraser. From Baker et al. (1978).

pendent sediment distributions and dispersal patterns that can be obtained from LANDSAT imagery is somewhat limited because most cloud-free days occurred during the summer; as a result, the majority of available images were from that season. Computer enhancement of images is being developed for future work. More details of the overall program and of the techniques of using the LANDSAT images are in Baker et al. (1978).

During summer the southward flows of the Fraser River's Main Arm (south) and Middle Arm were so strong that the resultant plume maintained its identity for a considerable distance and, in some cases, traversed the entire length of the Strait of Georgia (Fig. 19). Depending upon local changes in tidal currents, the plumes extended either southeast or southwest from the mouths of

the river. Tidal mixing was rapid and numerous eddies could be seen. Also, the Skagit River plume flowed into Skagit Bay and Saratoga Passage during the summer months. Some plume material passed through Deception Pass into Rosario Strait during ebb tide.

The winter plumes from the Fraser and Skagit Rivers, as shown by the three images LANDSAT was able to make in wintertime between January 1973 and March 1976, were much less distinct and less well-defined than the summer plumes (Fig. 20). For instance, the Fraser River plumes were only visible in the near-shore regions just a few kilometers seaward of the river mouth, where the primary flow pattern was to the southeast. During this period, the discharge of both water



Figure 21. MSS Band 5 of LANDSAT image 5465-17484, showing a southeasterly dispersal (10) of suspended sediments from the Fraser River into the Strait of Georgia on July 27, 1976. Time of image acquisition was 1048 PST, between major ebb current and slack water. The dispersal pattern suggests movement of Fraser River sediments into Haro Strait from the passages on either side of Mayne and

Saturna Islands (11), and into Rosario Strait from the southeastern Strait of Georgia (12). Suspended sediment discharging into the Strait from the North Arm of the Fraser appears to flow northward past Point Grey, where it bifurcates, a portion flowing to the northwest, and the remainder flowing to the northeast into Burrard Inlet (13). From Baker et al. (1978).

and suspended sediments was at a minimum, resulting in dilution of suspended sediments to background levels. These conclusions were substantiated by the results of the seasonal surveys of suspended matter concentrations in the vicinity of the Fraser River. The winter decreases of fresh water and sediments were less for the Skagit River, and seasonal variations in the Skagit River plume were not nearly so pronounced. This material mixed rapidly with the offshore water, and the winter plumes did not maintain their identity beyond Deception Pass.

The LANDSAT satellites have produced eight or nine high-quality images which can be used for describing tidal effects on the dispersion of the Fraser River plume. During ebb tide, distinct sediment plumes originating from Main Arm and

Middle Arm initially flowed seaward in a southwesterly direction, and then were diverted in a southeasterly direction by the ebb flow in the Strait of Georgia (Fig. 19). The sediment plumes migrated with the flow across the Strait and under the influence of tidal and Coriolis forces flowed through various passages and eventually into Haro Strait. Occasionally the tidal flow was so strong that the sediment plume could be traced as far east as the passage between Orcas and Lummi Islands (shown in Fig. 39) and ultimately into Rosario Strait (Fig. 21). However, prevailing northwesterly winds at about 14 m/sec may have augmented this effect. Numerous cyclonic and anticyclonic eddies were associated with the plumes. For instance, a cyclonic eddy observed in the region north of Galiano Island (next island

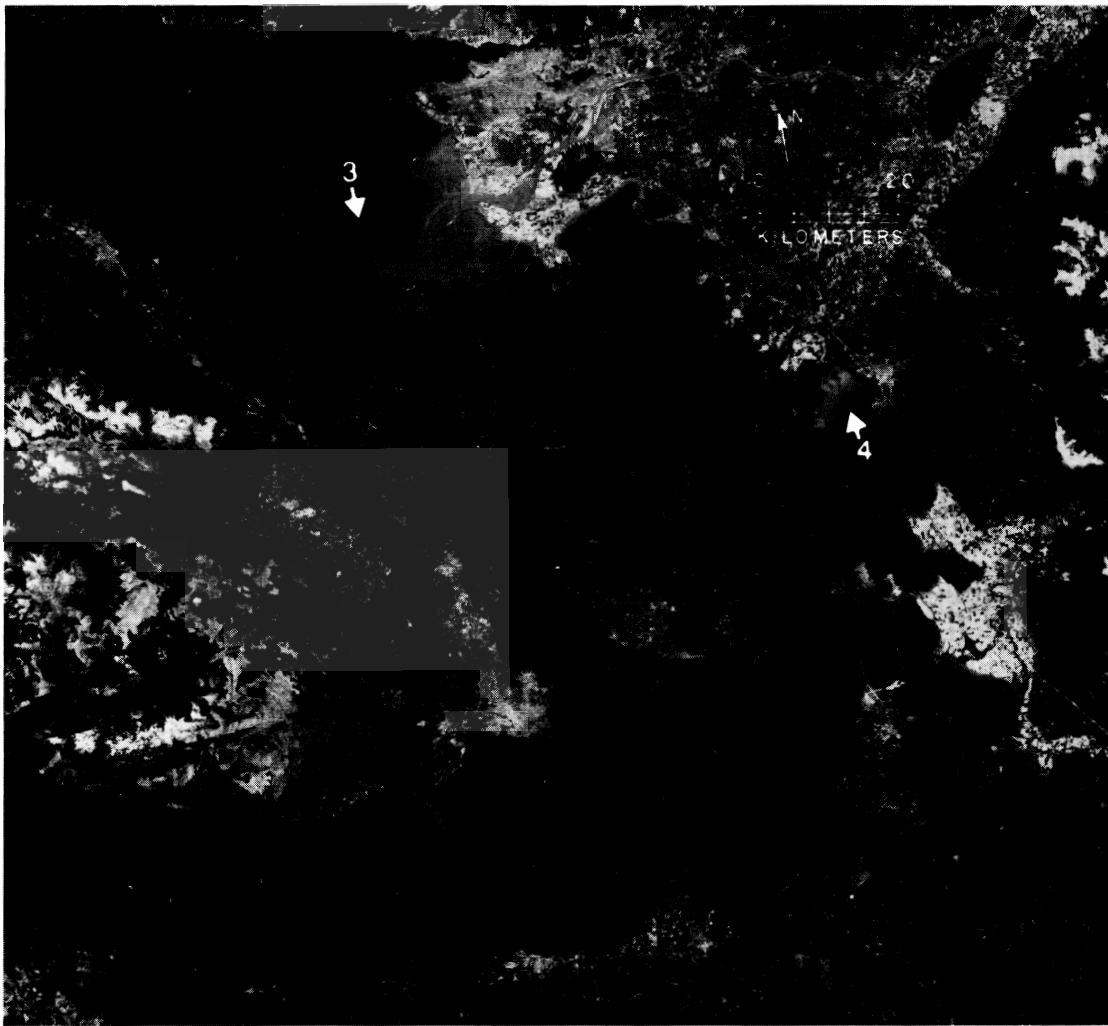


Figure 22. MSS Band 5 of LANDSAT image 2129-18254, showing a southwesterly dispersal of suspended sediments from the Fraser River into the Strait of Georgia on May 31, 1975. Time of image acquisition was 1025 PST, just after flood current. An anticyclonic gyre can be observed due west of Point Roberts (3). Sediment discharge from the Nooksack River can be seen in Bellingham Bay (4). Image is free of cloud cover. From Baker et al. (1978).

northwest of Mayne Island, Fig. 39) appeared to be detached from the major plume emanating from the Fraser River. It probably represented a relic plume that moved into the region during a previous tide. The sediment plumes emanating from the North Arm of the Fraser during ebb tide in Figs. 19 and 21 flowed to the north and west, and a portion of the plumes flowed to the northeast into Burrard Inlet (immediately north of the mouth of the Fraser's North Arm).

The sediment plumes originating from Main Arm and Middle Arm during flood tide initially flowed seaward in a southwesterly direction (Fig. 22). However, instead of being diverted to the southeast, as is the case during ebb tide, they were driven by the flood current across the Strait and to the northwest along the northern coast of

Galiano Island. There is evidence for small cyclonic and anticyclonic eddies in the plumes associated with the flooding tide. The sediment-laden plume from North Arm flowed to the north and into Burrard Inlet during flood tide.

The LANDSAT images showed fronts separating light-colored, particle-laden river water from clearer, darker sea water. There also were light streaks that must show the concentration of particles or of foam and debris at the convergence of water masses having different directions of motion. Fronts of this type frequently appeared in the Strait of Juan de Fuca at the entrance to Haro Strait, forming parallel arcs east of Victoria and south of San Juan Island. Fronts separating two colors were seen in the western Strait of Juan de Fuca, stretching from Vancouver Island across to

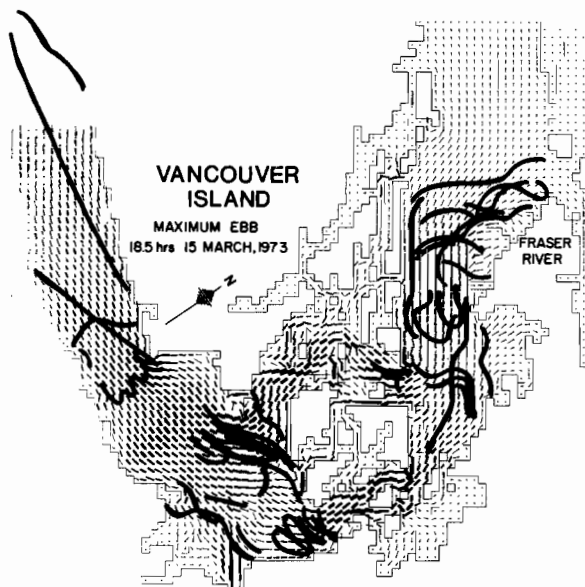


Figure 23. Composite sketch of fronts seen in 24 LANDSAT images during ebb tides. Adapted from Crean (1978) for this report by Sawyer.

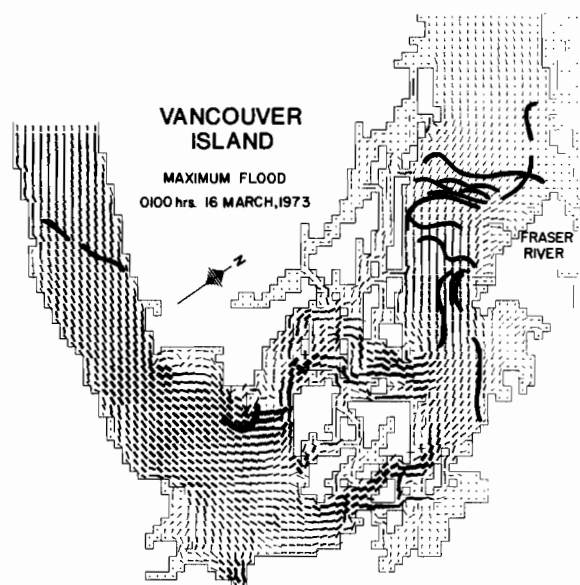


Figure 24. Composite sketch of fronts seen in 9 LANDSAT images during flood tides. Adapted from Crean (1978) for this report by Sawyer.

the Olympic Peninsula in a southwesterly direction. On one occasion a pair of parallel curved fronts crossed the Strait about 50 km apart. These had a parabolic form similar to flow in a pipe or channel, with faster flow in the center and slower flow toward the boundaries.

The sharpest and most obvious fronts seen on LANDSAT images of the Strait of Georgia and the Strait of Juan de Fuca have been sketched on charts of tidal currents from a barotropic model of this system (Figs. 23 and 24; P. B. Crean, Environment Canada, personal communication; Thomson, 1975). Fronts are found inclined to the current at all angles, but tend to parallel the ebb current which is stronger and has stronger lateral shear. Plumes that were visible during ebb tide at Admiralty Inlet, at Deception Pass, and at the mouths of some of the smaller rivers disappeared during flood tides. Fronts parallel to strong currents appeared at the boundary of the Fraser plume (especially during flood tide), at the entrances to Haro and Rosario Straits, and in the western Strait of Juan de Fuca. The parallel fronts suggested strong cross-channel shear of the along-channel current, and the cross-channel fronts suggested a gentler sloshing back and forth of the sediment-laden water. Separation of data according to wind direction showed little dependence of frontal structure on wind.

The separation of cross-channel fronts was up to 20 or 30 km. The tidal excursions estimated were 31 km for the ebb tide and 11 km for the

flood, and they reasonably explained the spacing of fronts that crossed the Strait of Juan de Fuca and San Juan Island passages.

3.3 Western Strait Currents and Water Properties

The western Strait of Juan de Fuca is the relatively straight reach extending about 90 km eastward from the Pacific Ocean to just west of Port Angeles. During two winters (February–May 1976 and November 1976–February 1977) and one summer (June–September 1977), an extensive series of near-surface (upper 25 m) current and temperature measurements and over-the-water wind measurements was made from surface moorings at three sites (A, B, and C) positioned longitudinally in the western Strait (Fig. 25). Only Site C was occupied during the first winter. Each surface mooring contained from one to five vector-averaging current meters (VACM's) suspended within the upper 25 m of the water column and one tower-mounted vector-averaging wind recorder (VAWR). The shallowest VACM was generally placed at a depth of 4 m. More details are discussed in Holbrook and Halpern (1978).

In addition, subsurface moorings were deployed for about 40 days each during February–April 1976, October–December 1976, and June–August 1977, using Aanderaa current meters with temperature and conductivity sensors (Fig. 25).

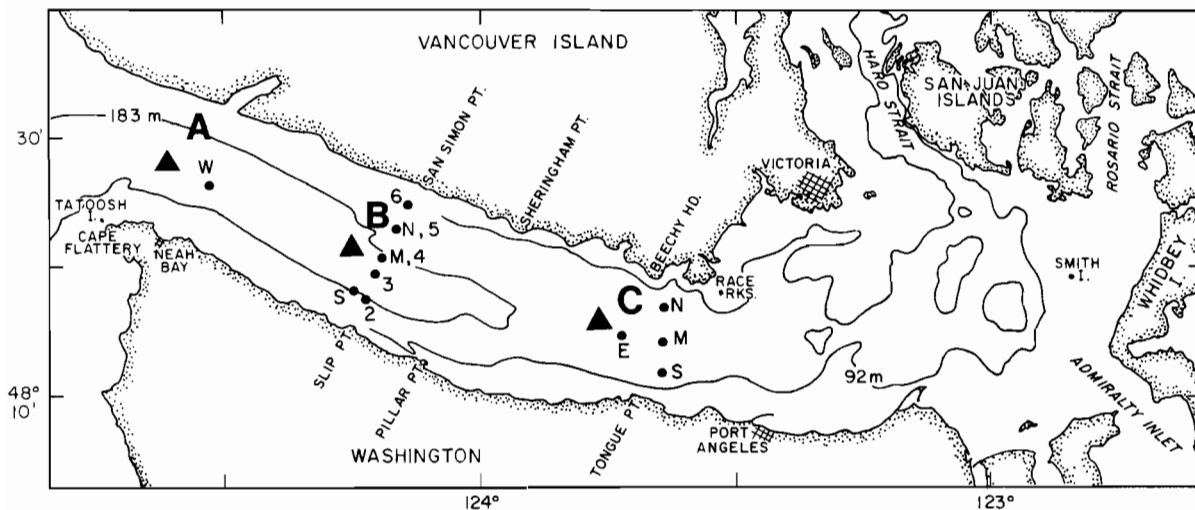


Figure 25. The Strait of Juan de Fuca, showing Sites A, B, and C and associated subsurface moorings.

Various numbers of meters were used on each mooring. The shallowest placement of instruments was at about 15 m depth and the deepest about 5 m off the bottom. During the first winter three subsurface moorings (N, M, and S), each with four current meters, were positioned across the Strait at Site C between Tongue Point and Beechy Head. During the second winter five subsurface moorings (2, 3, 4, 5, and 6) were moored across the Strait at Site B north of Slip Point. A sixth mooring (W) was located in mid-channel near the mouth of the Strait at Site A off Neah Bay. Finally, during the summer three subsurface moorings (N, M, and S) were deployed across the Strait at Site B off Slip Point, and two more (W and E) were deployed in mid-channel off Neah Bay at Site A and off Tongue Point at Site C. The middle mooring was lost. More details of the subsurface moorings are discussed in Cannon and Laird (1978).

Numerous separate CTD (conductivity, temperature, and depth) surveys of the region were made to extend the spatial coverage and to calibrate the Aanderaa sensors. In addition, various auxiliary data were collected to support the primary measurements. Typically, river runoff was low during the winter experiments and high during the summer experiment.

Examples of the along-channel and across-channel components of hourly averaged 10-m currents at Site C showed along-channel velocities in

excess of 150 cm/sec during both winter and summer and across-channel components up to about 60 cm/sec (Fig. 26). The records were dominated by a mixed tidal signal with semidiurnal and diurnal constituents. These have been removed from the records by low-pass filtering for the remainder of this study. The resultant low-frequency along-channel velocity showed greater variability during winter with amplitudes comparable to the tidal currents and at times actually reversed to flow up-channel. During summer the low-frequency along-channel component was relatively steady and was not observed to reverse direction. The low-frequency across-channel components did not change greatly with season, except at Site A where there was a substantial across-channel seasonal variation (factor of two). Although small compared to the along-channel currents, these low-frequency across-channel currents must be considered an important process in the movement of foreign substances shoreward. Some details are given in the reports by Holbrook and Halpern (1978) and by Cannon and Laird (1978).

Mean flow. The near-surface currents, when vector-averaged over the record length, were all directed seaward (Fig. 27). This is in qualitative agreement with the classical picture of outflowing, near-surface estuarine circulation. The mean along-channel component of currents at 4 m decreased seaward from Sites C to A, with greater

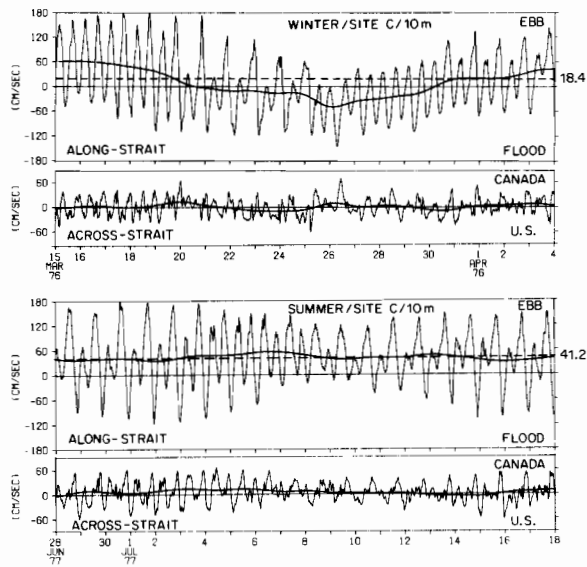


Figure 26. Along- and across-channel currents at 10 m at Site C during winter and summer, showing hourly averages, low-pass filtered and total-record average values. From Holbrook and Halpern (1978).

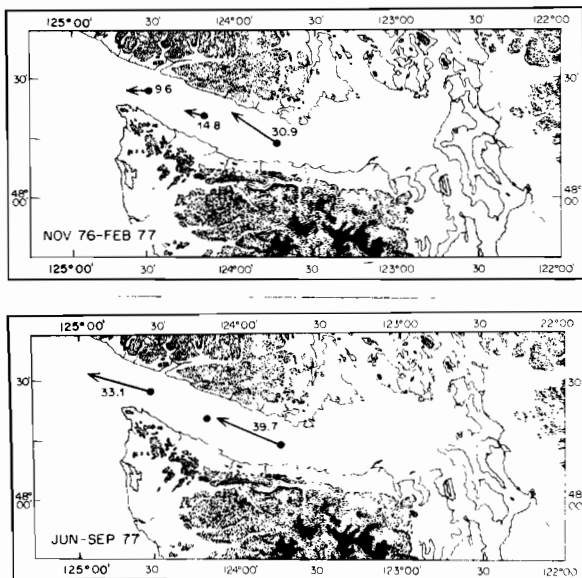


Figure 27. Vector mean currents (cm/sec) at 4 m during winter and summer. From Holbrook and Halpern (1978).

longitudinal variability during winter. During summer the magnitudes were greater.

Flow through the sections averaged over the total records showed the estuarine characteristics of outflow in the surface waters and inflow in the deeper waters (Fig. 28). At Site C the largest average seaward currents occurred nearer the surface and in mid-channel, being somewhat symmetrical about the middle station. The largest averaged landward currents favored the northern side and the deeper part of the channel. The level of no-net-motion was relatively flat, possibly sloping up

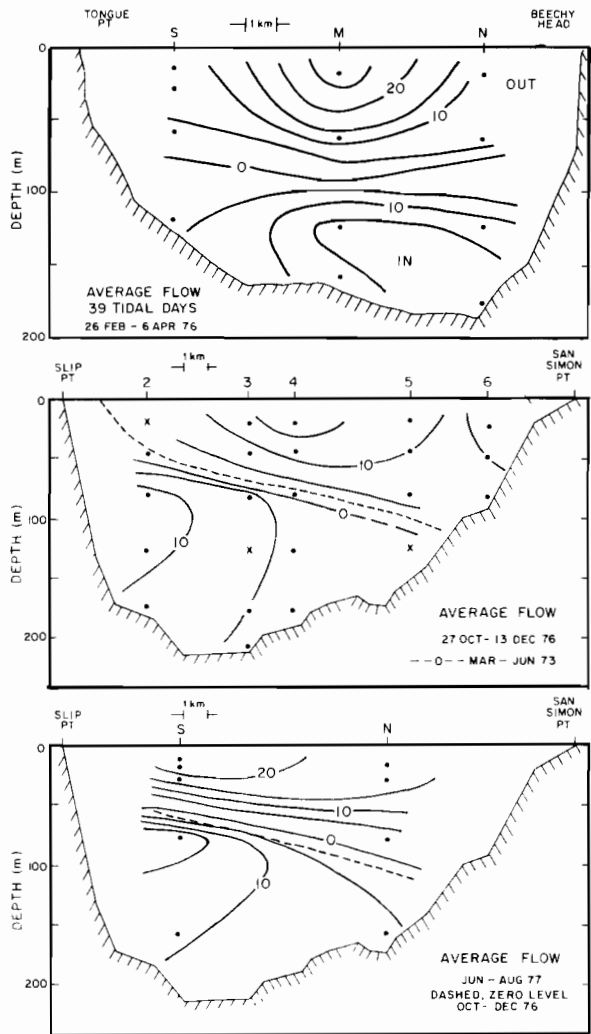


Figure 28. Along-channel total-record average currents (cm/sec) through sections at Tongue Point (top) and Slip Point (middle and bottom). From Cannon and Laird (1978).

slightly from the middle to both sides. If real, there were possible geostrophic effects associated with the down-sloping level of no motion between the south and middle moorings. The upslope from the middle to the north mooring possibly indicated effects of curvature in opposition to and greater than the geostrophic effect. This section was located at a position where the channel width undergoes a relatively abrupt change, all of which occurs on the northern side of the Strait.

Flow through the section at Site B was very similar in winter and summer and also was similar to a section in winter-spring 1973 at Pillar Point, about 10 km to the east (Huggett et al., 1976). The level of no-net-motion was at about 50 m on the south side and about 100 m on the north, similar to that shown by Herlinveaux (1954) at Pillar Point. Landward flow occurred in the deeper water with the strongest currents on the southern side, and seaward flow occurred above the level of

no-net-motion with the strongest currents also appearing to occur on the southern side during summer but in mid-channel during winter. This may be the result of having only two moorings during summer. The recent Canadian observations in spring showed some differences, however, in that the level of no-net-motion was observed to rise to the surface before reaching the southern shore. It is possible that the no-motion level reached the surface south of our southern mooring. If this were so, then one might expect to find net landward flow (parallel to the coast locally) near the southern shore of this part of the Strait during much of the winter and spring. The average salinity across this section in summer showed isohalines sloping down to the north except near the bottom. However, there were large salinity variations (described below) during winter.

Variations. The total variance of the current, which is equal to twice the kinetic energy of the fluctuations, changed both seasonally and spatially. At Site A, the winter variance was 76% greater than the summer variance. Most of this difference was due to seasonal changes in the amount of low-frequency and diurnal energy. At Site C, there was less seasonal change, with winter variance exceeding summer variance by only 11% at the 4-m depth. Winter-to-winter differences in total variance were small. Variance decreased with depth during both winter and summer.

Tidal energy dominated the along-channel component of variance, accounting for about 65%-90% of it. Tidal variance expressed as percentage of total variance increased with depth near the surface during winter and summer, and root mean square (rms) amplitudes of the semi-diurnal tidal currents decreased seaward from 47 cm/sec at Site C to 31 cm/sec at Site A with no significant seasonal variation. During summer, however, large longitudinal variations were observed in the diurnal tidal currents, with rms amplitudes of 18 cm/sec at Site A increasing to 29 cm/sec at Site C. Apparently, the diurnal tidal current oscillations were not stationary and had an important seasonal baroclinic component that may be related to the physical oceanography of the Washington coast. Major fluctuations in the diurnal energy band have been found during the course of summer upwelling off the Oregon coast (Hayes and Halpern, 1976).

Observations from the subsurface moorings showed that the standard deviation about the total-record average in the east-west direction was greater across the Site C section than across the Site B section by about 10 cm/sec. The cross-section area is smaller at Site C than it is at Sites A and B, which also implies larger tidal currents

across the Site C section. Values were maximum in mid-channel and decreased toward the sides. There also was a decrease close to the bottom due to friction. The total variance in the records decreased with depth at each mooring except during summer when there was initially a slight increase with depth followed by a decrease. Of particular interest was that the near-surface variance at the subsurface mooring at Site C, as measured by the Aanderaa meter, was the same as measured by a VACM suspended from the nearby surface mooring.

Low-frequency variance represented a significant percentage of the total along-channel variance during winter. At Site A, near the mouth of the Strait, 27% of the variance at 4 m occurred in this range. At Site C, the variance at 10 m was 140% greater during the first winter experiment than during the second winter. Some of this difference may be attributed to the greater meteorological forcing during the first winter as described in Section 2.3. Low-frequency variance during summer was much lower than in winter and was amazingly uniform. More details are given in Holbrook and Halpern and in Cannon and Laird.

Although the along-channel component of variance accounted for 84%-92% of the total variance, important across-channel fluctuations also occurred. At Sites A and B during winter, more than twice as much variance occurred in the low-frequency band as in the combined tidal bands. However, at Site C the low-frequency variance was less than half the tidal variance. In the cross-channel direction the low-frequency rms currents were much larger than the long-term averaged (total record) currents. For example, during winter at Site B at 4 m depth, the subtidal rms amplitude was 13 cm/sec while the long-term mean was 1.6 cm/sec. Low-frequency fluctuations, with time scales greater than 5 days, dominated cross-channel advective processes. At a speed of 13 cm/sec, a distance equivalent to the width of the western Strait may be traveled in less than two days. It is known from the drifter studies described in Section 3.1 that a significant percentage of drifters ended up on the beaches after several days.

Winter wind forcing. During winter in the western Strait, a major oceanographic feature not previously described is the significant amount of current variance occurring at frequencies lower than the tidal frequencies. This low-frequency variance decreased with distance landward from the Pacific and varied greatly from winter to winter. Descriptions of the two winters show the general characteristics.

During the first winter the variations of flow through the Site C section were large, and a pro-

gressive vector diagram (PVD) of the 16-m records showed two periods of inflow and two periods of outflow at the south mooring (Fig. 29). Inflow occurred from mooring deployment (February 26, 1976) to March 2 and from March 21 to 28.

The second inflow started later and lasted longer at the middle and north moorings at this level. Flow reversed second at the north mooring and last at the middle. Also, the PVD at the middle mooring was closely parallel to the axis of the Strait, but at the side moorings there were across-channel components. These reversals from the normal outflow near the surface to inflow were similar to those observed by Cannon et al. (1972) at the mouth of the Strait. Here they occurred about 90 km from the mouth. The implied excursion during the second inflow at the south mooring was about 150 km, a distance from the mooring greater than that from the mouth of the Strait to the west, or to land toward the east. The excursions at the middle and north moorings were about 100 km. These reversals appeared directly related to storm winds along the coast which raised the sea level sufficiently to reverse the pressure gradient contribution of the sea surface slope and which are shown in more detail below for the second winter. There were two major periods of persistent southerly winds measured at the mouth of the Strait on Tatoosh Island that corresponded with the two flow reversals (Fig. 13). Southerly winds on March 9–13 evidently were insufficient to cause reversal of the flow. During the strongest southerly coastal winds, westerly winds were observed in the Strait near the northern end of the section at Race Rocks. The north-south component of winds measured at Tatoosh Island accounted for approximately 61% of the low-frequency along-channel current variations at 10 m at the Site C surface mooring.

The spatial effects of an intrusion can be seen from the surface temperature and salinity distributions measured at the beginning of the observations. Relatively fresher and warmer water was observed along the south side (Fig. 30). Near-surface water with temperature exceeding 7°C and with salinities less than 30‰ occupied a large fraction of the Strait and penetrated almost to the mooring section. Flow was landward at the 15- and 29-m depths at the south mooring and was slightly seaward at 19 m at the middle and north moorings. The higher salinity water presumably has come from Haro Strait just east of Victoria. This was opposite to the case occurring during more normal estuarine flow, when the lowest salinities were observed in water coming from Haro Strait and highest surface salinities were on the south side of each section.

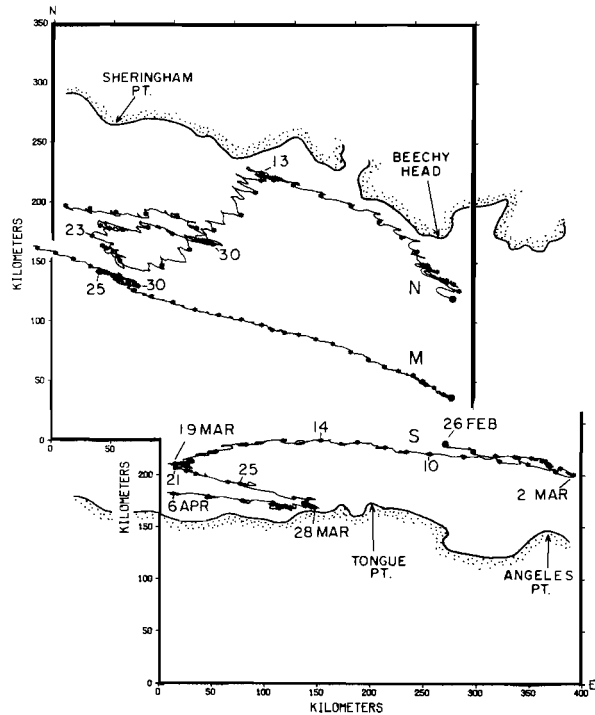


Figure 29. Progressive vector diagrams of 15-m flow across the Tongue Point section during winter. From Cannon and Laird (1978). All records start at the mooring locations on February 26, 1976. Scale for mooring M is double that shown. Coast is shown but the scale is only about 20 km from Beechy Head to Tongue Point. North is along the vertical axis.

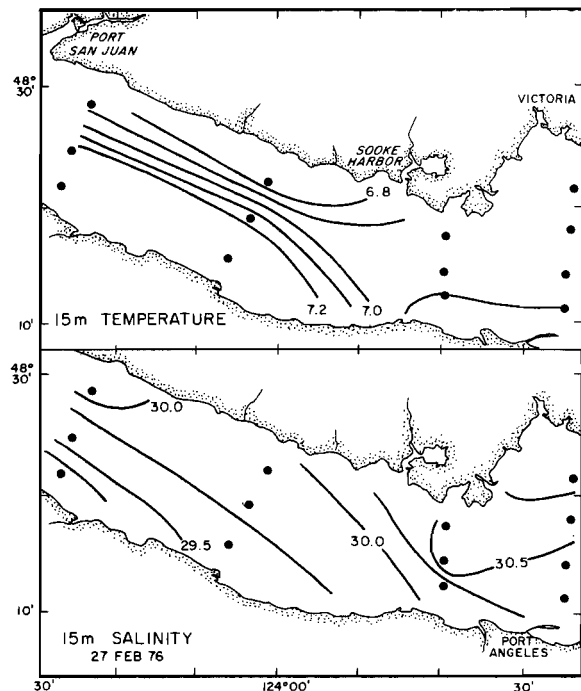


Figure 30. Near-surface temperature (°C) and salinity (‰) following deployment of Tongue Point moorings. From Cannon and Laird (1978).

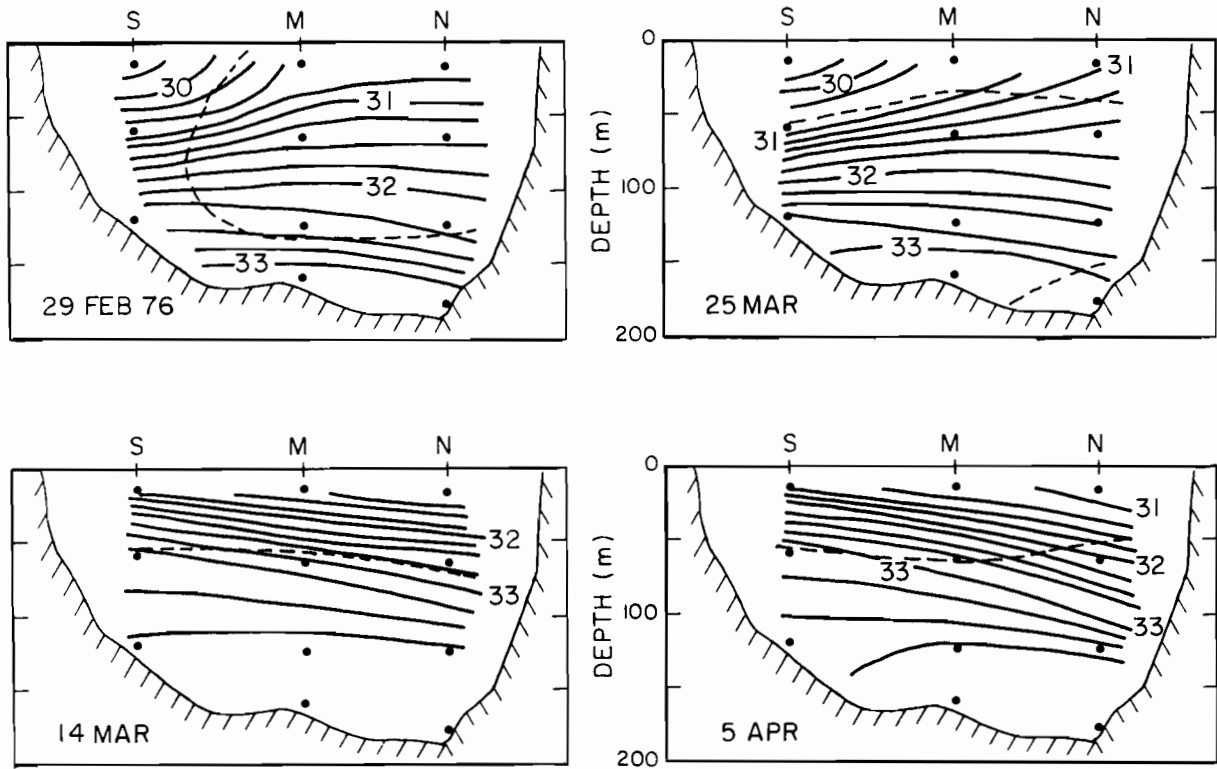


Figure 31. Daily average salinity across Tongue Point section. From Cannon and Laird (1978). Dashed line is daily average zero-motion level.

The salinity distributions across the section (measured by the Aanderaa meters) also had different characteristics, depending on whether there was an intrusion or the more normal estuarine flow (Fig. 31). During both intrusions (February 29 and March 25, 1976) the freshest water was less than $30^{\circ}/_{\infty}$ and occurred on the south side. The $32^{\circ}/_{\infty}$ isohaline was relatively flat at about 100 m. Above this level the isohalines tended to slope up toward the north. The $33^{\circ}/_{\infty}$ isohaline was near the bottom as was indicated on a longitudinal STD section. During more normal estuarine flow (March 14 and April 5), the freshest water was about $31^{\circ}/_{\infty}$ and occurred on the north side. The isohalines all sloped down toward the north. The $32^{\circ}/_{\infty}$ isohalines occurred at much shallower depths with the $33^{\circ}/_{\infty}$ isohaline about 50–70 m shallower. Hourly average salinity sections during flood tide at all meters resembled the daily averages very closely both during intrusions and during the more normal estuarine flow. However, at the end of ebb tide during part of the first intrusion, all water greater than $33^{\circ}/_{\infty}$ had moved seaward. Near-surface distributions remained very similar to the daily average.

During the second winter, low-frequency current fluctuations with amplitudes in excess of 50

cm/sec occurred in all near-surface records. Visual correlations between currents measured at 4, 10, and 15 m at Site A were remarkably high (Fig. 32). Visual correlation for currents at 4 m at Sites A, B, and C, however, were much less striking. Approximately 55% of the along-channel variance at Site C was linearly correlated with Site A, with C lagging A by 47 hours. The amplitudes of the correlated fluctuations at Site C were 57% of Site A. Five major reversals occurred at Site A with maximum landward (along-channel) currents of 25–55 cm/sec, lasting from 3–10 days, and accounting for 35% of the observational period (Fig. 33).

Longitudinal sections of temperature, salinity, and density made on November 5, 1976, just prior to mooring deployments, showed a lens of warm ($>11^{\circ}\text{C}$), low-salinity ($<31.75^{\circ}/_{\infty}$) water located just west of Site A. Near-surface water temperatures eastward were fairly uniform, with values generally less than 9°C . The temperature characteristics of this less-dense lens were used as a tracer during periods of near-surface net landward currents (Fig. 34). Vertical lines drawn at times of arrival of the warm water lens at Site A show that the arrival of the front occurred within a tidal cycle of the major low-frequency current reversals

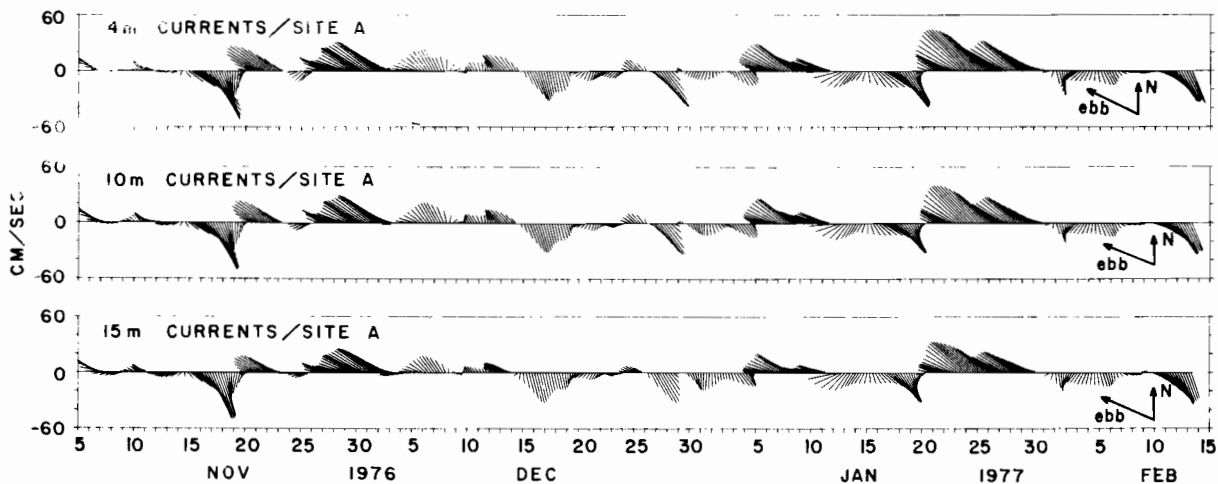


Figure 32. Vector plots at 6-h intervals of low-pass filtered currents at 4, 10, and 15 m at Site A. From Holbrook and Halpern (1978).

(seaward to landward). During all the major reversals, the warm lens arrived several days later at Site C. The minor reversals on December 8, 1976, and January 4 and February 1, 1977, were not strong enough to advect the lens front 65 km up-channel to Site C.

The main intrusion and flow reversals had their maximum extents across the Site B section on November 18 (Fig. 35). Landward flow occurred entirely across the surface, and seaward flow occurred throughout the deeper water except at the bottom on the south side. The near-surface average daily speed of 14 cm/s at the middle mooring

was about what was required to transit the distance between the moorings near Sites A and B in about three days. The freshest water and warmest temperatures indicated by the daily averages occurred near the surface on the south side with the isolines sloping up toward the north. The deeper isolines were relatively flat with $33^{0/00}$ at about 120 m and 8°C at about 110 m. Highest salinities were near bottom on the north side.

More normal estuarine flow during an interval of weak winds showed a level of no-net-motion sloped down toward the north more steeply than

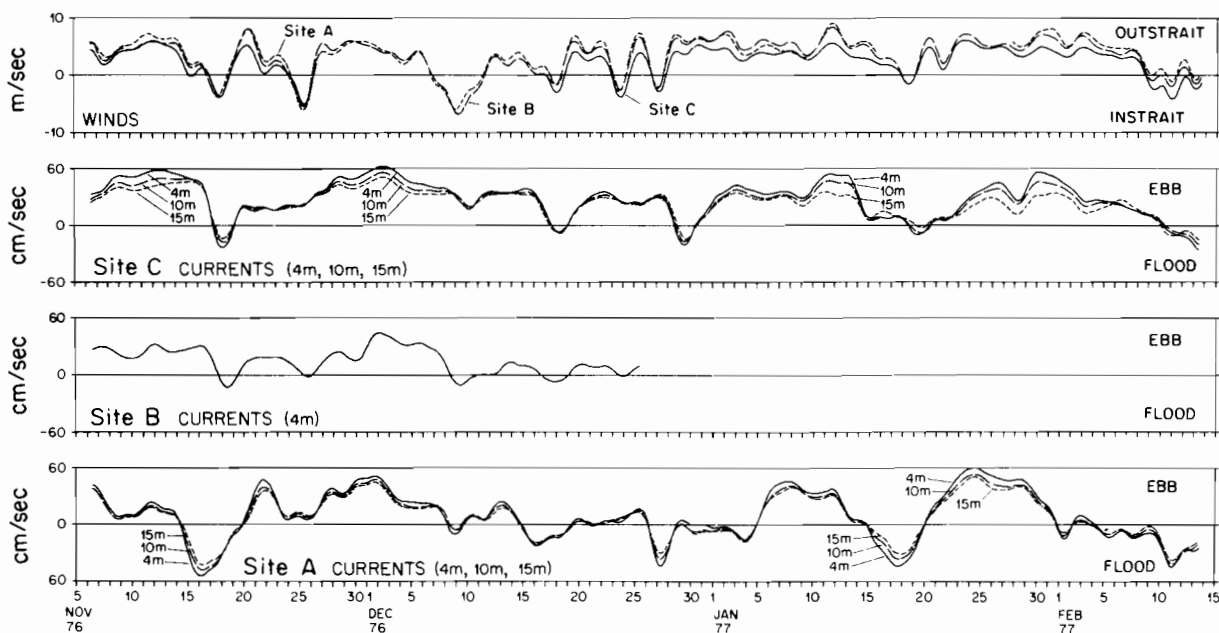


Figure 33. Along-channel components of low-pass filtered near-surface currents and winds at Sites A, B, and C. From Holbrook and Halpern (1978).

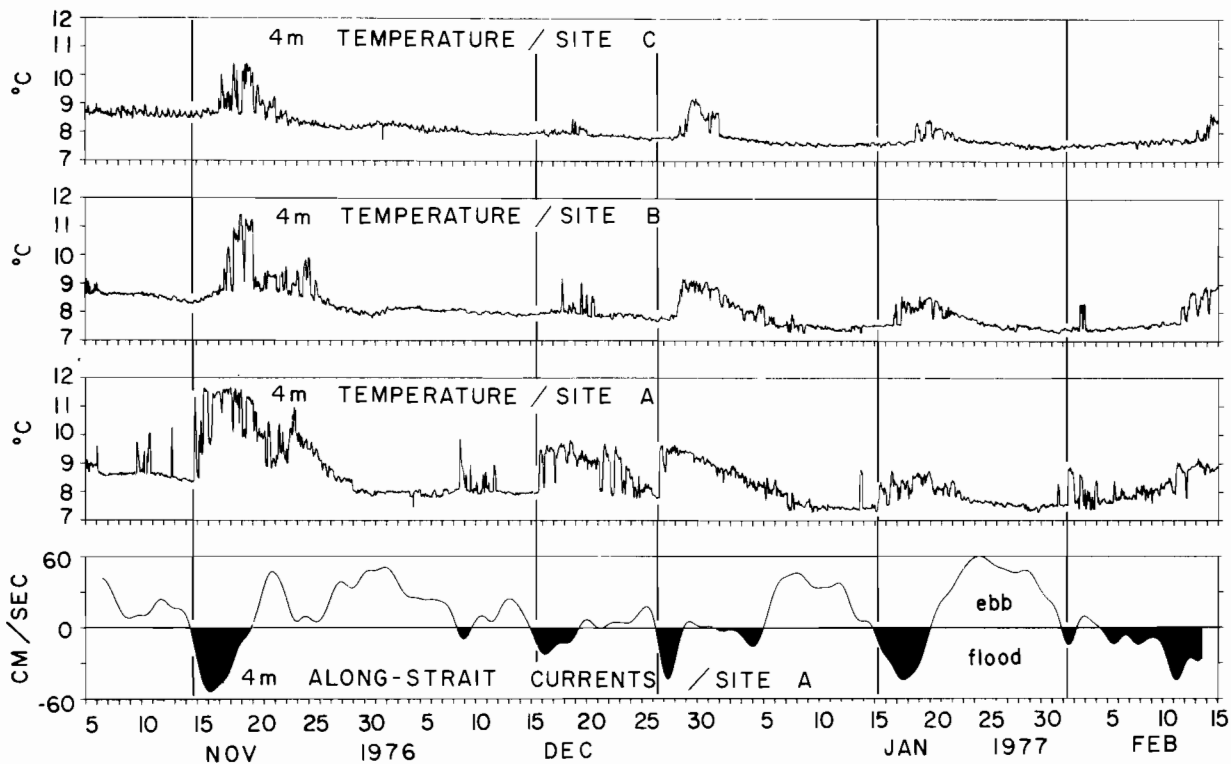


Figure 34. Hourly values of near-surface temperature at Sites A, B, and C and low-pass filtered along-channel currents at Site A. From Holbrook and Halpern (1978).

the total-record average, but its location in mid-channel was about the same. Maximum seaward speeds were located farther north, and maximum landward speeds remained near the south side. Isohalines and isotherms in the upper water sloped down toward the north, and the freshest, warmest water was near the surface on the north side as in the first winter. Below about 100 m the isolines sloped down toward the south. Isohalines of 33 and 32⁰/oo were located considerably nearer the surface and sloped more steeply than during the intrusion, which was also characteristic of the previous winter. Strong easterly winds occurred in late November-early December, the seaward flow became greater and extended deeper on the north side, and the isohalines sloped more steeply than during the no-wind observations. Temperatures were almost uniform throughout the upper water, and the highest salinities remained near bottom on the north side.

Although the winds at Site A were consistently directed seaward (positive) at 7 m/sec, the low-frequency currents reversed from seaward to landward during the largest reversal, on November 14, causing net landward advection. The temperature front passed Site A during the middle of the tidal flood on November 14 and returned during the following ebb (Fig. 34). After several days of

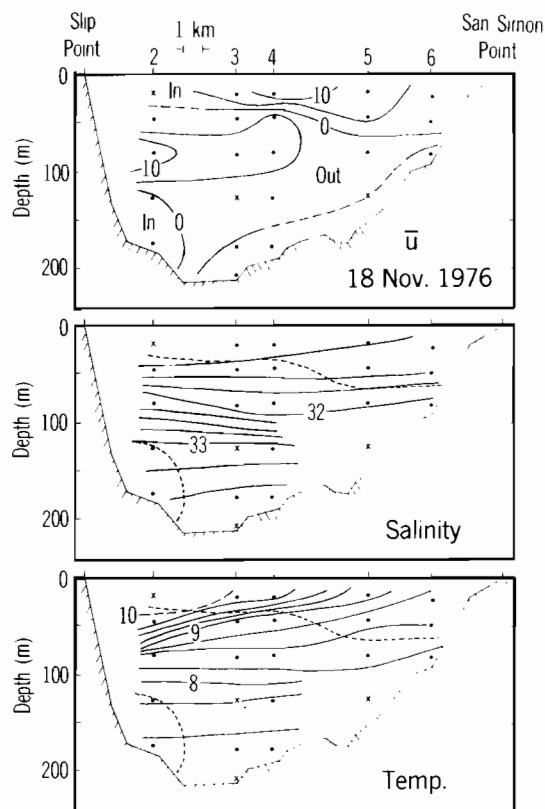


Figure 35. Daily average along-channel currents, salinity, and temperature across the Slip Point section during the largest intrusion. From Cannon and Laird (1978).

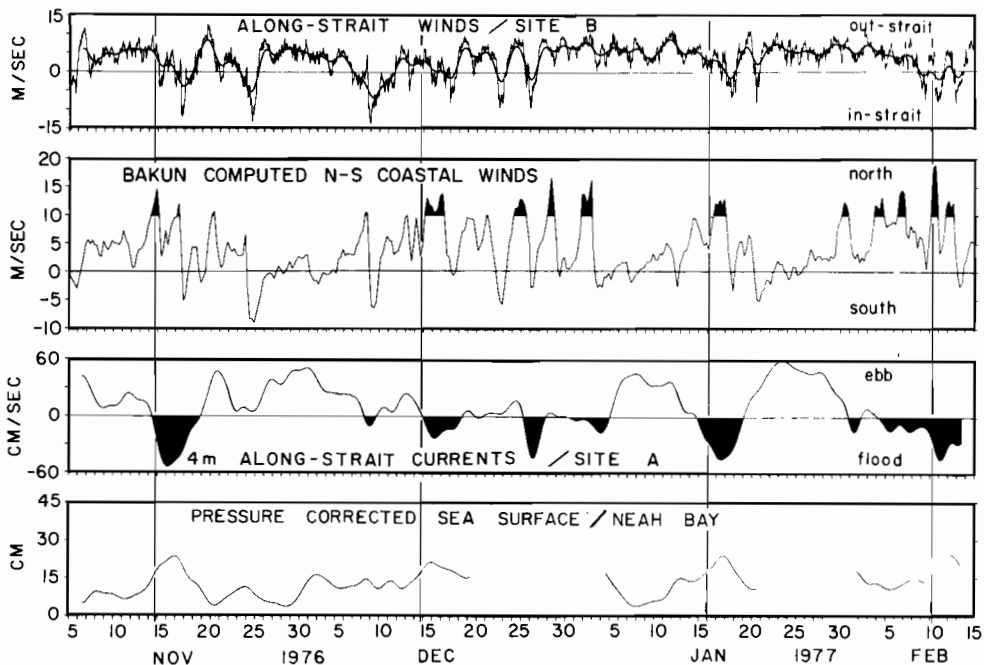


Figure 36. Along-channel and coastal winds, along-channel currents, and sea-surface elevations showing various correlations. From Holbrook and Halpern (1978).

sloshing back and forth, the warm lens was located far enough landward that short periods of tidal ebbs did not advect it seaward through Site A. Although the along-channel components of winds at Sites A, B, and C (Fig. 22) were strongly correlated with each other, local wind forcing of the near-surface currents was weak and only barely significant.

The wind-stress field off the Washington coast can indirectly influence the along-channel currents through induced sea-surface height fluctuations. During winter, southerly winds may be expected to pile up water along the coast through onshore Ekman transport. This increases the coastal sea-surface elevation, which in turn decreases the longitudinal sea-surface slope in the Strait, causing a deceleration of the seaward near-surface circulation.

During the second winter surface winds were computed for a 3°-square pressure grid centered at 48°N, 125°W (25 km off the Washington coast) by rotating directions 15° counterclockwise and by reducing speeds by 30% to approximate the surface frictional effects (A. Bakun, NOAA, National Marine Fisheries Service, personal communication) (Fig. 36). Vertical lines were drawn at times of maximum deceleration of the along-channel currents when accompanying sea-surface height data existed at Neah Bay. Generally, decelerations occurred during strong southerly

winds off the coast and during increasing sea-surface height at Neah Bay. Significant correlations were found: (1) between the along-channel 4-m currents at Site A and the north-south Pacific winds, with currents lagging winds by 42 hours; (2) between the along-channel 4-m currents at Site A and sea-surface height at Neah Bay, with currents lagging sea-surface height by 6 hours; and (3) between the north-south Pacific winds and sea-surface height at Neah Bay, with sea-surface height lagging winds by 24 hours. Temporal decelerations as large as 140 cm/sec in 4 days were observed at Site A (Fig. 34). A sea-surface slope of 4 cm/10 km would be necessary to balance such decelerations. Low-frequency sea-surface elevation fluctuations of 15–20 cm near the entrance may be large enough to set up local 10–20-km slopes, which travel slowly (30 cm/sec) eastward as baroclinic waves. The existence of the strong local density gradient associated with the warm-water lens would complicate such a picture. Regardless of the coupling mechanism, strong coherence existed between the north-south Pacific winds and the low-frequency along-channel near-surface currents in the Strait. Winds measured during the first winter at Tatoosh Island also support this concept (Figs. 14 and 28).

The largest seaward flows at Site A tended to parallel the axis of the Strait. During the mid-November intrusion, the flow had a large south-

ward component at Site A (Fig. 32) and at Site B (not shown). Presumably, this was the result of southerly coastal winds forcing surface water up against the Vancouver Island coast, creating large secondary across-channel flows. Statistically, at midchannel Sites A and B, across-channel flow was correlated with along-channel flow, with intrusions having a south-shore transport and seaward flow having a north-shore transport. Intrusions on the south side of the Site B cross-section, however, tended to parallel the shore line, while seaward flow had more of an across-channel component away from the shore (Fig. 37). There was little evidence of shoreward flow at this location. However, seaward flow at the northern mooring showed a persistent shoreward component, but the intrusion flowed parallel to the axis. This is significant because winter-released drifters tended to beach on Vancouver Island as shown above in Section 3.1. Summer observations (not shown) were less conclusive. Although there were intervals of 2-3 days with shoreward components to the flow at the south and north moorings, there were no extended intervals as shown at the north mooring during winter.

These intrusions of coastal water probably include a mixture of Columbia River water, which is known to flow northward along the Washington coast in winter (Barnes et al., 1972). Observations by Barnes et al. showed the plume extremely close to the coast during major storm periods. Predominantly southerly winds tended to cause an onshore component of surface-water flow. Canadian investigators also have observed fresher water near the surface on the southern side of the Strait of Juan de Fuca during similar winter storm conditions (Crean and Ages, 1971). The flow reversals have been observed across the entire continental shelf in the glacial trough which cuts the shelf (Cannon et al., 1972), and Canadian investigators recently have shown PVDs with similar reversals near Pillar Point (Hugget et al., 1976). Drifter studies on the continental shelf also have indicated winter northward flow along the coast. Some drift bottles released during the winters of 1960-63 near and south of the latitude of the Columbia River have been recovered in the Strait of Juan de Fuca (Burt and Wyatt, 1964). A few were recovered east of Port Angeles. Some bottom drifters released along the coast also have been recovered in the Strait, but these are not necessarily indications of the surface intrusions (Barnes et al., 1972).

3.4 Eastern Strait-San Juan Island Currents

The transport of water and material between the Strait of Juan de Fuca and the Strait of Georgia

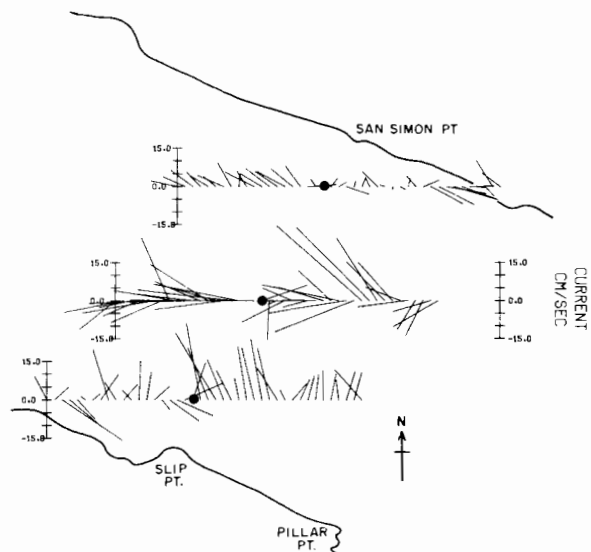


Figure 37. Vector plots of daily averages of low-pass filtered currents at the 15-m level across the Slip Point section. From Cannon and Laird (1978). Dots represent mooring locations.

systems is accomplished principally by estuarine and wind-driven currents superimposed on the tidal currents. The importance of winter reversals in the eastern Strait is unknown at this time, but they may play a major role in the circulation and even dominate the local wind-driven near-surface currents. The moored current meter data obtained by the National Ocean Survey (Section 2.2) were intended primarily to define the tidal currents. Although the current records were relatively short (a month or less in duration) they can be used to make initial estimates of the longer period estuarine and wind-driven currents without regard for seasons. No summer observations were made. A new PMEL current observation program is measuring currents in the eastern Strait for 1978. The data are not available for this report, but will be available about one year after the study ends.

The mean surface currents for the eastern Strait of Juan de Fuca and for the region in and around the San Juan Archipelago were calculated for the total, but varying, record lengths (Figs. 38 and 39). The data were scattered in time so that they do not give an instantaneous picture of the mean flow. Instead, they are suggestive of the magnitude and direction of the currents with periods longer than those of tidal currents and of the variations in the magnitude with location. The numbers beside the current vectors are related to standard deviations of the components and are measures of the reliability of the mean current vectors. A number much less than one indicates that the scatter of the individual currents, which were sampled every six hours after the tidal currents had been removed, was relatively small and demonstrates that the mean current was relatively steady during the period of observation. Numbers

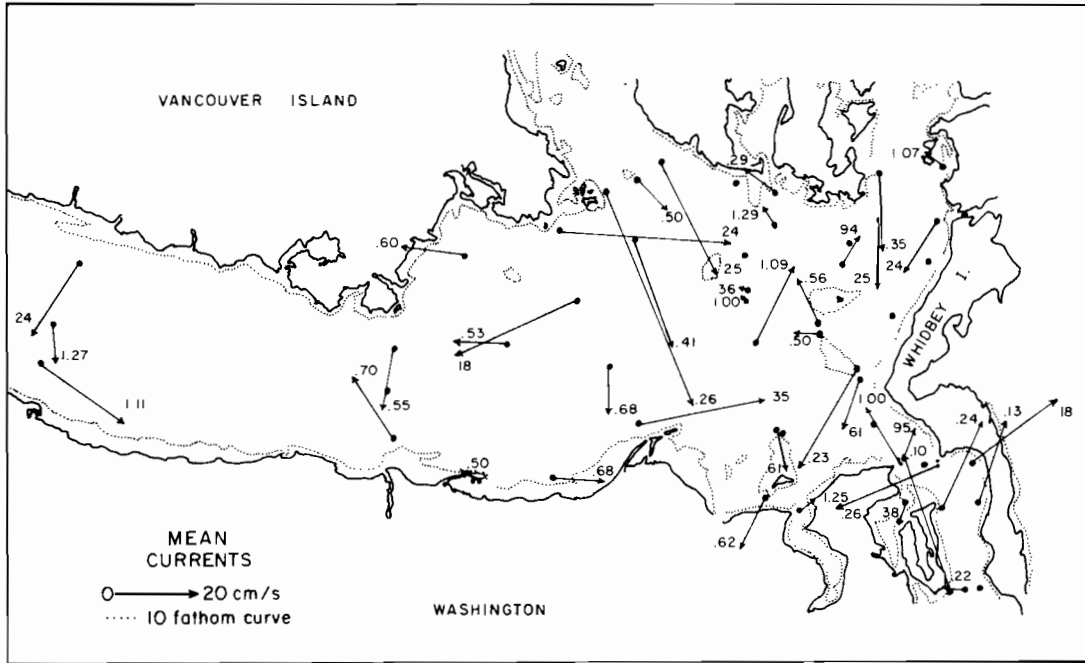


Figure 38. Near-surface mean currents observed during spring and fall in the Strait of Juan de Fuca. Prepared for this report by Mofjeld. Numbers near the current vectors indicate the scatter in the long period currents.

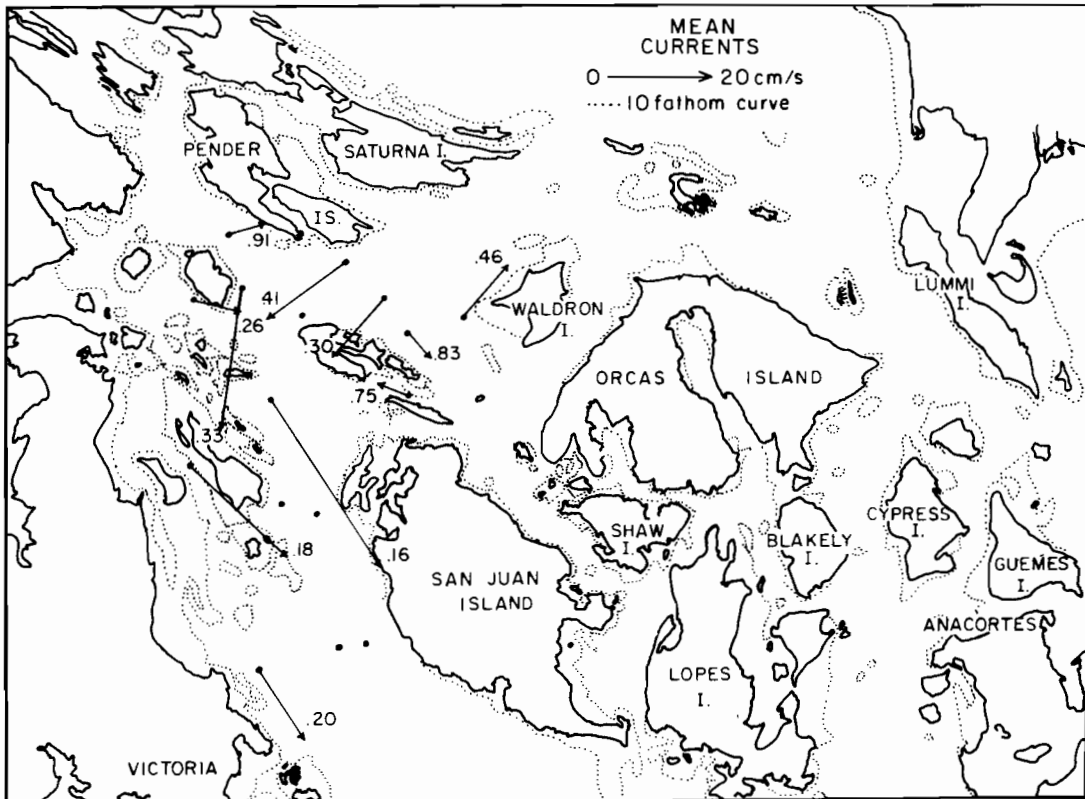


Figure 39. Near-surface mean currents near the San Juan Archipelago. Prepared for this report by Mofjeld.

equal to or greater than one indicate that the long-period currents varied considerably and that the mean therefore was not representative of the non-tidal current at those locations. The variability was due in large part to fluctuations in the wind-driven currents. However, no wind records were available for the varying times of observation. Small variability probably indicated that the long-period flow was controlled by the estuarine circulation, although rectification of tidal currents in near-shore eddies also produces a local mean current observed by a moored current meter. Several of the large mean currents directed toward the beach at near-shore locations are thus suspect. Most of the largest mean currents were observed in the more confined passages. The vertical distribution of the long-period currents in the system are not defined with precision by the NOS data because of the limited number of meters deployed on each mooring to measure tidal currents. The

data have verified, however, that the deeper, long-period motions tend to be opposed in direction to the near-shore surface flow, which is consistent with estuarine flow.

Similar calculations were made for the mean current vectors for the region immediately north of the San Juan Islands in the southern Strait of Georgia and in the immediate vicinity of Cherry Point (Schumacher et al., 1978; Tracy, 1975). Mean flow during late winter-early spring 1975 on the western side of the southern Strait of Georgia was found to be predominantly driven by Fraser River discharge (Fig. 40). River water crossed the Strait and proceeded along its western side in a southeasterly direction. Bathymetry north of Boundary Pass (between Saturna and Pato Islands) caused a portion of the less saline surface waters to bifurcate, with one portion flowing eastward and southeastward along the San Juan Archipelago and the remainder flowing seaward

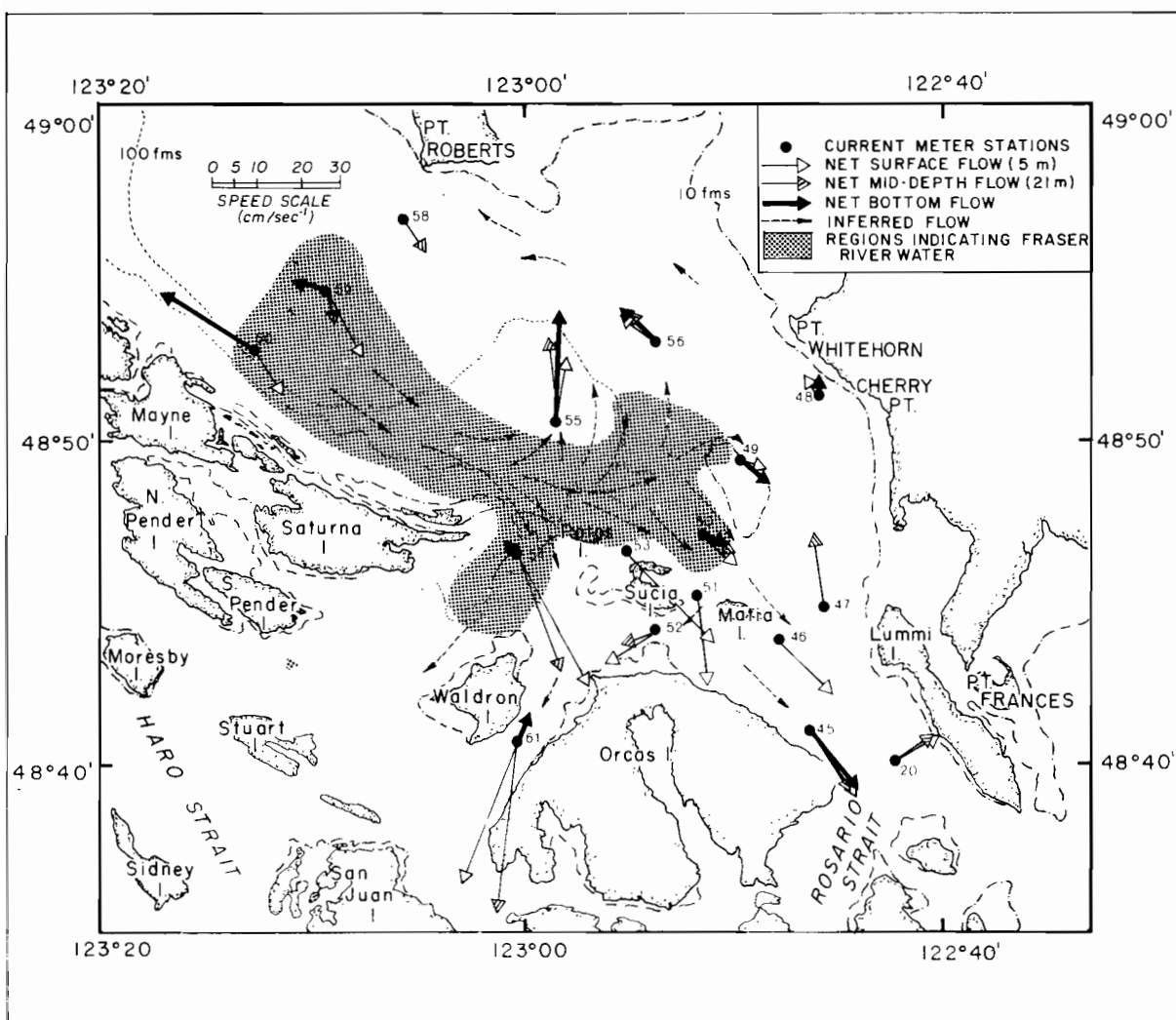


Figure 40. Mean currents north of the San Juan Archipelago. From Schumacher et al. (1978). Numbers near current vectors are station numbers.

through Haro Strait. Oceanic water entered the system flowing landward at depth through Haro Strait (the deepest connection with the sea) in response to the fresh-water runoff. A two-layered flow regime also was observed in the Strait of Georgia across the section from Point Roberts to Mayne Island. On the shallower eastern side of the Strait of Georgia, surface waters showed a weaker mean current flowing northwestward, and the water column was well-mixed. There was little or no evidence of mean northward flow through Rosario Strait. This work and the satellite studies of the Fraser River plume are mutually supportive. The indications of Fraser River water in this study (Fig. 40) are the same as shown previously for ebb flow partly exiting into Haro Strait (Fig. 19).

It has been reported that in the southern Strait of Georgia the flooding tidal current was stronger and of longer duration than the ebb on the eastern side. The opposite existed for the western side, and this tidal inequality tended to drive the observed counterclockwise circulation (Waldichuck, 1957). However, more recent data have indicated no net flow northward through Rosario Strait (Schumacher and Reynolds, 1975). These two studies suggest that the apparent tidal inequality results from superimposition of tidal current upon mean estuarine flow.

The wind field during this study was relatively uniform over the entire area; topography controlled the flow, which resulted in axial winds. Strong estuarine flow on the western side reduced the impact of wind-induced movement, and thus there was little direct correlation between mean flow and winds. On the eastern side of the Strait near Cherry Point, winds played a more dominant role in driving the circulation, and a relatively high correlation coefficient existed between axial winds and currents. During periods when winds exceeded 10 m/sec, approximately 71% of the variation in the mean current velocity was accounted for by a linear relationship with axial winds, and axial current speeds were approximately 1% of axial wind speeds.

The southern Strait of Georgia encompasses a relatively small area. However, its geomorphology divides this small area further into two distinct subregions. Circulation response to local forcing mechanisms in each of these subregions is substantially different. The western half is dominated by gravitationally convected estuarine circulation, while the eastern half responds almost solely to wind-forcing. Some recent Canadian studies have examined various aspects of flow in the Strait of Georgia in considerably more detail (Chang et al., 1976; Tabata, 1972; Crean, 1978).

Little work is currently available describing flow in the passages between the San Juan Islands, and that which is available is of short duration. Drogue observations made in various places along Rosario Strait for durations of $\frac{1}{2}$ -1 day showed no groundings of the drogues except for a few released very near to shore (Schumacher and Reynolds, 1975). Current observations in the southern half of Haro Strait showed two-layered flow with the depth of no-net-motion at about 50 m near the junction with the Strait of Juan de Fuca and deepening northward to about 100 m (D. Evans and E. E. Collias, University of Washington, unpublished manuscript). The no-motion layer sloped across channel and upward toward the east, or to the left looking seaward. Cross-channel surface flow was observed near periods of slack water, a phenomenon which is common to many of the more restricted passages. Some recent Canadian work in Haro Strait is noted below in Section 5.

3.5 Plankton Observations

Cruises were made in the Strait of Juan de Fuca for over a year during 1976-77 to determine seasonal distributions of plankton. The sporadic occurrence of a group of coastal surface-living plankton species was unexpected in view of the quasi-constant surface outflow (Table 1). Initially, the zooplankton species were believed to be deep strays entering the Strait at depth. However, these zooplankters were not seen in deep samples, and they were not found in summer, when they can be very abundant offshore.

In November 1975 a large bloom of phytoplankton occurred off Neah Bay together with typical offshore phytoplankton and zooplankton species. Physical oceanographic observations independently taken at that time revealed an intrusion of relatively warm coastal water into the western Strait. During two cruises in 1977 there were no independent physical data to support the occurrence of some of these coastal species. But at all other times these coastal species were only found in the Strait in association with or very close to incidents of documented coastal water intrusion and current reversals from seaward to landward flow. The correlation is excellent.

These plankton species could act as indicators for surface coastal water, which at times might influence even the easternmost limits of the Strait. Also the distribution of deep-water plankton is limited within the Strait system by the presence of the various sills. More details of this work are discussed in Damkaer and Larrance (1978).

Table 1. Occurrences of various species of plankton in the Strait of Juan de Fuca.

| REVERSALS | CRUISES | ZOOPLANKTON | | | | | | | | | | PHYTOPLANKTON | | | | |
|--------------|-----------|---------------------|-----------------------|---------------------------|------------------------|---------------|---------------------|------------------------|----------------------|--------------|-------------------|----------------------------|-------------------------|--------------------|------------------------|--|
| | | Calanus tenuicornis | Clausocalanus lividus | Clausocalanus parapergens | Calocalanus styliremis | Acartia danae | Phronima sedentaria | Dictyocysta reticulata | Parafavella gigantea | Radiolarians | Coccolithophorids | Bacteriastrium delicatulum | Asteromphalus heptactis | Rhizosolenia alata | Chaetoceros convolutus | |
| Feb 16-22 | Feb 23-24 | • | • | • | | • | | | | | • | | | | | |
| Feb 28-Mar 2 | Apr 5-6 | | • | • | | | | | | | • | | | | | |
| Mar 20-30 | May 17-18 | | | | | | | | | | | | | | | |
| | Jun 28-30 | | | | | | | | | | | | | | | |
| | Aug 3-5 | | | | | | | | | | | | | | | |
| | Sep 14-16 | | | | | | | | | | | | | | | |
| Nov 14-19 | Nov 12-15 | • | • | • | | | | • | • | • | • | • | • | • | | |
| Dec 8-9 | | | | | | | | | | | | | | | | |
| Dec 14-18 | | | | | | | | | | | | | | | | |
| Dec 26-28 | | | | | | | | | | | | | | | | |
| Jan 1-5 | Jan 12-13 | • | • | • | | • | | | | • | • | • | | • | | |
| Jan 14-19 | | | | | | | | | | | | | | | | |
| Feb 2-3 | | | | | | | | | | | | | | | | |
| Feb 5-14 | Feb 23-24 | • | • | • | • | • | • | | | • | • | | | • | | |
| | Apr 7-8 | | • | • | | | | | | • | • | | | | | |
| No data | | | | | | | | | | | | | | | | |
| | June 2-3 | | | | | | | | | | | | | | | |
| | Jul 26-27 | | | | | | | | | | • | | | | | |
| Aug 31-Sep 2 | | | | | | | | | | | | | | | | |
| Sep 6-8 | | | | | | | | | | | | | | | | |
| Sep 21-25 | Oct 3-5 | | • | | | | | | | | • | • | | | | |

4. OIL-SPILL TRAJECTORY MODELING

4.1 Model Description

An oil-spill-trajectory computer model consists of three basic components. The first is a collection of tables and/or numerical formulas that specify the time and spatial behavior of wind and current. These tables represent the movement and mixing of ocean and coastal waters at some nominal resolution independent of the possibility of an added pollutant. The second component is a motion equation that relates the movement of a central element of an oil spill, treated as a particle, to the specified local wind and current. The third component is a set of quantitative relations that specify the spreading, sedimentation, and weathering of the oil following a trajectory path. The latter clearly depends upon the physical and chemical characteristics of the oil as well as environmental conditions. The results to follow have neglected those factors which depend upon the volume and type of oil and have concentrated simply upon trajectory plots of idealized particles advected by currents and drifted by the wind.

All oil-spill trajectory models are essentially the same with respect to the motion equation. They rely on empirical and uncertain relationships that link oil-spill velocity with the vector sum of the local current velocity and a fraction, e.g., 3%, of the wind velocity. Such estimates are obtained from after-the-fact analysis of the trajectories of major oil slicks. Drift factors represent an approximate composite response for the complicated interaction between wind, waves, oil, and water. Comparison of observed and predicted trajectories for the grounding of the *Torrey Canyon* showed daily variability of drift factors of 2.5%–4.5% for best fit. For the cases shown here particles were advected with the velocity of the tidal current plus 3.5% of the wind speed in the direction toward which the wind is blowing.

The method of handling the wind and current data largely distinguishes one model from another. The crudest models assume spatially uniform and time-steady currents or winds, or both.

Models increase in complexity from this point. In the present study, for example, the time behavior of the current has been simulated by using locally measured tidal amplitude and phase data for the five most significant tidal harmonics. The spatial behavior of the current was interpolated between measurement points using hand-derived coefficients. The spatial behavior of the wind field was deduced by using a combination of local measurements and the results of the numerical model discussed in Section 2.3 that accounted for the effects of the local topography and air stability.

Because the equation of motion is empirical and based on only a few observations; there currently is little knowledge of the errors inherent in any particular calculation of spill motion. Without a knowledge of these errors, it is not possible to estimate quantitatively the effects of errors in the specification of the wind and current fields on the spill trajectory, because the trajectory and the driving forces are coupled by these poorly understood equations. However, some conclusions are still possible regarding the properties that should be built into the wind and current simulations, irrespective of the spill motion model. Of prime importance is the proper simulation of the evolution of the winds and currents in time. In this regard, the ebb and flood phases of the tides are obviously important, but so is the persistence of the wind. Most winds only remain in a given octant for a few hours, and the changes after that are fundamentally random, although they may exhibit certain patterns. The reason this time-wise evolution is important is that the assessment of oil-spill risk from a location requires that the ensemble of all possible spill scenarios be examined. Spills can happen at all phases of the tide and in all wind conditions. Each initial condition will result in a collection of trajectory possibilities consistent with the temporal evolution of the wind and current fields from the initial state. It is this time-wise behavior that will determine which beaches are most likely to be impacted.

An algorithm to simulate the tidal currents in the Straits of Juan de Fuca, Georgia (U.S. part), Rosario, Haro, and in other connected channels and bays was written for use with the oil-spill trajectory model. The principal purpose of this algorithm was to furnish components of the tidal velocity when interrogated with appropriate information about position and time. The two major sources of tidal current information were 57 stations from NOAA/National Ocean Survey (1976), in conjunction with the NOS standard harmonic constants for the prediction of currents at six primary stations, and 90 stations from Parker (1977) with standard harmonic constants for each station. Stations from Parker were considered the primary data set, with NOS tidal tables supplying information primarily in the secondary channels.

The computations were carried out using a one-kilometer grid over the entire region of interest. Each square in the grid was assigned a sequence number related to the current configuration in that square. Several neighboring squares might have similar currents and all have the same sequence number. The groupings varied in size from groups of one or two squares in small channels to groups of 80 or more in areas of less complicated flows. Each sequence number was assigned a direction of flow at flood current, and up to three NOS stations were used to interpolate the current and the respective proportionality fractions of their influence. The direction of ebb was assumed to be opposite that of flood.

The currents at the reference stations were calculated by the numerical harmonic method described in U.S. Coast and Geodetic Survey (1958). The five largest contributing tidal constituents, M_2 , S_2 , N_2 , K_1 , and O_1 , were used.

The routines were tested in parts and as a module in the trajectory model. A test run was made for March 1976 off Port Angeles. The diurnal inequality was well represented in the results, and the phasing matched the predicted values in the NOS tables. While a mean drift is specified for each station from the tidal analysis, it represents a climatological mean value of non-tidal drift over the period recorded by each instrument. The model, therefore, does not include the instantaneous effects of non-tidal drift such as extremes in the estuarine flow described above in several sections.

The procedure for providing spatially dependent winds to the trajectory model was to specify two keying parameters, the direction and wind speed measured at Tatoosh Island at the entrance to the Strait of Juan de Fuca. Amplitude ratios and local directions were estimated for a four-kilometer-square grid overlying the region to convert the keying parameters to local winds for each 45° segment of wind direction at Tatoosh

Island. These local wind patterns were estimated from observations for each synoptic case supplemented by subjective guidance provided by the regional meteorological model described in Section 2.3. To date and for this report, two local wind fields have been completed, corresponding to the more persistent cases of east and west winds (Fig. 41). An important omission is the short-duration storm situation with strong southerly winds in the eastern Strait and light winds at Port Angeles in the lee of the Olympic Mountains.

4.2 Sample Trajectories

The unity of the oil-spill trajectory model stems from its ability to incorporate wind and current fields that are variable in both time and space. Tidal currents are nearly periodic in time at a given location over the period of several days but can change magnitude and direction over short spatial distances. The wind field varies significantly in both time and space. The trajectory model provides a testing ground for determining the importance of these features to the oil-spill motion problem. This section discusses three experiments with the trajectory model. The first two specify winds constant in time corresponding to the east and west wind fields outlined in the previous section. The third specifies time-varying but spatially uniform winds for a release site near Port Angeles. Five release sites in the eastern Strait of Juan de Fuca were used in the first two cases (Fig. 42). Sites a, b, and e correspond to intersections in the vessel traffic-control system, while Sites c and d are the entrances to major shipping routes through Rosario and Haro Straits.

Figure 42 shows the plotted trajectories for easterly winds in the Strait (Fig. 41) keyed to a wind magnitude at Tatoosh Island of 10 m/sec. Crosses on trajectories are at 24-h intervals. Start time for the current field was noon on March 15, 1976. Trajectories a and b were under the influence of strong winds at the outer end of the Strait. Drift toward the west was on the order of 10 km/day. The release in Haro Strait (Site c) traveled south under the influence of the cold air winds from the north. It reached the central Strait far enough west that the trajectory continued west under the influence of the gap winds in the central-western part of the Strait. The release in Rosario Strait (Site d) was blown south similarly to that at Site c but approached a region of lighter winds in the vicinity of Site e, where the response was primarily tidal.

For time-invariant winds from the west (Fig. 41), the same five release sites have been simulated (Fig. 43). The keying wind magnitude is again 10 m/sec, and the currents were initialized

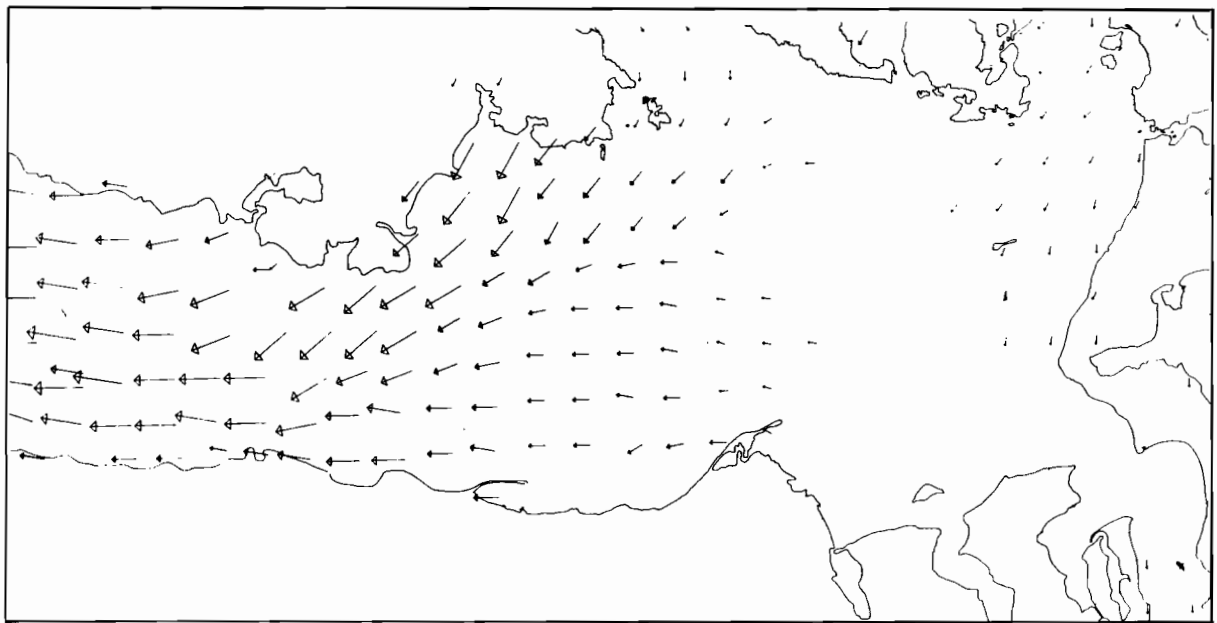
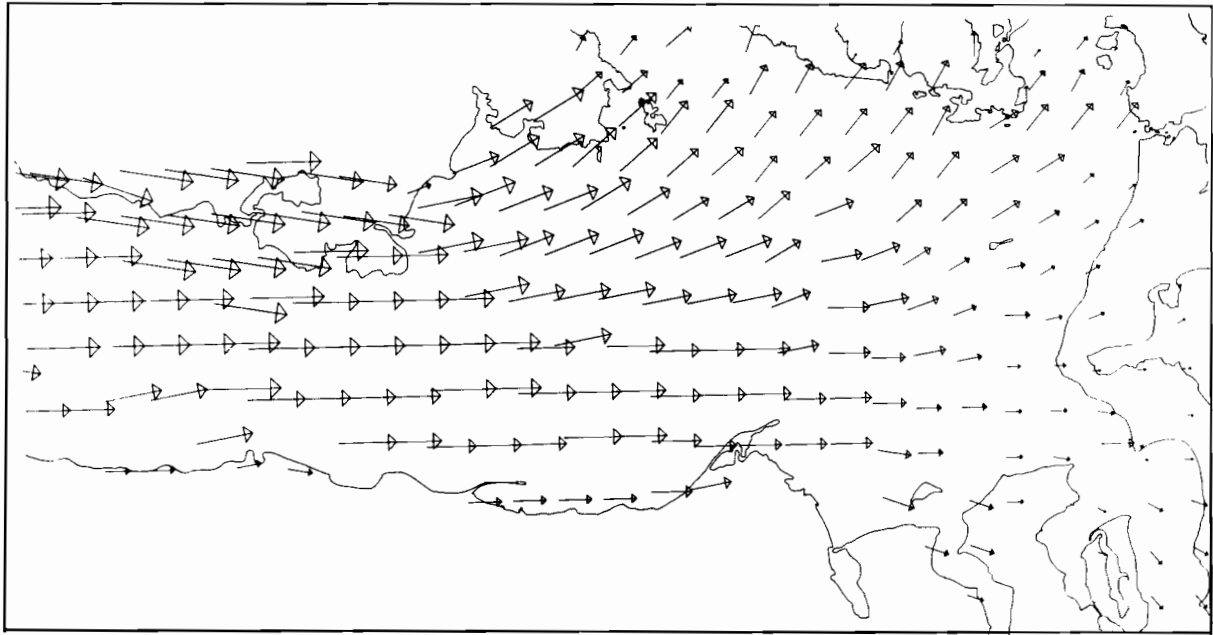


Figure 41. Local wind field for offshore winds from the west (top) and east (bottom). Relative wind speed is scaled by the length of the arrow.

at noon on March 26, 1976. Trajectories starting west of Port Angeles (Sites a and b) traveled east at a rate of 10–15 km/day, separating with a diverging current pattern at the east end of the Strait. Landfall occurred in five days, which is much longer than west winds can be expected to persist. Releases from points at the eastern sites (c, d, and e) quickly reached landfall in the San Juan

Islands. West winds in this part of the Strait of Juan de Fuca diverge on a line running due east of Race Rocks, blowing toward the San Juan Islands above this line and toward Admiralty Inlet and Whidbey Island south of this line. The trajectories reflect this behavior.

Figures 44 through 46 show 24-, 48-, and 72-hour trajectories for a release site southwest of

124.0.0w

122.35.0w

48.30.0n

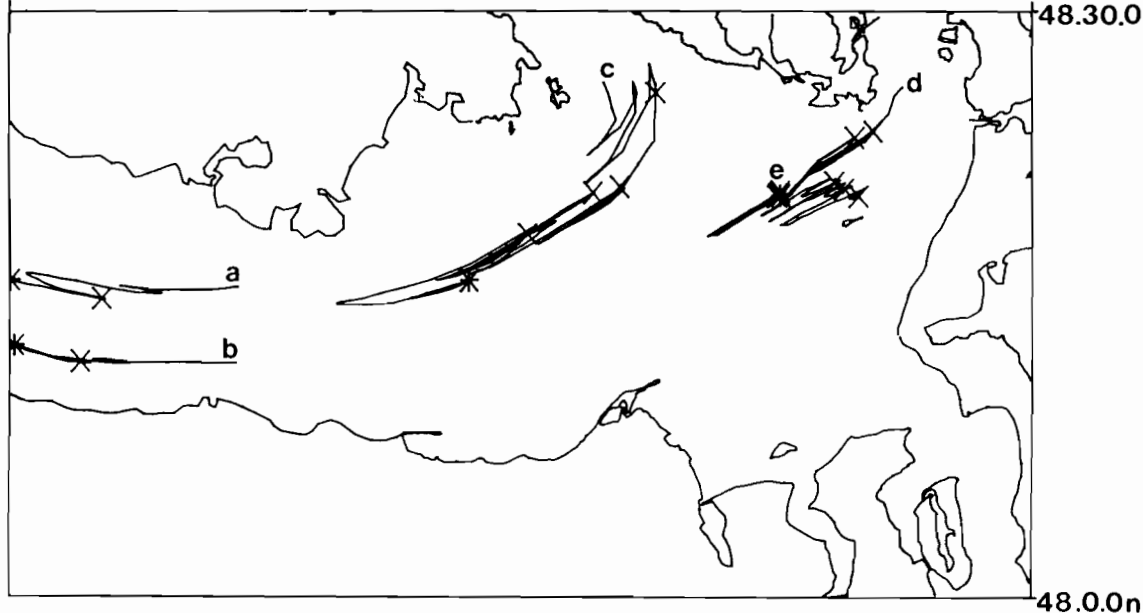


Figure 42. Trajectories from five release sites during easterly winds. Crosses (X) represent twenty-four hours of travel time. Stars (*) represent landfall or termination at five days.

Race Rocks with six releases at 1200 PST on March 12, 15, 18, 21, 24, and 27, 1976. The wind was assumed uniform over the region, and the time variations were based on hourly wind observations made at Race Rocks in March 1976. Due to the known spatial variability in the wind field, these trajectories can only be trusted while they remain in the vicinity of Race Rocks. For purposes here, "vicinity" was loosely interpreted as meaning west of New Dungeness and south of Race Rocks. During a typical March the average wind is from the west in the Strait of Juan de Fuca, so spills should be expected to have predominantly eastward trajectories subject to tidal currents and the local wind. This behavior is reflected in all three figures. After 24 hours, two spills had traveled 15 km to the east, three spills had traveled about 5 km to the east, and only one spill showed a net transport to the west (Fig. 44). After 48 hours, four spills were clustered in the region northwest of Admiralty Inlet, one spill returned to the vicinity of the launch site south of Race Rocks, and the last spill still showed a net westward movement (Fig. 45). Finally, after 72 hours, two spills were as far east as Admiralty Inlet, two spills were between New Dungeness and the launch site, and two spills were 3-5 km west of the launch site (Fig. 46). Because of the assumption of a spatially uniform wind field, the location of the spills farthest east must be considered questionable but nevertheless suggestive.

A prominent feature of all three figures is the east-west orientation of the trajectories. This re-

sults both from the strong channeling effect of the Strait on the tide and the east-west orientation of the wind in the vicinity of Race Rocks. This is something of an artifact because of the spatially uniform wind field assumption. Based on Figs. 42 and 43, some northward component in the trajectories can be expected once they get as far east as New Dungeness and as far north as Race Rocks. The two spills that traveled into Admiralty Inlet both spent some time in this region, and some north-south perturbations might have been expected. Spills with a net westward transport also could be expected to have some northward component once they were beyond the lee of the Olympic Mountains.

There are several qualifications that should be emphasized regarding these trajectories. First, they are not intended to be an exhaustive sampling of all the trajectory possibilities. They are simply six trajectories from a typical March. If six trajectories had been drawn from March of 1977, which was atypical, the predominant transport would have been to the west, not to the east. No attempt has been made to present a spectrum of results that would have indicated this potential for variability. Second, only wind and tidal currents have been considered. Besides these, there are strong low-frequency currents associated with wind setup along the coast and with fresh water runoff, as described in various parts of Section 3. These are not included in the current field. Transport from these currents could easily overwhelm a relatively weak wind transport. Unfortunately, these

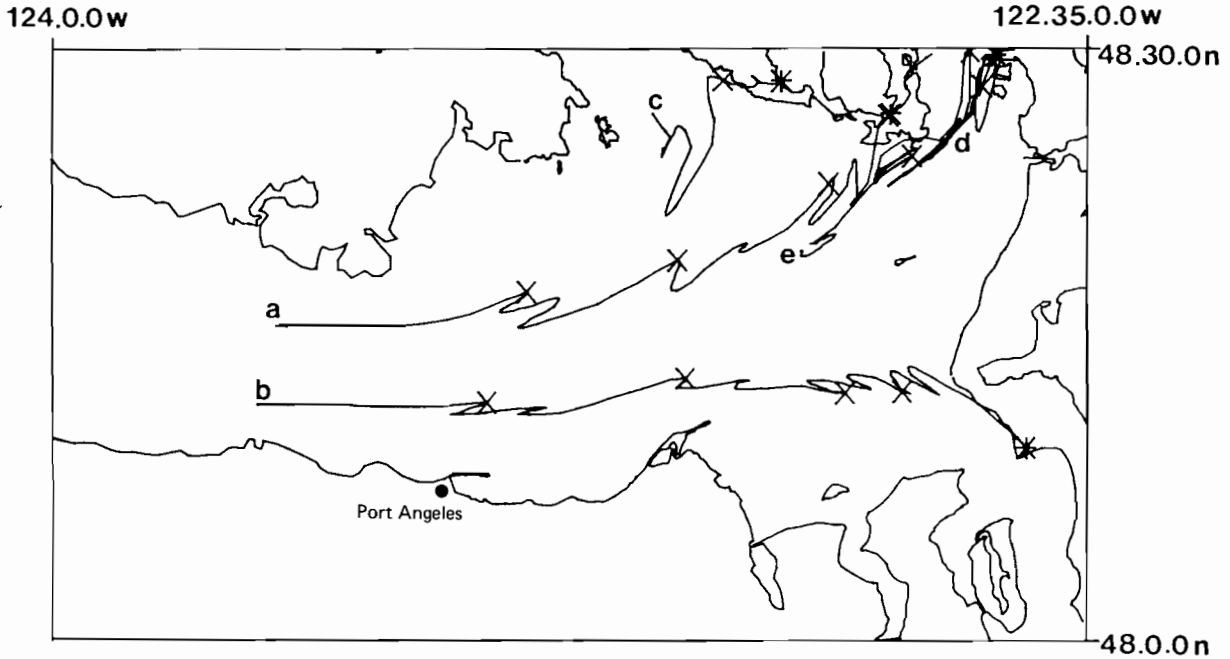


Figure 43. Trajectories for five days during westerly winds.

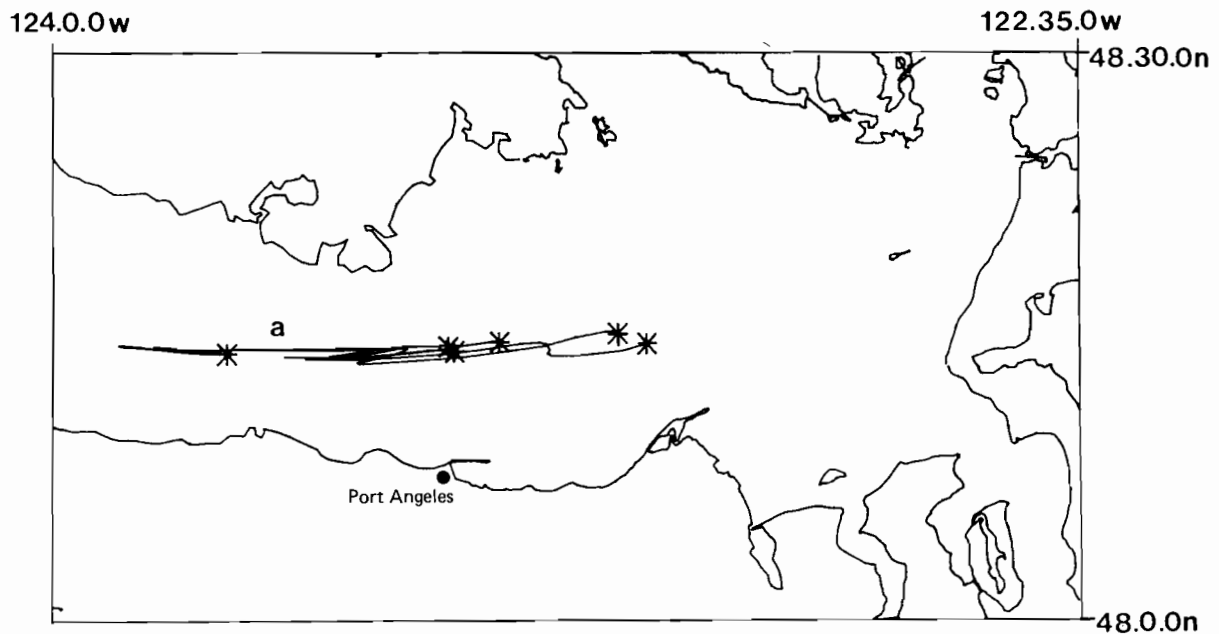


Figure 44. Trajectories for six releases at site northwest of Port Angeles. The releases were at three-day intervals starting at noon on March 15, 1976. Each trajectory is based upon hourly winds at Race Rocks initialized on the six days. Each trajectory is for twenty-four hours.

currents are not yet sufficiently understood to be modeled. Third, no explicit consideration was given the effect of storm passage on spills in the eastern strait region. Within several days of a release, a frontal passage could be expected, channeling strong southerly winds through Puget Sound. Such events may be responsible for the

strong dispersion evident in the drift card trajectories shown in Section 3.1. Finally, no consideration was given to summer cases, which are characterized by persistent high pressure offshore, resulting in predominantly west winds modified by diurnal sea breeze. Further work, including the summer examples, is underway in the numerical

124.0.0w

122.35.0w

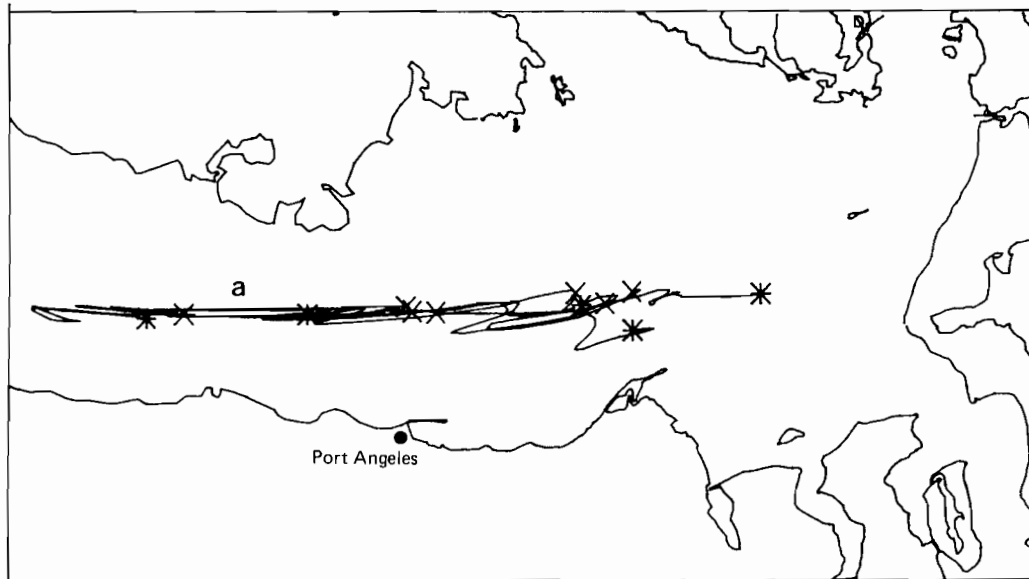


Figure 45. Trajectories after 48 hours for releases shown in Fig. 44.

124.0.0w

122.35.0w

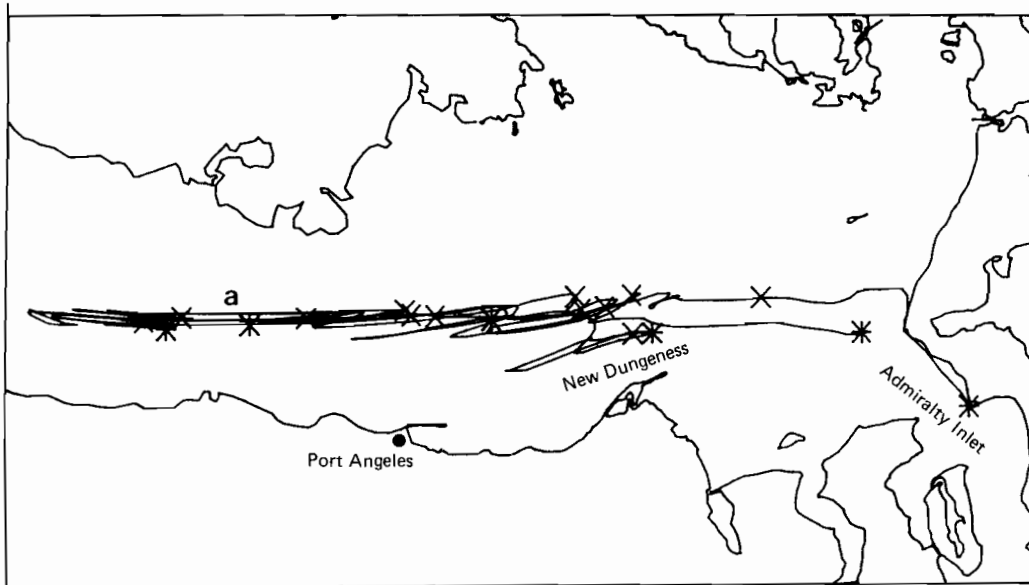


Figure 46. Trajectories after 72 hours for releases shown in Fig. 44.

studies group at PMEL, and the results should be available in a separate report late in 1978. Results to date from their ongoing study have been described here.

5. OTHER STUDIES

Canadian investigators conducted a number of studies in the western Strait of Juan de Fuca in the vicinity of Pillar Point during 1973 and 1975 and in the southern part of Haro Strait northwest of Victoria during 1976. Results from these studies are beginning to be published, and brief summaries from their reports follow. These are part of ongoing studies, and the results should be considered preliminary until completed by the respective scientists. Recent Canadian work in the Strait of Georgia was noted in Section 3.4. Also, the tidal modeling work in the Strait of Juan de Fuca-Strait of Georgia system is a continuing endeavor, and the most up-to-date descriptions are in Crean (1978). PMEL trajectory modeling will be continued this year as outlined in Section 4, and further results will be in a future modeling report. Major field investigations in 1978 are underway in the eastern Strait of Juan de Fuca because of a lack of information about this area. This is a joint investigation between PMEL and the Institute of Ocean Sciences, Environment Canada, and a brief summary of the study follows. Preliminary results for the eastern Strait work are planned for summer 1979 as a supplement to this report.

The 1973 Canadian oceanographic program in the Strait of Juan de Fuca was both an investigation into the flushing process of the Strait of Georgia and an attempt to obtain current observations as input to the Strait of Georgia numerical tidal model. Continuous records of currents (and temperature and conductivity at some locations) were obtained for three months, and at two stations for over five months, all commencing in March (Huggett et al., 1976). Time series of temperature and salinity profiles were taken at a number of stations during the time the current meters were in place and at a few stations from June to December when there were no current observations.

Their data showed current speeds from just under 125 cm/sec on the surface to 75 cm/sec near

the bottom. The principal semidiurnal component M_2 changed very little near the cross-section, averaging around 48 cm/sec with a phase angle of 245° . Similarly, K_1 averaged 29 cm/sec with a phase angle of 254° . The residual currents showed a seaward or westward current in the upper portion of the Strait and a landward or eastward current in the lower half. The line of null velocity sloped upward from around a depth of 110 m on the north side of the Strait to the surface on the southern side about one-half mile offshore. The two layers had the same maximum speed (around 14.5 cm/sec) with the maximum seaward current being on the surface in the center of the Strait and the maximum landward current centered about the middle of the lower layer. The close similarity of our overall averages was indicated in Section 3.3. Also, reversals were observed in their current records, but no attempt was made to correlate them with storms or wind events. A significant finding is the possibility of net eastward flow at all depths near the southern shore at this time of year at this location.

The 1975 Canadian observations of currents, bottom pressures, and various auxiliary data were obtained in the Strait of Juan de Fuca from May to July. The primary purpose of these measurements was to investigate the relationship between the currents flowing along the Strait and the difference in bottom pressures across the Strait. A close correspondence between these two quantities would provide a method for computing the currents from pressure measurements made on opposite sides of the Strait (Fissel and Huggett, 1976; Fissel, 1976).

The Canadian group calculated currents from these differences of pressure, which generally agreed within 20% with the measured current. Errors in the method were determined to be due to physical phenomena which also caused differences in the pressure across the Strait. These phenomena

were thought to be local accelerations of the cross-channel current and variations in the density on either side that were not in isostatic balance with the sea-surface elevation. Thus, for the full signal the accuracy of the pressure difference method will depend largely on the size of these other factors relative to the pressure differences resulting from the Coriolis force. The method could not be tested properly for residual currents, because large spatial variations of residual current fluctuations across the Strait indicated that sampling the current at five locations was not adequate to compute a meaningful cross-channel averaged residual current. However, correlation with the pressure differences was surprisingly good.

The 1976 Canadian study in Haro Strait was conducted from July to September to determine some of the major water characteristics and flow in that region for late summer. The study included observations of currents across a section, temperatures using thermistor chains, several time series of CTD profiles over 25 hours, and winds (D. M. Farmer, Environment Canada, personal communication; Webster, 1977).

This study showed estuarine circulation, and the level between inflow and outflow was observed to vary between 40 and 100 m on the eastern side to greater than 100 m on the western side. Deepening to the west was similar to that noted in Section 3.4. Following spring tides, the velocity, temperature, and salinity gradients were found to be minimums, and following neap tides they were maximums. Tidal phases were smallest in the surface on the eastern side. Phases increased with depth and towards the western side. Pronounced changes occurred in the water characteristics in the whole water column of Haro Strait over periods of a day. For example, coinciding with the

occurrence of spring tides, the maximum northward flowing tidal current was associated with the appearance of a 250-m-thick layer of almost uniform salinity in the southern end of Haro Strait.

The 1978 PMEL program in the eastern Strait of Juan de Fuca consists of two separate experiments, one in winter (December 1977–April 1978) and one in summer (July–September 1978), utilizing moored current meter arrays, surface wind, sensors, and CTD data. Supporting meteorological and circulation data will be obtained from NWS, NOS, FNWC, and Environment Canada. Three surface and three subsurface moorings will be positioned as centrally as possible in the main channels connecting the eastern Strait with the western Strait, Haro Strait, and Admiralty Inlet. A triangular configuration of these arrays will be used to describe flow. Additional subsurface moorings will be placed near the Admiralty Inlet sill and farther west at the same locations occupied during the program in the western Strait described in Sections 2.2 and 3.3. At the same time, Canadian scientists will place several moorings near the north end of Haro Strait in the Strait of Georgia. Winds measured at the surface moorings will be supplemented by wind measurements from anemometers located on Smith Island, Tatoosh Island, New Dungeness spit, and from the weather station at Port Angeles on Ediz Hook. Tidal heights will be available from NOS tide gauges at Neah Bay, Port Angeles, and Port Townsend. CTD sampling of the entire Strait of Juan de Fuca including the Admiralty Inlet sill region will be done during deployment and recovery of the moored arrays and once about midway. Other observations of surface flow on a broader scale may take place at short intervals during the summer deployment.

6. SUMMARY AND CONCLUSIONS

The Strait of Juan de Fuca estuary is a major shipping route for both the United States and Canada. The most recent published oceanographic description of this estuary is now over fifteen years old, and much new work has since taken place. Recently, the Pacific Marine Environmental Laboratory (PMEL) has been studying near-surface circulation and its driving mechanisms and has been developing a computer model to predict possible trajectories of spilled oil. The National Ocean Survey of NOAA has been measuring tides and tidal currents in order to provide improved predictions. Environment Canada also has been investigating various circulation problems in these waters and has been developing a numerical tidal model. This report summarizes some of the results to date.

Because of potentially increased tanker traffic in these waters, this synthesis of ongoing environmental studies has been written so that the most recent results will be readily available for use in decisions regarding these waters. The primary emphasis of these studies has been either directly or indirectly on transport mechanisms that might affect the redistribution of spilled oil. The primary questions that the studies have been attempting to answer are: Given an oil spill at some location in the Strait of Juan de Fuca or near the San Juan Islands, what would tidal currents, river discharges, and wind-driven currents do to the oil? Would it come ashore, and if so where, or would it be transported out to sea and away from the shorelines? No attempt has been made yet to relate these results to specific ecosystems in the Strait. More details will become available, especially for the waters east of Port Angeles, about one year after completion of the 1978 field studies.

It is well known that tidal currents dominate the water motion in this estuarine system. The tidal currents are navigational hazards because the currents are quite large in the more restricted passages

of the San Juan Islands and in Admiralty Inlet, exceeding 4–5 knots in some places. In addition, tidal currents away from shorelines can mix and disperse floating and suspended material, but they tend to produce concentrations in near-shore eddies and at tidal fronts. Satellite photographs have shown large numbers of tidal fronts, particularly on either side of the San Juan Islands (Figs. 23 and 24). Studies in the Puget Sound laboratory hydraulic model at the University of Washington have shown, in the vicinity of Admiralty Inlet (the northern limit of the model), the existence of near-shore eddies almost everywhere on the down-current side of points-of-land and in some embayments (Fig. 7). Canadian numerical tidal model studies also have shown similar eddies in the Strait of Juan de Fuca, and they probably exist throughout these waters. Tidal currents appear much more sensitive than tidal elevations (the rise and fall of the sea surface) to local variations in water depth and details of the shore line. This zone very close to shore has had very little study.

Superimposed on the tidal motions are the estuarine (river discharge) and wind-driven currents which transport floating and suspended material through the system or toward the shores. Studies of these motions have been carried out at PMEL using, for example, surface drift cards (Section 3.1), satellite photographs of suspended sediment (Section 3.2), moored current meters for extended durations (Sections 3.3 and 3.4), and an oil-spill trajectory model (Section 4).

Drift cards released during spring and summer south of San Juan Island in the middle of the eastern basin of the Strait have been found on all beaches surrounding the eastern basin (Fig. 18). Cards released in Puget Sound flowed out Admiralty Inlet and were similarly dispersed around the eastern basin. Cards released closer to the southern shore throughout the Strait moved seaward and were found primarily on the southern shore. Drifters that were tracked during several

days in summer in the vicinity of Slip Point to Pillar Point showed flow parallel to the shore during ebb currents and toward the shore during flood currents. Cards released in winter were found mostly on Vancouver Island (Fig. 18). Summer recoveries on the southern shore and winter recoveries on the northern shore of the western basin of the Strait were consistent with the concept of current drift to the right of prevailing winds. Westerly winds dominated in summer, and easterly winds dominated in winter. Also, moored current-meter observations in winter showed seaward flow with a persistent shoreward component near the coast of Vancouver Island (Fig. 37). Observations in summer were not as close to the southern shore, and flow towards that shore was observed only during relatively short intervals.

Satellite observations of suspended sediment were most useful north of the San Juan Islands in summer when sediment concentrations were largest because of the nearness of the Fraser River and its large volume of sediment-laden river runoff. Mixing in the San Juan Island passages considerably reduced the sediment concentrations in the near-surface water. Sediment plumes and eddies were observed where the Fraser first enters the Strait of Georgia. The plumes moved seaward primarily along the western shore of the Strait of Georgia, then through various passages, and eventually into Haro Strait (Fig. 19). However, during strong northwesterly winds the flow was modified sufficiently so that the sediment plume extended further southeast along the northern coasts of the San Juan Islands, flowed between Orcas and Lummi Islands, and then into Rosario Strait (Fig. 21). Parts of these plumes remained in the southern Strait of Georgia at times, and they continued eastward and then northward along the Washington coast in the vicinity of Cherry Point. Tidal currents were small in the relatively shallow water near Cherry Point, and variable wind-driven currents dominated. Flow patterns deter-

mined by moored current meters and by observations of water properties showed patterns similar to the Fraser plume (Fig. 40). Many of the plumes were very close to shore.

Moored current-meter observations in the western basin of the Strait showed that the near-surface currents averaged over long times were seaward (or westward). During summer shorter-term averages yielded seaward flow. However, during winter considerable variability was observed, and there were extended periods of 3-10 days when the averaged near-surface flow was directed landward (or eastward). One month's observations across the Strait at Tongue Point showed two periods of inflow and two periods of outflow on the southern side (Fig. 28). During the second interval of inflow, the eastward-directed surface flow extended entirely across this section, and significant changes in the deeper flow also were observed. In another winter five major flow reversals occurred, accounting for 35% of the observation interval (Fig. 33). These flow reversals were accompanied by intrusions of coastal oceanic waters which were relatively fresher and warmer (Fig. 30) and which contained coastal species of both phytoplankton and zooplankton (Table 1). The intrusions probably were mixtures of Columbia River discharge, which is known to flow northward during winter under the influence of southerly winds. These reversals and intrusions appeared to be directly related to storm winds along the coast, which raised the sea level at the mouth of the Strait enough to reverse the flow within the western basin (Fig. 36). Significant correlations were observed between along-channel currents at the mouth and sea-surface height at Neah Bay, and between coastal winds and the sea-surface height. The intrusions were observed south from Race Rocks as far as 90 km from the mouth. The speed and duration of these current reversals implies that oceanic water on occasion could possibly reach as far east as Whidbey

Island. However, it is not certain whether the intrusions of coastal water actually enter the eastern basin of the Strait; nor is it certain to what extent storm-related conditions drive the circulation in the eastern basin. These questions are being addressed during the present field investigations.

The oil-spill trajectory model, while still incompletely developed, has nevertheless provided considerable useful information. A simulated oil spill, assumed to be under the influence of easterly winds that were variable in space but constant in time, had trajectories starting from five release sites in the eastern basin, all of which remained in open water for the duration of the calculations. The simulation for westerly winds showed trajectories ending on beaches after a day or two when the release sites were near the San Juan Islands, and after about five days when the sites were west of Port Angeles (Fig. 43). However, it is unlikely that the winds would remain constant for as long as five days. A third case was run for time-varying but spatially uniform winds for a release site west of Port Angeles and south of Race Rocks. Six releases were simulated at noon at three-day intervals, using computerized data from winds observed at Race Rocks for March 1976. After three days, two spills had been transported as far east as Admiralty Inlet, two were between New Dungeness and the release site, and two were slightly west of the release site (Fig. 46). Because of the assumption of spatially uniform winds, the easternmost predicted trajectories should be regarded as preliminary results only. Also, the east-west channeling of these mid-channel releases may be an artifact, because the model does not include all the details of the actual currents (data from the drifter experiment indicate that oil would likely reach the northern or southern shore).

These test cases were trajectories from a typical March. However, March 1977 was not typical, and had oil been spilled then, its transport would have been to the west. Also, no summer cases

have yet been run. Finally, the model includes wind and tidal currents, but time has not allowed inclusion of the winter current reversals arising from wind setup along the coast. These currents are not yet sufficiently well understood to be modeled in the computer.

Drift cards have been found on some beaches at all times of the year. Their recovery in the western basin appeared related to local winds. Recovery in the eastern basin throughout the year appeared to be independent of season; however, the flow patterns distributing the cards around the eastern basin remain unknown. The initial trajectory model experiments described here also indicate that beachings would occur, but more comparisons remain to be made with actual observations for details of the paths, particularly for those exceeding a day or two in time.

The details of the circulation for the southern Strait of Georgia and for the western basin of the Strait of Juan de Fuca are better known than those for the eastern basin. Considerably more information should be available from the ongoing studies in the latter region in about a year and the gaps in knowledge partially filled. However, little is known about processes occurring in the nearshore zone extending about a mile or so offshore anywhere in the estuary, in the passages between the San Juan Islands, at the mouth of the Strait of Juan de Fuca, and at the junction with Admiralty Inlet. These areas must await future research.

So far, these studies have shown that in the Strait of Juan de Fuca a variety of transport processes exist which could result in considerable redistribution of spilled oil (or any other contaminant). Although much work remains to better describe and quantify the cause and effect relationships, much evidence has been presented that indicates the strong possibility of significant volumes of contaminant reaching beaches within the estuary instead of being transported out of the estuary and into the ocean.

7. ACKNOWLEDGMENTS

Funding for a significant part of these studies was provided by the U.S. Environmental Protection Agency to NOAA and managed by NOAA's Puget Sound Project Office of the Marine Ecosystems Analysis (MESA) Program. MESA provided additional funding for this report. This support is gratefully acknowledged. In addition, these funds were supplemented by the Pacific Marine Environmental Laboratory (PMEL). The National Ocean Survey (NOS) was supported primarily by its own funds with a small supplement from MESA. The NOS also provided ship support for many of the PMEL field activities, and assistance by the officers and crews was invaluable.

Special thanks are due Dr. Patrick B. Crean, Dr. Richard E. Thomson, and Mr. W. Stan Huggett of Environment Canada's Institute of Ocean Sciences at Patricia Bay. Many discussions of their work as well as assistance in the field have greatly aided carrying out much of our own work.

Special credit is due many at PMEL who have contributed to and made these studies successful. Dr. John R. Apel provided many helpful suggestions during the final writing.

8. REFERENCES

- Baker, E. T., J. D. Cline, R. A. Feely, and J. Quan, 1978. Seasonal distributions, trajectory studies, and sorption characteristics of suspended particulate matter in the northern Puget Sound region, unpublished manuscript.
- Barnes, C. A., B. A. Morse, and A. C. Duxbury, 1972. Circulation and selected properties of the Columbia River effluent at sea. In: *The Columbia River estuary and adjacent ocean waters*, A. T. Pruter and D. L. Alverson (editors), Univ. of Washington Press, Seattle, 41-80.
- Burt, W. V. and B. Wyatt, 1964. Drift bottle observations of the Davidson Current off Oregon. In: *Studies on oceanography*, K. Yoshida (editor), Univ. of Washington Press, Seattle, 156-165.
- Cannon, G. A., N. P. Laird, and T. V. Ryan, 1972. Currents observed in Juan de Fuca submarine canyon and vicinity, 1971. NOAA Tech. Rep. ERL 252-POL 14, 57 pp.
- Cannon, G. A. and N. P. Laird, 1978. Circulation in the Strait of Juan de Fuca, 1976-1977, unpublished manuscript.
- Chang, P., S. Pond, and S. Tabata, 1976. Subsurface currents in the Strait of Georgia, west of Sturgeon Bank. *J. Fish. Res. Bd. Canada*, 33: 2218-2241.
- Crean, P. B., 1978. A numerical model simulation of barotropic mixed tides in the Strait of Georgia. In: *Hydrodynamics of estuaries and fjords*, J. Nihoul (editor), Elsevier Scientific Publ. Co., Amsterdam, Elsevier Oceanography Series #23, 283-313.
- Crean, P. B. and A. B. Ages, 1971. *Oceanographic records from twelve cruises in the Strait of Georgia and Juan de Fuca Strait, 1968*. Department of Energy, Mines and Resources, Mar. Sci. Branch, Victoria, B.C., 5 vols.
- Damkaer, D. M. and J. D. Larrance, 1978. Seasonal distributions of plankton in the Strait of Juan de Fuca, unpublished manuscript.
- Ebbesmeyer, C. C., J. M. Helseth, and J. M. Cox, 1977. Surface drifter movements observed in outer Strait of Juan de Fuca, July 1977. NOAA Tech. Memo. ERL MESA-22, 70 pp.
- Fissel, D. E., 1976. Pressure differences as a measure of currents in Juan de Fuca Strait. Inst. of Ocean Sciences, Patricia Bay, Victoria, B.C., Pac. Mar. Sci. Rep. 76-17, 63 pp.
- Fissel, D. E. and W. S. Huggett, 1976. Observations of currents, bottom pressures and densities through a cross-section of Juan de Fuca Strait. Inst. of Ocean Sciences, Patricia Bay, Victoria, B.C., Pac. Mar. Sci. Rep. 76-6, 68 pp.
- Gargett, A. E., 1976. Generation of internal waves in the Strait of Georgia, British Columbia. *Deep-Sea Res.*, 23:17-32.
- Harris, R. G. and M. Rattray, Jr., 1954. The surface winds over Puget Sound and the Strait of Juan de Fuca and their oceanographic effect. Univ. of Washington, Seattle, Tech. Rep. 37, 101 pp.
- Hayes, S. P. and D. Halpern, 1976. Observations of internal waves and coastal upwelling: Oregon, July 1973. *J. Mar. Res.*, 33:247-267.
- Herlinveaux, R. H., 1954. Tidal currents in Juan de Fuca Strait. *J. Fish. Res. Bd. Canada*, 11:799-815.
- Herlinveaux, R. H. and J. P. Tully, 1961. Some oceanographic features of Juan de Fuca Strait. *J. Fish Res. Bd. Canada*, 18:1027-1071.
- Holbrook, J. R. and D. Halpern, 1978. Variability of near-surface currents and winds in the western Strait of Juan de Fuca, unpublished manuscript.
- Huggett, W. S., J. F. Bath, and A. Douglas, 1976. Juan de Fuca Strait, 1973. In: *Data record of current observations, Volume XV*. Inst. of Ocean Sciences, Patricia Bay, Victoria, B.C., 169 pp.

- Klemas, V. and D. F. Polis, 1976. Remote sensing of estuarine fronts and their effects on oil slicks. College of Marine Studies, Univ. of Delaware, Newark, Report CMS RANN 4-76, 480 pp.
- Lilly, K. E., Jr., 1978. Northwest Washington weather for the small boat operator. Seattle Forecast Office, National Weather Service, unpublished manuscript.
- Little, A. D., Inc., 1977. The onshore impact of Alaskan oil and gas development in the state of Washington. Report to the Department of Ecology, State of Washington, Olympia, 2 vols.
- McGary, N. and J. H. Lincoln, 1977. Tide prints: surface tidal currents in Puget Sound. Univ. of Washington, Seattle, Washington Sea Grant Publ., WSG 771-1, 51 pp.
- Maunder, W. J., 1968. Synoptic weather patterns in the Pacific Northwest. *Northwest Sci.*, 42:88.
- NOAA/National Ocean Survey, 1976. *Tidal current tables 1977: Pacific coast of North America and Asia*. NOAA/National Ocean Survey, Rockville, MD, 254 pp.
- Nelson, C. S., 1977. Wind stress and wind stress curl over the California Current. National Marine Fisheries Service, Seattle, NOAA Tech. Rep. NMFS SSRF-14, 87 pp.
- Oliver, B. M. and J. F. R. Gower, 1977. Airborne measurements of horizontal wind. Inst. of Ocean Sciences, Patricia Bay, Victoria, B.C., Pac. Mar. Sci. Rep. 77-15, 23 pp.
- Overland, J. E., M. H. Hitchman, and Y. J. Han, 1978. A regional surface wind model for mountainous coastal areas, unpublished manuscript.
- Overland, J. E. and J. C. Vimont, 1979. Marine climatology of western Washington. To be published in: *Puget Sound: oceanography of the in-shore waters of Washington*, L. K. Coachman (editor), Univ. of Washington Press, Seattle.
- Parker, B. B., 1977. Tidal hydrodynamics in the Strait of Juan de Fuca-Strait of Georgia. NOAA Tech. Rep. NOS-69, 56 pp.
- Pashinski, D. J. and R. L. Charnell, 1978. Recovery rate for surface drift cards released in the Puget Sound-Strait of Juan de Fuca during 1976-77, unpublished manuscript.
- Phillips, E. L., 1966. *Washington climate for these counties: northeast Clallam, northeast Jefferson, Island, San Juan, Skagit, Snohomish, and Whatcom*. Cooperative Extension Service, Washington State University, Pullman, Washington, 64 pp.
- Redfield, A., 1950. The analysis of tidal phenomena in narrow embayments. *Papers in physical oceanography and meteorology*, Vol. XI, No. 4, Massachusetts Institute of Technology and Woods Hole Oceanographic Institution, Cambridge and Woods Hole, Massachusetts, 36 pp.
- Reed, T. R., 1931. Gap winds of the Strait of Juan de Fuca. *Mon. Weather Rev.*, 59:473-576.
- Schumacher, J. D. and R. M. Reynolds, 1975. STD, current meter, and drogue observations in Rosario Strait, January-March 1974. NOAA Tech. Rep. ERL 333-PMEL 24, 212 pp.
- Schumacher, J. D., C. A. Pearson, R. L. Charnell, and N. P. Laird, 1978. Regional response to forcing in southern Strait of Georgia. Accepted for publication in *Estuarine and Coastal Mar. Sci.*
- Tabata, S., 1972. The movement of Fraser River influenced surface water in the Strait of Georgia as deduced from a series of aerial photographs. Inst. of Ocean Sciences, Patricia Bay, Victoria, B.C., Pac. Mar. Sci. Rep. 72-6, 69 pp.
- Thomson, R. E., 1975. Currents in Juan de Fuca Strait: the physical oceanography of the B.C. coast—Part VII. *Pac. Yachting*, August, 84-91.
- Tracy, D. E., 1975. STD and current meter observations in the north San Juan Islands, October 1973. NOAA Tech. Memo. ERL PMEL-4, 77 pp.
- U.S. Coast and Geodetic Survey, 1958. *Manual of harmonic analysis and prediction of tides*. Government Printing Office, Washington, D.C., 316 pp.
- Waldichuck, M., 1957. Physical oceanography of the Strait of Georgia, British Columbia. *J. Fish. Res. Bd. Canada*, 14:321-486.
- Webster, I., 1977. A physical oceanographic study of Haro Strait: a data summary and preliminary analysis. Report for Inst. of Ocean Sciences, Patricia Bay, Victoria, B.C., Contractors Report Series 77-3, 90 pp.